

UNIVERSIDAD CARLOS III DE MADRID

DEPARTMENT OF CONTINUUM MECHANICS AND STRUCTURAL ANALYSIS



# SIMPLIFIED DESIGN OF A COMMERCIAL AIRCRAFT WING MADE OF CARBON FIBER

Bachelor Thesis  
Aerospace Engineering

Author: Viet Toan Hoang Hoang  
Tutor: Carlos Santiuste Romero

June 2015



# Acknowledgements

I would like to express my sincere gratitude to my tutor, Dr. Carlos Santiuste Romero for guiding and supporting me through the development of this bachelor thesis. I would like to highlight the confidence he has placed in me and my possibilities, allowing me to work in comfort and motivated.

Also, I would like to thank all people that have helped me to get where I am today, finishing my bachelor thesis and closing a wonderful stage of my life. In special, I would like to thank my incredible mother, an example of perseverance and effort, allowing me to have an opportunity thanks to her desire in search for a better life. Thank you for your unconditional love, support and understanding throughout my studies.



---

# Abstract

The current project consists on the design of a simplified commercial aircraft wing made of carbon fiber material. A real commercial aircraft is used as a model in order to create a wing model by using finite element modelling techniques through the use of ABAQUS software. The development of the wing model involves the creation of each of the structural members of the wing, the joint of them in order to create the final model, the creation of the mesh necessary for the analysis and the application of the loads to perform an analysis that accurately predicts the stresses and displacement that the wing withstands. Two different models are presented, one consisting on one tapered section wing and the second consisting on a wing with two tapered sections. These models are subjected to two different wing loads in cruise conditions, a simplified triangular load and a load that represents a real distribution of aerodynamic loads in the wing. In order to create the final wing model made of carbon fiber material, the wing is analyzed first by using the two different geometries presented and aluminum material. The wing model evolves from the one tapered section wing under triangular loads using aluminum material to the second model under real distribution loads using carbon fiber material. The models have been optimized to decrease the weight as much as possible by taking into account the design restrictions imposed. Then, the first wing model created is a simple tapered section wing made of aluminum and subjected to a triangular distribution, and it has a mass of 8749.52 kg, while the last wing model is formed by two tapered sections made of carbon fiber material and subjected to a real aerodynamic load, and it has a mass of 4765.44 kg, which is about 45 percent lower than the first created model.

---

---

---

# Table of contents

<b>Abstract .....</b>	<b>I</b>
<b>Table of contents.....</b>	<b>III</b>
<b>Table of figures.....</b>	<b>V</b>
<b>Table of tables.....</b>	<b>IX</b>
<b>1. Introduction.....</b>	<b>1</b>
1.1. Motivation.....	1
1.2. Objectives of the project.....	4
1.3. Description of the project .....	5
<b>2. State of the art.....</b>	<b>7</b>
2.1. Previous projects.....	7
2.2. Airbus A330-300 characteristics.....	8
2.2.1. General dimensions.....	8
2.2.2. Aircraft wing .....	9
2.3. Finite Element Method .....	9
2.3.1. Theoretical background .....	9
2.3.2. ABAQUS software.....	13
<b>3. Models .....</b>	<b>16</b>
3.1. Model 1 .....	16
3.2. Model 2 .....	21
<b>4. Materials and design restrictions .....</b>	<b>25</b>
4.1. Materials .....	25
4.2. Failure criteria .....	26
4.3. Maximum vertical displacement.....	27

---

<b>5. Applied loads .....</b>	<b>28</b>
5.1. Triangular load distribution.....	29
5.2. Real loads distribution.....	33
<b>6. Studied cases .....</b>	<b>40</b>
6.1. Case 1 .....	40
6.2. Case 2 .....	48
6.3. Case 3 .....	51
6.4. Case 4 .....	54
6.5. Summary of the results .....	63
<b>7. Conclusions.....</b>	<b>65</b>
<b>8. Future projects.....</b>	<b>67</b>
<b>9. Project planning and budget.....</b>	<b>68</b>
<b>Bibliography .....</b>	<b>70</b>



---

# Table of figures

## Chapter 1

Figure 1.1 – Lift produced by an airfoil [1] .....	1
Figure 1.2 – Wing components [3] .....	2
Figure 1.3 – Pyramidal hierarchy of a model .....	3
Figure 1.4 – Effect of Finite Element Modeling in the pyramidal hierarchy of the model .....	3
Figure 1.5 – Finite Element Modelling of a full scale aircraft [5] .....	4

## Chapter 2

Figure 2.1 – Airbus A330-300 [7].....	7
Figure 2.2 – Previous designed wing models .....	7
Figure 2.3 – General A330-300 aircraft dimensions [9] .....	8
Figure 2.4 – A330-300 aircraft wing [9].....	9
Figure 2.5 – Meshing of the spatial domain in FEM [4] .....	10
Figure 2.6 – Numbering of the finite elements and nodes of the spatial domain [4] .....	10

## Chapter 3

Figure 3.1 – Wing models used in the project .....	16
Figure 3.2 – NACA 2415 airfoil and system of coordinates used in the project. ....	17
Figure 3.3 – Distribution of ribs in the FEM. Model 1 .....	18
Figure 3.4 – Creation of the spars in the FEM. Model 1 .....	18
Figure 3.5 – Internal structure of the wing. Model 1 .....	19
Figure 3.6 – Creation of the wing skin on the wing. Model 1 .....	19
Figure 3.7 – Wing skin (left) and complete structure of the wing (right). Model 1 .....	19
Figure 3.8 – Numbering of the panels in the upper skin of the wing. Model 1 .....	20
Figure 3.9 – Meshing of the ribs and the spars through the use of triangular and square elements. Model 1 .....	20
Figure 3.10 – Meshing of the skin through the use of square elements. Model 1 .....	21
Figure 3.11 – Internal structure of the wing. Model 2 .....	22
Figure 3.12 – Wing skin. Model 2 .....	22
Figure 3.13 – Wing skin (left) and complete structure of the wing (right). Model 2 .....	22
Figure 3.14 – Numbering of the upper skin panels. Model 2 .....	23
Figure 3.15 – Numbering of the lower skin panel. Model 2 .....	23
Figure 3.16 – Meshing of the ribs and the spars through the use of triangular and square elements. Model 2 .....	24
Figure 3.17 – Meshing of the skin through the use of square elements. Model 2 .....	24

---

## Chapter 5

Figure 5.1 – Triangular load distribution in the wing. Example of triangular distribution in Model 1. ....	29
Figure 5.2 – Triangular load distribution across the span of the wing. Model 1 and model 2. ...	30
Figure 5.3 – Triangular load distribution across the chord of the wing. Model 1 and model 2. ...	31
Figure 5.4 – Angle of the panel resultant load with respect to the vertical component load....	33
Figure 5.5 – Span-wise and chord-wise lift distribution in a tapered wing [21] .....	33
Figure 5.6 – Example of pressure distribution in a general airfoil [22].....	34
Figure 5.7 – Pressure distribution in NACA 2415 airfoil ( $\alpha = 5$ deg; $Re = 1000000$ ) .....	34
Figure 5.8 – Pressure distribution along the NACA 2415 airfoil ( $\alpha = 5$ deg; $Re = 1000000$ ) .....	35
Figure 5.9 – Elliptical load distribution across the span of the wing.....	36
Figure 5.10 – Ellipse characteristics .....	37
Figure 5.11 – Angle of the vertical component versus the resultant of the forces in the second model .....	39

## Chapter 6

Figure 6.1 – Tapered wing with triangular distribution of loads.....	42
Figure 6.2 – VM in Pascal (upper) and vertical displacements in meters (lower) with thickness of 2 mm. Model 1 .....	42
Figure 6.3 – VM in Pascal (upper) and vertical displacements in meters (lower) with thickness of 15 mm. Model 1.....	43
Figure 6.4 – Influence of thickness in the vertical displacement in each part with the remaining at 2mm of thickness. ....	44
Figure 6.5 – Influence of thickness in the Von Mises Stress in each part with the remaining at 2mm of thickness. ....	44
Figure 6.6 – Influence of thickness in the mass in each part with the remaining at 2mm of thickness.....	45
Figure 6.7 – Von Mises in Pascal of the optimized aircraft wing. Case 1 .....	46
Figure 6.8 – Vertical displacement in meters of the optimized aircraft wing. Case 1 .....	46
Figure 6.9 – Mesh sensitivity analysis. Case 1.....	47
Figure 6.10 – Two tapered sections wing with triangular distribution of loads. ....	49
Figure 6.11 – Von Mises stress in Pascal of the optimized aircraft wing. Case 2.....	49
Figure 6.12 – Vertical displacement in meters of the optimized aircraft wing. Case 2 .....	50
Figure 6.13 – Two tapered sections wing with real distribution of loads.....	52
Figure 6.14 – Von Mises in Pascal in the upper panel of the optimized aircraft wing. Case 3 ...	52
Figure 6.15 – Vertical displacement in meters in the upper panel of the optimized aircraft wing. Case 3 .....	53
Figure 6.16 – Von Mises stress in Pascal in the lower panel of the optimized aircraft wing. Case 3.....	53
Figure 6.17 – Vertical displacement in meters in the lower of the optimized aircraft wing. Case 3.....	53

---

Figure 6.18 – Ply orientation (defined by light blue arrows) and normal direction (red arrows) in the wing model .....	55
Figure 6.19 – Vertical displacement in meters for $[45/-45/0/90]_{20S}$ in all the wing components. ....	55
Figure 6.20 – HSNMTCRT in the lower skin of the wing under $[45/-45/0/90]_{20S}$ in all the wing components .....	56
Figure 6.21 – Skin Sensitivity Analysis for HSNMTCRT failure criteria and vertical displacement. ....	56
Figure 6.22 – Spar Sensitivity Analysis for HSNMTCRT failure criteria and vertical displacement .....	57
Figure 6.23 – Vertical displacement in meters for last model .....	58
Figure 6.24 – HSNFCCRT in the upper skin of the wing under optimized ply sequence in all the wing components.....	58
Figure 6.25 – HSNMTCRT in the lower skin of the wing under optimized ply sequence in all the wing components.....	58
Figure 6.26- Internal structure of the wing with circular holes in the outer ribs. Model 4 .....	59
Figure 6.27 – Location and section of the stringers in the upper and lower skin of the wing. Model 4 .....	60
Figure 6.28 – Mesh of the internal structure of the wing. Example from Rib 2 to Rib 5. Model 4 .....	61
Figure 6.29 – Longitudinal stresses in Pascal for the stringers .....	62
Figure 6.30 – HSNFCCRT in the upper skin of the wing with holes and stringers.....	62
Figure 6.31 – HSNMTCRT in the lower skin of the wing with holes and stringers .....	62
Figure 6.32 – Vertical displacement in meters for last model .....	63

---

---

# Table of tables

## Chapter 2

Table 2.1 – Dimensioning of A330-300 aircraft wing .....	9
--	---

## Chapter 3

Table 3.1 – NACA 2415 airfoil coordinates .....	17
Table 3.2 – Characteristics of the ribs in the FEM. Model 1 .....	17
Table 3.3 – Mesh characteristics of Model 1 .....	21
Table 3.4 – Characteristics of the ribs in the FEM. Model 2 .....	21
Table 3.5 – Mesh characteristics of Model 2 .....	24

## Chapter 4

Table 4.1 – Aluminum 7475-T761 properties [14] .....	25
Table 4.2 – Carbon Epoxy MTM45-1/IM7 properties [15] .....	26

## Chapter 5

Table 5.1 – Aircraft Weight data of A330-300 [19] .....	28
Table 5.2 – Factors in the sections of the wing span. Model 1 and model 2 .....	30
Table 5.3 – Total force in the sections of the wing span. Model 1 and model 2 .....	31
Table 5.4 – Factors in the panels of the wing chord. Model 1 and model 2 .....	31
Table 5.5 – Maximum force in the sections of the wing span. Model 1 and model 2 .....	32
Table 5.6 – Vertical force applied in each panel of the wing. Model 1 and model 2 .....	32
Table 5.7 – Value of the angles formed by the resultant and the vertical component .....	33
Table 5.8 – Pressure coefficients in the upper part of the NACA 2415 airfoil .....	34
Table 5.9 – Pressure coefficients in the lower part of the NACA 2415 airfoil .....	35
Table 5.10 – Factors (Calibrated pressure coefficients) used in the upper part of the NACA 2415 airfoil .....	35
Table 5.11 – Factors (Calibrated pressure coefficients) used in the lower part of the NACA 2415 airfoil .....	36
Table 5.12 – Factor for distribution of loads across the wing span .....	37
Table 5.13 – Total force in the sections of the wing span .....	37
Table 5.14 – Factors for distribution of loads across the chord (upper and lower skin) .....	38
Table 5.15 – Maximum force in the wing span .....	38
Table 5.16 – Force on the upper panels of the wing .....	38
Table 5.17 – Force in the lower panel of the wing .....	39
Table 5.18 – Value of the angles formed by the resultant and the vertical component .....	39

---

## Chapter 6

Table 6.1 – Area of the upper panels of the simple tapered wing model .....	41
Table 6.2 – Pressure applied in the upper panels of the simple tapered wing model .....	41
Table 6.3 – Thickness in mm of the ribs, spars and skin. Case 1.....	46
Table 6.4 – Results of optimization process. Case 1 .....	47
Table 6.5 – Area of the upper panels of the two tapered sections wing model.....	48
Table 6.6 – Pressure applied in the upper panels of the two tapered sections wing model.....	48
Table 6.7 – Thickness in mm of the ribs, spars and skin. Case 2.....	50
Table 6.8 – Results of optimization process. Case 2 .....	50
Table 6.9 – Area of the lower panels of the two tapered sections wing model .....	51
Table 6.10 – Pressure applied in the upper panels of the two tapered sections wing model....	51
Table 6.11 – Pressure applied in the lower panels of the two tapered sections wing model ....	52
Table 6.12 – Thickness in mm of the ribs, spars and skin. Case 2.....	54
Table 6.13 – Results of optimization process. Case 2 .....	54
Table 6.14 – HASHIN Failure Criteria for [45/-45/0/90] <sub>205</sub> in all the wing components. ....	55
Table 6.15 –Optimized ply sequence in the wing components .....	57
Table 6.16 – HASHIN Failure Criteria for optimized ply orientation in all the wing components. .....	59
Table 6.17 – Characteristics of the stringers in the upper and lower panels. ....	60
Table 6.18 – Isotropic Carbon Epoxy MTM45-1/IM7 properties .....	60
Table 6.19 – Mesh characteristics of Model 4 (with holes and stringers) .....	61
Table 6.20 –Optimized ply sequence in the wing components (with holes and stringers) .....	61
Table 6.21 – HASHIN Failure Criteria for optimized ply orientation in all the wing components. .....	63
Table 6.22 – Results for wing models made of Al 7475-T761 .....	63
Table 6.23 – Results for wing models made of Carbon Epoxy MTM45-1/IM7 .....	64

## Chapter 9

Table 9.1 – Hours per work package .....	68
--	----

# Chapter 1

## Introduction

### 1.1. Motivation

Wings produce the aerodynamic force necessary for flight. This force is produced due to the airfoil shape (streamlined cross-sectional shape) of the cross section of the wing and it is called lift, as shown in Figure 1.1. Due to the aerodynamic shape, the stream velocity flows faster over the top of the airfoil, producing lower pressure than in the bottom part of the airfoil, creating therefore a net force upwards that allows the wing to lift up.

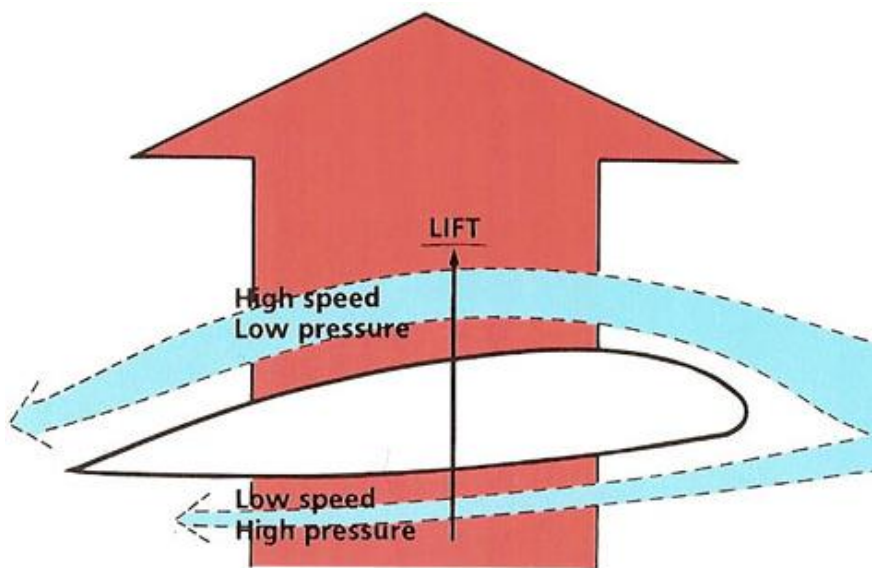


Figure 1.1 – Lift produced by an airfoil [1]

The wing is composed by different components that allow to obtain the required aerodynamic shape for flight as well as to accommodate the loads developed during all the flight phases. The wing is also composed by different parts that are used as controls to allow the different motions of the aircraft, like flaps, ailerons and spoilers.

From the structural point of view, the main parts that compose the wing shown in Figure 1.2 are the following:

- Skin: covers the internal structure of the wing and constitutes a continuous surface to withstand the aerodynamic pressures. The skin pressure loads are then transmitted from the skin to the stringer, ribs and spars.

- Stringers: structural members that run in the longitudinal direction of the wing. They are attached to the skin in order to avoid buckling of the panels of the skin under relatively small compression loads.
- Spars: structural members of the wing that run straight through the span of the wing, from the fuselage to the wing tips. They support the flight loads and the weight of the wings while on the ground, providing the wing rigidity needed to enable the aircraft to fly safely.
- Ribs: forming elements of the structure of a wing attached perpendicularly to the spars and distributed across the span at frequent intervals to form the skeletal shape for the wing and to help the skin to withstand aerodynamic pressure loads. They usually have the airfoil shape necessary for the wing to obtain the aerodynamic forces for flight. [2]

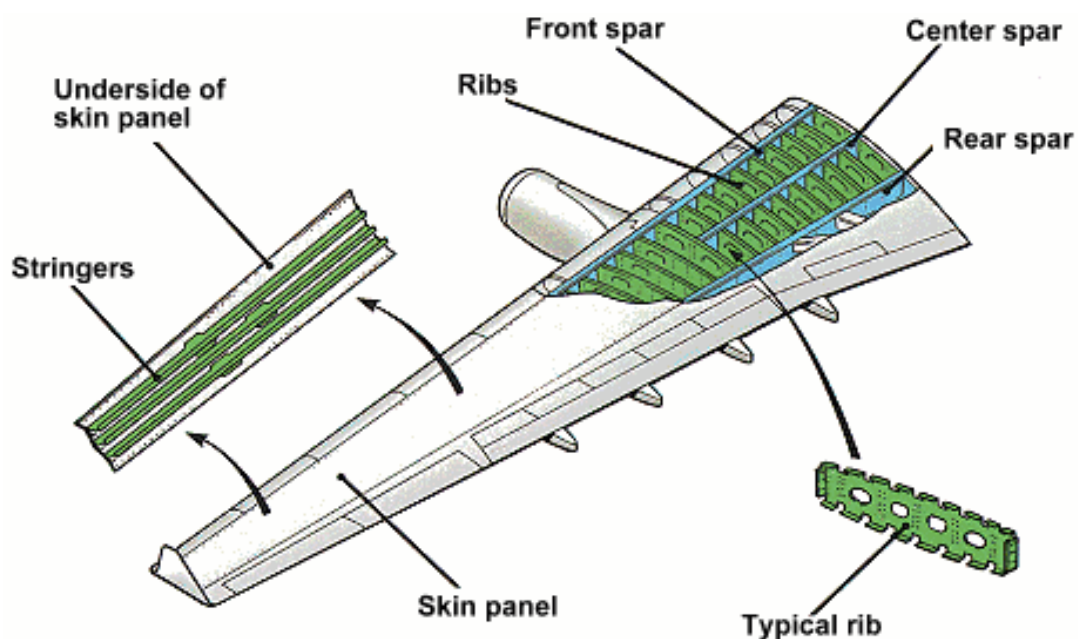


Figure 1.2 – Wing components [3]

Loads supported by these structural members are specified by using prototypes and models that are tested in general mechanical tests. These kinds of test are very expensive, so the use of *Finite Element Modelling* has been introduced in the aeronautical field thanks to the evolution of the technology that allows increasingly difficult numerical computations.

The simplified pyramidal hierarchy shown in Figure 1.3 shows the different sublevels that compose a full scale design. In order to obtain the complete scaled design, all the sublevels of this pyramidal hierarchy must be studied, starting from the bottom, which is the basic material, and going upwards, analyzing the different levels up to the full scale design.



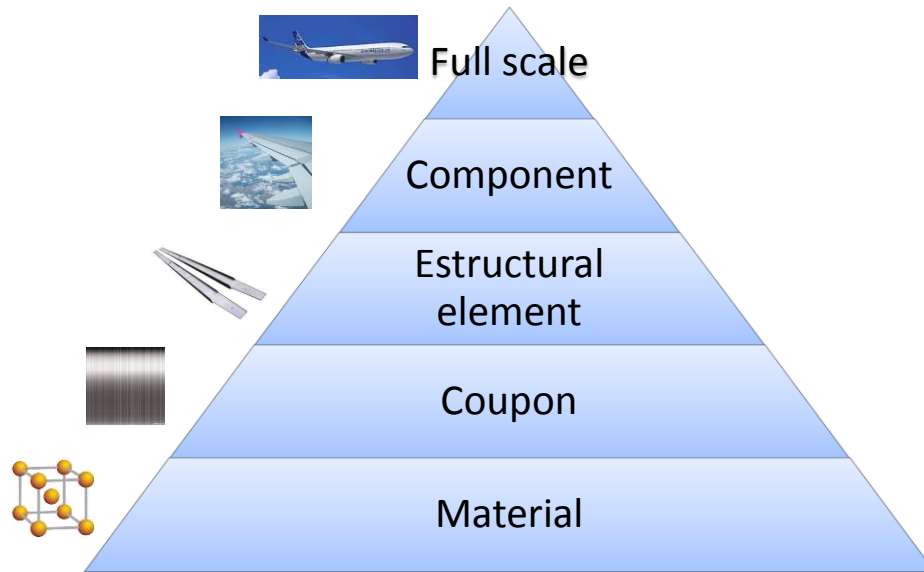


Figure 1.3 – Pyramidal hierarchy of a model

The analysis of these different stages within the pyramid brings a significant money and time involved, as the construction and the test of the different models for each of the levels must be performed.

The use of Finite Element Method (FEM) for virtual testing lead to a significant money and time saving because the construction and the test of the structural elements and components can be removed from the pyramidal hierarchy. These expensive experimental tests can substituted by the finite element models, used for the analysis of a simulated design that allows going into the full scale model without the construction of real and expensive models, as shown in Figure 1.4.

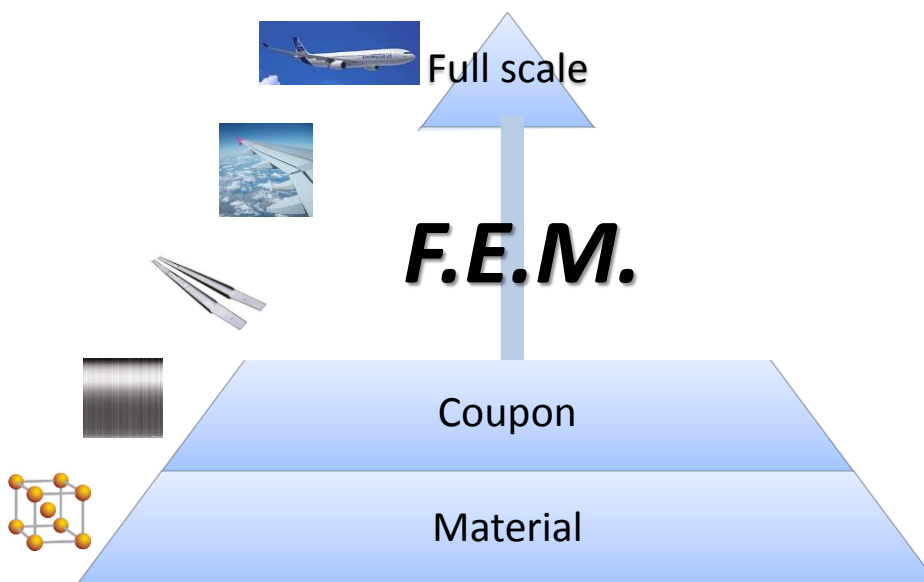


Figure 1.4 – Effect of Finite Element Modeling in the pyramidal hierarchy of the model

Then, when analyzing an engineering problem, that is, a component or a structural element, a closed-form solution to the problem must be obtained. However, complexities in

the geometry, properties and in the boundary conditions that are seen in most real-world problems usually mean that an exact solution cannot be obtained in a reasonable amount of time. Here is where the Finite Element Method comes in, used to obtain approximate solutions that can be obtained in a reasonable time frame and with reasonable effort. In the FEM, the computer simulated region defining the studied system is discretized into simple geometric parts called elements. The properties and the governing relationships are specified over these elements and expressed mathematically in terms of unknown values at specific points in the element called nodes. An assembly process is used to link the individual elements to the given system. Introducing loads and boundary conditions to the model, a set of linear or nonlinear algebraic equations is usually obtained, so the solution of these equations gives the approximate behavior of the system. [4]

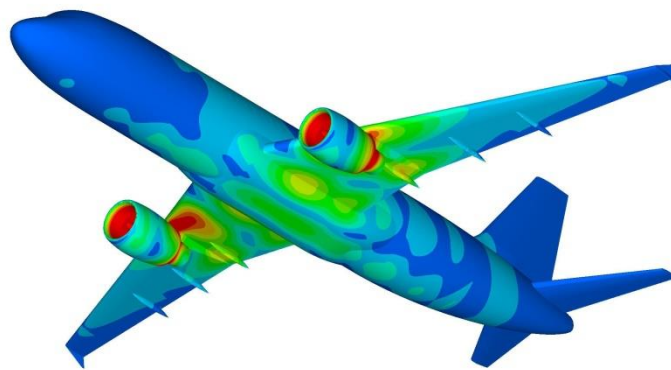


Figure 1.5 – Finite Element Modelling of a full scale aircraft [5]

## 1.2. Objectives of the project

The objective of this project is the design and the corresponding structural analysis of a simplified commercial aircraft wing subjected to loads that simulate the real aerodynamic loads during flight in cruise conditions. The wing design, as well as the loads used to perform this analysis, evolves in order to approximate the studied model to a model that exists in the real life.

In order to perform a correct analysis, the following objectives have been specified:

- Design of a simplified aircraft wing to perform a structural analysis on a finite element model.
- Optimize the design in order to minimize the wing weight.
- Perform a simplified study of the stress state of the aircraft wing under simplified and real aerodynamic loads.
- Learn and improve the knowledge about the finite element analysis and computer-aided engineering through the use of ABAQUS software.

- Perform a correct interpretation of the results obtained from the finite element model.
- Optimize the finite element model by using data collected from the results obtained.
- Understand the behavior of the composite materials used in the wing design under aerodynamic loads.
- Learn the main consequences of use composite material in the wing design instead of aluminum.
- Understand the different failure criteria used in the structural analysis of the wing.
- Demonstrate the function of each of the structural members of the wing.
- Compare the results obtained from the different model used under the different loads applied to these models.

### 1.3. Description of the project

The project is divided in nine different chapters according to the contents that they present.

The first chapter consists on this introduction to the project, in which the general characteristics of the wing and the basics of the finite element modelling are presented. Also, the objectives specified for this project and a brief description of the different contents of it are introduced in this section.

The second chapter contains the state of the art, in which previous projects are introduced. The real wing model used for the creation of the aircraft wing is also described in this section in order to create a similar wing model made through finite element modelling. Due to this, the finite element method and the theoretical basis of it are explained in this chapter. The chapter ends with the presentation of ABAQUS, the finite element modelling software used in the project [6].

To define the different cases analyzed in this project taking into account the geometry of the wing, the load distribution on the wing and the materials used, the following chapters are dedicated to each of these different options.

Thus, the third chapter presents the two different models used for the analysis. These models are evolved versions of the versions presented in the previous projects, being more similar to the real wing aircraft chosen. In this chapter, the creation of the different structural members that compose the entire model are explained.

The fourth chapter introduces the two different materials used in the project. Depending on the material assigned to each of the different parts of the wing, a failure criterion is defined in accordance to the properties that characterize the material. Apart from the failure criterion associated to the material, an additional restriction is introduced for the design, which is the maximum vertical displacement that is allowed in the wing.

The fifth chapter of the project presents two different load distributions on the wing models. Both of them are calculated from the maximum take-off weight that is associated to the aircraft chosen for the project.

The sixth chapter collects the analysis of the different wing models by using the different wing geometries, materials and load distributions presented in the previous chapters. Processing and post-processing of the results are included in this section.

The next two chapters are dedicated to the conclusions and the future projects. The different results obtained are explained here as well as the introduction of future possible projects that can be developed by using the results obtained in the current project.

Finally, the project planning and the budget related to this project are presented. The project ends with the bibliography, which collects all the sources used for the realization of this project.

# Chapter 2

## State of the art

### 2.1. Previous projects

The current project is based in a previous project that consists also in the simplified design of a commercial aircraft wing. The structural analysis has been performed over a wing model that corresponds to the Airbus 330, commonly named A330 and more specifically, the A330-300 version, shown in figure below.



Figure 2.1 – Airbus A330-300 [7]

The created designs performed in the previous projects are shown in Figure 2.2. They consist on straight wings with the general A330-300 dimensions and made of aluminum, one with a simplified cross-section, and the other with the corresponding improvement of the cross section with the introduction of a streamlined cross-sectional shape. These models are subjected to triangular loads distribution and are structurally analyzed by using the Finite Element Method. [8]

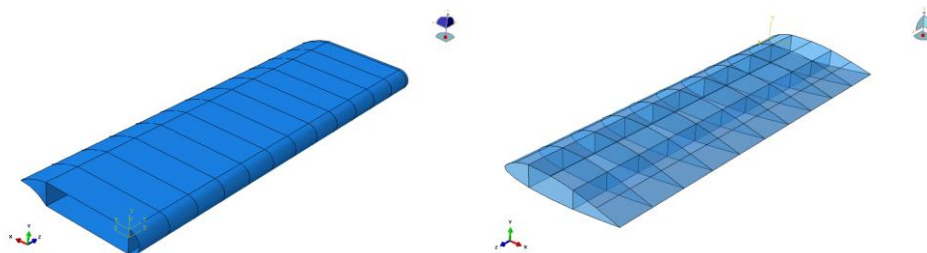


Figure 2.2 – Previous designed wing models

The improvement of the design of these models is an objective of this project, as well as the improvement of the loads applied in order to obtain a realistic distribution of aerodynamic loads. Improvement of the aircraft weight is also performed with the introduction of carbon fiber material.

## 2.2. Airbus A330-300 characteristics

The Airbus A330 is a medium wide-body twin-engine jet airliner made by Airbus and that dates to the mid-1970s as one of the several conceived derivatives of the Airbus A300. The A330-300 was the first aircraft variant, based on a stretched A330 fuselage long but with new wings, stabilizers and fly-by-wire systems, matching twin-engine efficiency with increased passenger capacity (carry 300 passengers in a typical two-cabin arrangement) while retaining the A330 family's highly comfortable, low-noise cabin and operating commonality with the entire Airbus fly-by-wire product line. [7]

### 2.2.1. General dimensions

The general dimensions of the A330-300 aircraft are shown in figure below:

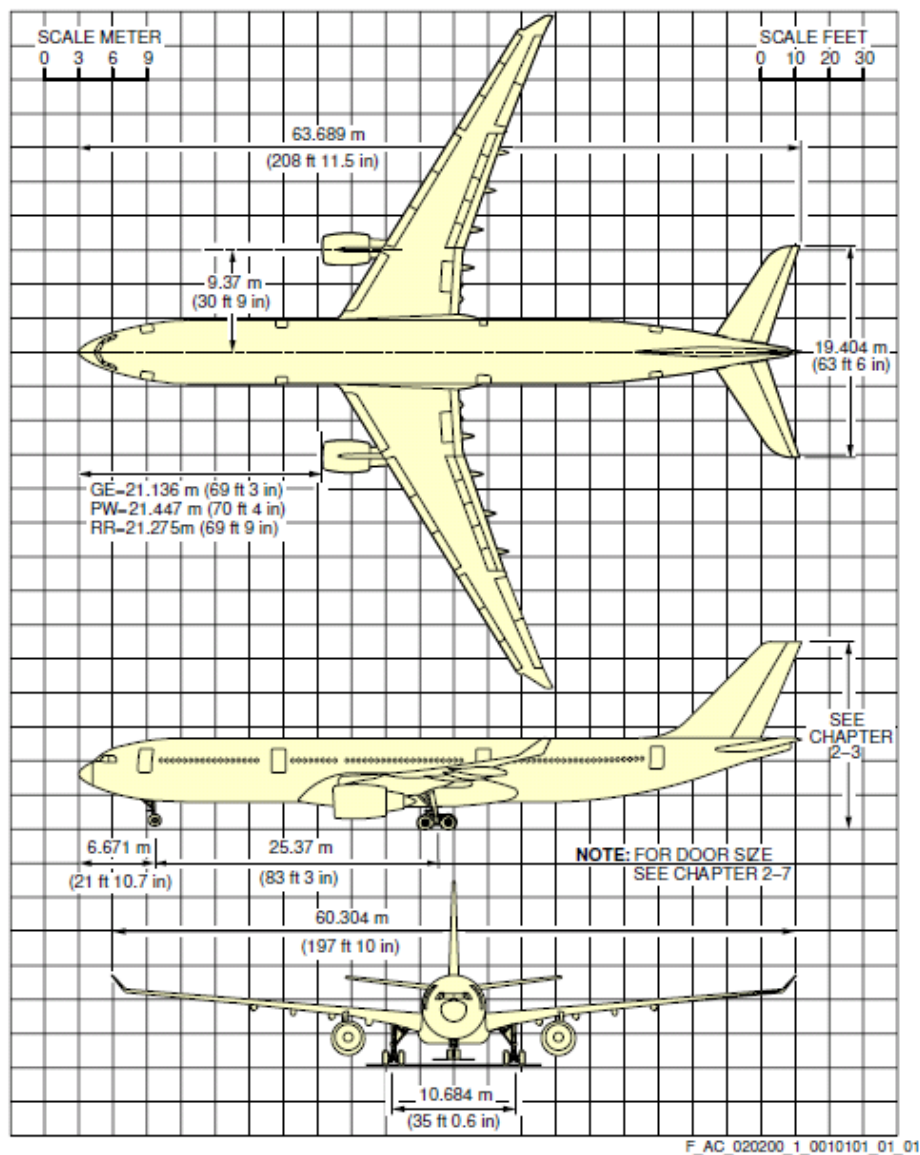


Figure 2.3 – General A330-300 aircraft dimensions [9]

### 2.2.2. Aircraft wing

The A330-300 aircraft wing is shown in more detail in Figure 2.4. As it is shown, it is a swept-back wing that is formed by two tapered sections. Also, the control surfaces are shown in the figure. The A330-300 wing equipment is composed by seven slats, inner and outer flaps, six spoilers and inner and outer ailerons.

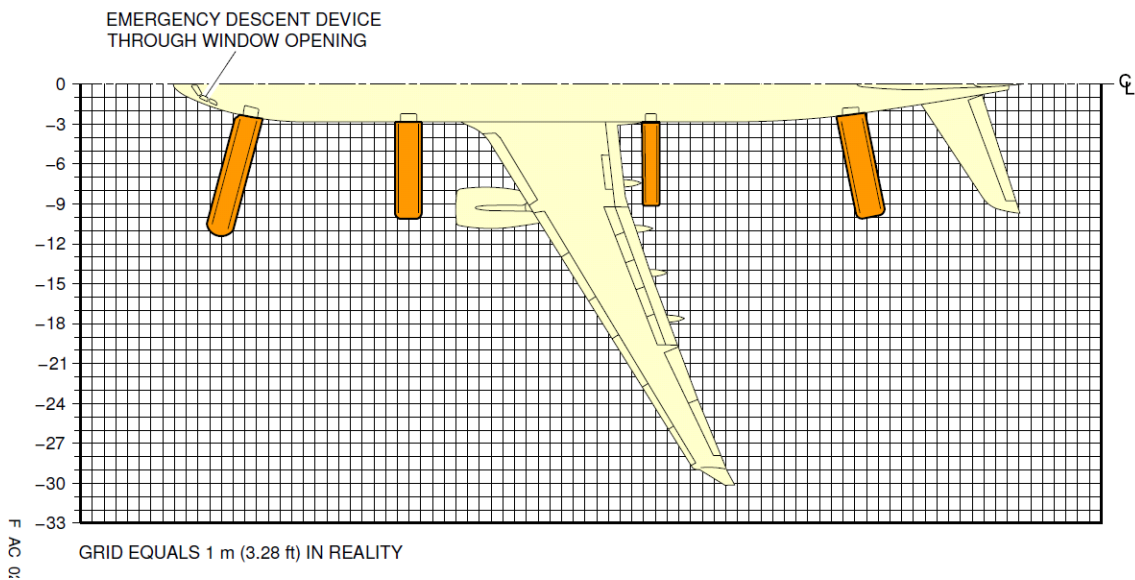


Figure 2.4 – A330-300 aircraft wing [9]

In order to perform an initial dimensioning of the wing for the project model, one can take measures by knowing that a square is formed by four sides of one meter long. Therefore, the wing can be defined with the following dimensions:

	Length [m]
Wing Span	27
Root Length	11
Tip Length	3

Table 2.1 – Dimensioning of A330-300 aircraft wing

In this project, the dihedral of the wing appreciated in Figure 2.3 is not taken into account for simplicity of the design. For the same reason, the control surfaces of the wing and the winglets are not modeled.

## 2.3. Finite Element Method

### 2.3.1. Theoretical background

The Finite Element Method is a numerical procedure for obtaining approximate solutions to many of the problems encountered in engineering analysis with reasonable accuracy. The theoretical background is presented in the following lines. [4]

The spatial domain  $V$  under consideration is decomposed into a set of elements called finite elements, creating thus a mesh that has to verify the following restrictions: the elements cannot leave any zone of the domain uncovered and cannot overlap.

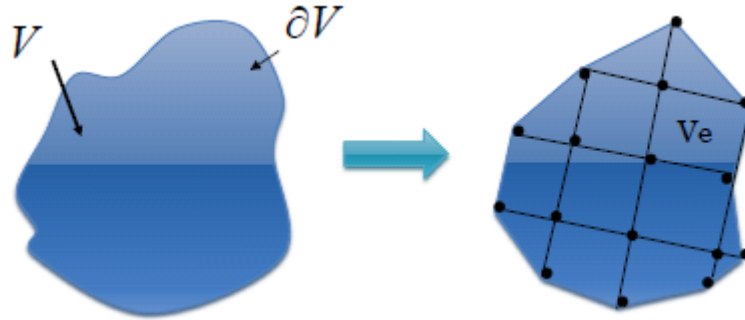


Figure 2.5 – Meshing of the spatial domain in FEM [4]

Therefore, each generic finite element “ $e$ ” ( $e=1,...,E$ ) contains a specific number of nodes  $m_e$ , locally numbered with an index  $i$  ( $i=1, ..., m_e$ )

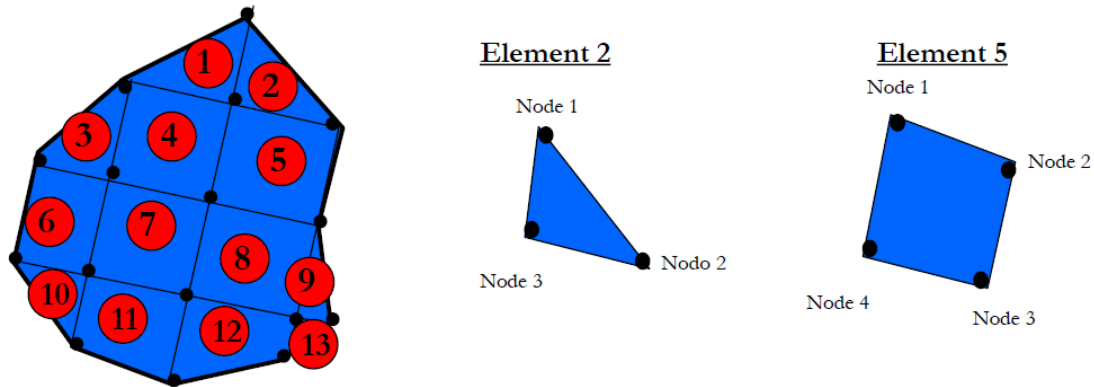


Figure 2.6 – Numbering of the finite elements and nodes of the spatial domain [4]

The discretization procedures reduce the problem to one of a finite number of unknowns by dividing the solution region into elements and by expressing the unknown field variable in terms of assumed approximating functions within each element. These approximating functions are called interpolation functions and they are defined in terms of the values of the field variables at specified points called nodes.

Approximation of the displacement field function inside an element “ $e$ ” is a linear combination of these interpolation functions.

$$\{u^{(e)}\} = [N^{(e)}]\{q^{(e)}\} \quad (1)$$

where:

- $\{q^{(e)}\}$  contains the  $N_e$  (the  $e$ -th element degrees of freedom) displacements of the  $m_e$  nodes in element “ $e$ ”.
- $[N^{(e)}]$  is a matrix which contains the  $e$ -th element interpolation functions.
  - o  $N^{(e)}(x) = 0$  if  $x$  is outside the element  $e$  ( $x$  is the vector of spatial coordinates)



$$\circ \quad u_i = \sum_{j=1}^N N_{i,j}^{(e)}(x, y, z) \cdot q_j^{(e)} = u_i^{(e)}(x, y, z) \text{ for } \mathbf{x} \text{ inside the element } e$$

Using the *variational approach*, in which the potential energy is used, the material properties are formulated:

$$\pi \approx \sum_{e=1}^E \pi_e \quad \text{where } \pi_e \text{ is the total potential energy of an element "e"}$$

Then, the total potential energy of the system is defined as:

$$\pi_e = \int_{V_e} U dv - \int_{V_e} \vec{u} \vec{f}_v dv - \int_{S_{et}} \vec{u} \vec{t} dv \quad \begin{array}{l} V_e \text{ volume of element "e"} \\ S_{et} \text{ is the } e\text{-th surface} \\ f_v \text{ is the body force} \end{array} \quad (2)$$

where:

- $\int_{V_e} U dv$  is the strain energy stored in the element
- $\int_{V_e} \vec{u} \vec{f}_v dv$  work potential of the body force
- $\int_{S_{et}} \vec{u} \vec{t} dv$  work potential of surface forces

The first term of the total potential energy can be expressed in terms of the deformation tensor and strain:

$$U = \frac{1}{2} \{D\}^T (\sigma) \rightarrow U^{(e)} = \frac{1}{2} \{D^{(e)}\}^T [C] \{D^{(e)}\} \quad (3)$$

Using nodal displacements to define the deformation of the element "e":

$$\{D^{(e)}\} = [L] \{u^{(e)}\} = [L][N^{(e)}]\{q^{(e)}\} = [B]\{q^{(e)}\} \quad (4)$$

Introducing eq. (4) in eq. (3) and substituting in eq. (2),  $\pi_e$  is defined as:

$$\pi_e = \int_{V_e} \frac{1}{2} ([B]\{q^{(e)}\})^T [C] [B]\{q^{(e)}\} dv - \int_{V_e} ([N^{(e)}]\{q^{(e)}\})^T \{f_v\} dv - \int_{S_{et}} ([N^{(e)}]\{q^{(e)}\})^T \{t\} ds$$

where the following definitions are used:

- $[K^{(e)}] = \int_{V_e} [B]^T [C] [B] dv$  is the element stiffness matrix which size is of order  $N_e \times N_e$
- $\{Q^{(e)}\} = \int_{V_e} [N^{(e)}]^T \{f_v\} dv - \int_{S_{et}} [N^{(e)}]^T \{t\} ds$  is the element load vector in the element "e", which size is  $N_e \times 1$

So that:

$$\pi^{(e)} = \frac{1}{2} \{q^{(e)}\}^T [K^{(e)}] \{q^{(e)}\} - \{q^{(e)}\}^T \{Q^{(e)}\} \quad (5)$$

The total potential energy is the sum over all the elements in the mesh, so:

$$\pi = \sum_{e=1}^E \pi^{(e)} = \sum_{e=1}^E \left( \frac{1}{2} \{q^{(e)}\}^T [K^{(e)}] \{q^{(e)}\} - \{q^{(e)}\}^T \{Q^{(e)}\} \right) \quad (6)$$

To find the properties of the overall system modeled by the network of elements, all the element properties must be assembled to combine the matrix equations expressing the

behavior of the elements and form the matrix equation expressing the behavior of the entire system. To do that, an element connectivity matrix has to be defined.

Using the following properties:

$$\{q^{(e)}\} = [A^{(e)}]\{q\} \quad \text{and} \quad \{q^{(e)}\}^T = ([A^{(e)}]\{q\})^T = \{q\}^T [A^{(e)}]^T \quad (7)$$

Where  $[A^{(e)}]_{N_e \times N_G}$  express the equivalence between local element nodal numbers and global node numbers ( $N_G > N_e$ ).  $[A^{(e)}] = 1$  when  $i=j$  and  $[A^{(e)}] = 0$  otherwise.

Thus:

$$\pi = \frac{1}{2} \{q\}^T \sum_{e=1}^E ([A^{(e)}]^T [K^{(e)}] [A^{(e)}]) \{q\} - \{q\}^T \left[ \sum_{e=1}^E ([A^{(e)}]^T \{Q^{(e)}\}) \right] \quad (8)$$

Therefore:

$$\pi = \frac{1}{2} \{q\}^T [K] \{q\} - \{q\}^T [Q] \quad (9)$$

where

- $[K]_{N_G \times N_G} = \sum_{e=1}^E ([A^{(e)}]^T [K^{(e)}] [A^{(e)}])$  is the global stiffness matrix
- $[Q]_{N_G \times N_G} = \sum_{e=1}^E ([A^{(e)}]^T \{Q^{(e)}\})$  is the global forcing factor

The assembly process gives a set of simultaneous equations that we solve to obtain the unknown nodal values of the problem. Minimizing the functional expression in terms of the unknown nodal displacement, leads an algebraic system of  $N_g \times N_g$  equations:

$$[K]\{q\} = \{Q\} \quad (10)$$

The stiffness matrix  $[K]$  and the forcing vector  $\{Q\}$  are known (calculate it using the material properties, the external forces applied and the chosen shape functions)

The nodal displacement  $\{q\}$  are unknown, but can be obtained as well as the following parameters:

- Nodal displacements:

$$\{q\} = [K]^{-1} \{Q\} \quad (11)$$

- Displacement field inside the finite elements:

$$\{u^{(e)}\} = [N^{(e)}] [A^{(e)}] \{q\} \quad (12)$$

- The components of the deformation tensor inside the elements:

$$\{D^{(e)}\} = [\mathcal{L}] \{u^{(e)}\} \quad (13)$$

- The stress tensor inside the elements:

$$\{T^{(e)}\} = [C] \{D^{(e)}\} \quad (14)$$

### 2.3.2. ABAQUS software

ABAQUS/CAE or "Complete ABAQUS Environment" is a software application used for both the modeling and analysis of mechanical components and assemblies (pre-processing) and visualizing the finite element analysis result obtained from the processing in ABAQUS/Standard of the dataset prepared by the pre-processor [10]. The finite element analysis (FEA) performed in ABAQUS can be divided in three principal steps [11]:

- 1- Pre-processing: the user constructs a model of the part to be analyzed in which the geometry is divided into a number of discrete sub-regions or elements, connected at discrete points called nodes, creating the mesh necessary for the analysis. Also, the material properties of the model, the boundary conditions and the applied loads are described in this first step.  
The importance of the assumptions when defining the material properties affects the final results as well as the size of the elements used in the meshing. Therefore, a sensitivity analysis of the mesh needs to be performed in order to obtain the optimal results.
- 2- Processing: The dataset prepared by the pre-processor is used as input to the finite element code itself, which constructs and solves a system of linear or nonlinear algebraic equations, as explained in section 2.3.1.
- 3- Post-Processing: Results of the analysis can be visualized through graphical displays. In the case of the structural analysis, the stress and deformations are the most important features to take into account. Depending on the results obtained, the pre-processing phase can be repeated in order to redefine the problem to obtain better results.

In ABAQUS, all these three phases are performed by working with different modules that are used in a sequential way in order to solve the complete problem [12]:

#### **PART MODULE**

In the *Part Module*, the following task can be performed:

- Create deformable, discrete rigid, analytical rigid or Eulerian parts. The part tools are also used to edit and manipulate the existing parts defined in the current model.
- Create the features (solids, shells, wires, cuts and rounds) that define the geometry of the part.
- Use the Sketcher to create, edit, and manage the two-dimensional sketches that form the profile of a part's features. These profiles can be extruded, revolved, or swept to create part geometry; or they can be used directly to form a planar or axisymmetric part.
- Create sets, partitions and datum geometry on the part in the current viewport.

Each of these created parts can be assembled in the assembly module in order to create the final structure.

**PROPERTY MODULE**

The *Property Module* is used to perform the following tasks:

- Define materials.
- Define beam section profiles.
- Define sections with an associated material and thickness in case of a shell.
- Assign sections, orientations, normal directions, and tangents to parts.
- Define composite layups.
- Define skin reinforcements.
- Define inertia on a part (point mass, rotary inertia, and heat capacitance).

**ASSEMBLY MODULE**

The *Assembly Module* is used to create and modify the assembly of the parts. The model contains only one assembly, which is composed of instances of parts from the model. The different parts can be moved along the three dimensions in order to obtain the desired design. The geometric part assembled therefore becomes to an instance or a unique part in case of merging all the pieces.

**STEP MODULE**

The *Step Module* is used to perform the following tasks:

- Create analysis steps.
- Specify output requests.
- Specify adaptive meshing.
- Specify analysis controls.

**INTERACTION MODULE**

The *Interaction Module* is used to define and manage the following tasks:

- Mechanical and thermal interactions between regions of a model or between a region of a model and its surroundings.
- Analysis constraints between regions of a model.
- Assembly-level wire features, connector sections, and connector section assignments to model connectors.
- Inertia (point mass, rotary inertia, and heat capacitance) on regions of the model.
- Cracks on regions of the model.

It is useful when no merging has been selected in order to constrain different movements in the structure.

**LOAD MODULE**

The *Load Module* is used to define and manage the following conditions:

- Loads.
- Boundary conditions like imposed displacements or constrained movements.
- Predefined fields.
- Load cases.

In this module, the different loads applied to the model to simulate a specific case are introduced to the model. The same occurs to the boundary conditions that the model has, like imposed displacement or constrained movements.

**MESH MODULE**

The discretization of the model is performed in this module, which contains tools to generate meshes on parts and assemblies created in ABAQUS/CAE, and functions that verify an existing mesh. The structure is therefore divided in finite elements to obtain the complete meshing. Finite Element Method suppose that the mechanical behavior of the whole structure is similar than the structure composed by a finite number of elements. As explained in section 1.1, these elements are connected between them by points called nodes, which can be discretized in order to assess the size of the elements, which can also have different shapes (triangular, square, beam, etc.)

**OPTIMIZATION MODULE**

The *Optimization Module* is used to create an optimization task that can be used to optimize the topology or shape of the model given a set of objectives and a set of restrictions.

**JOB MODULE**

In this module the interaction with the processing phase is carried out, creating and managing adaptivity analyses and co-executions. An input file that collects all the data created in the previous modules (pre-processing) is sent to the processor in order to perform the analysis job.

**VISUALIZATION MODULE**

Results obtained after the processing are collected in this module, in which all the deformations as well as the stresses obtained in the model from the analysis are shown in a graphical way.

# Chapter 3

## Models

In this section, the design of the different models created is explained. The complexity of the models is increased in order to approximate the model to the real one. In figure below, an upper view of the two models created is shown. As it can be seen, second model presented is very similar to the one shown in Figure 2.4, taking into account the simplifications performed on the wing creation.

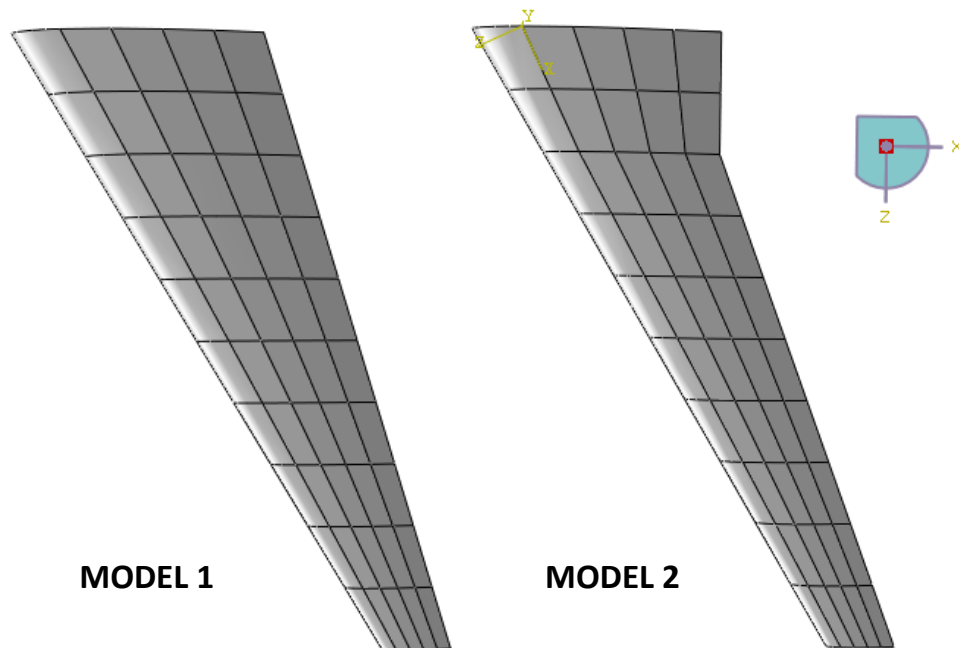


Figure 3.1 – Wing models used in the project

### 3.1. Model 1

The initial model consists on a tapered and swept wing that is the evolution of the previous models presented in section 2.1. The section that used in the wing is a standard NACA airfoil in order to give to the wing the required aerodynamic shape. The selected airfoil is the NACA 2415 [13], whose points are presented in table below.

**Extrados**

x/c	1.0000	0.9000	0.7000	0.6000	0.4000	0.2500	0.2000	0.1000	0.0500	0.0125	0.0000
y	0.0000	0.0245	0.0610	0.0750	0.0925	0.0917	0.0870	0.0683	0.0507	0.0271	0.0000

**Intrados**

x/c	0.0000	0.0125	0.0500	0.1000	0.2000	0.2500	0.4000	0.6000	0.7000	0.9000	1.0000
y	0.0000	-0.0206	-0.0384	-0.0490	-0.0566	-0.0570	-0.0525	-0.0390	-0.0305	-0.0117	0.0000

Table 3.1 – NACA 2415 airfoil coordinates

The NACA 2415 airfoil is used for the creation of the entire wing as a simplification, because nowadays the wing fabrication processes do not use a constant airfoil across the span.

The NACA 2415 airfoil created in the *Part Module* of ABAQUS software is shown in Figure 3.2, as well as the system of coordinates used in the project. In this case, the coordinates  $z$  and  $x$  define the span-wise and chord-wise direction, respectively.

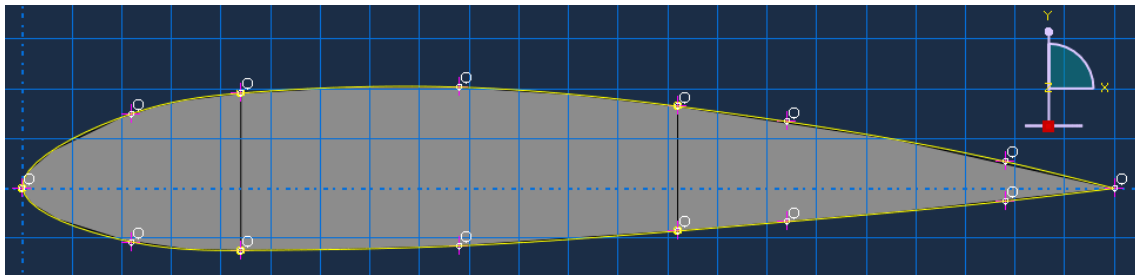


Figure 3.2 – NACA 2415 airfoil and system of coordinates used in the project.

This airfoil is used to create the ribs that form the wing and they are arranged across the span of the wing separated at the same distance between them, decreasing proportionally in length from the root to the tip to give the required wing shape. In Table 3.2, the characteristics of the 11 ribs that form the wing are shown in order to create each of them in the *Part Module* of ABAQUS program.

	Rib 0	Rib 1	Rib 2	Rib 3	Rib 4	Rib 5	Rib 6	Rib 7	Rib 8	Rib 9	Rib 10
Rib Length (m)	11	10.2	9.4	8.6	7.8	7	6.2	5.4	4.6	3.8	3
LE x-coord (m)	0	1.6	3.2	4.8	6.4	8	9.6	11.2	12.8	14.4	16
LE z- coord (m)	0	2.7	5.4	8.1	10.8	13.5	16.2	18.9	21.6	24.3	27

Table 3.2 – Characteristics of the ribs in the FEM. Model 1

To create the ribs arrangement, the  $x$ -coordinate of the leading edge of each rib is increased as the rib position is further than the root (at  $z=0$ ) to create the desired sweep of the wing. The arrangement of the ribs is performed in the *Assembly Module* and is shown in figure below:

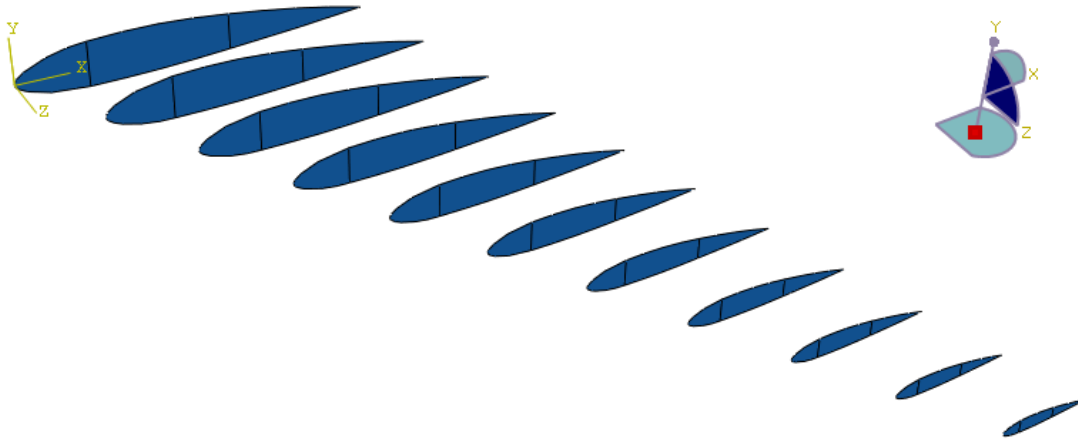


Figure 3.3 – Distribution of ribs in the FEM. Model 1

The creation of two spars is carried out by joining the vertical partitions performed in the ribs through the use of the lofting tool in the *Part Module*, so that they are extended from the root to the tip of the wing, as shown in the Figure 3.4.

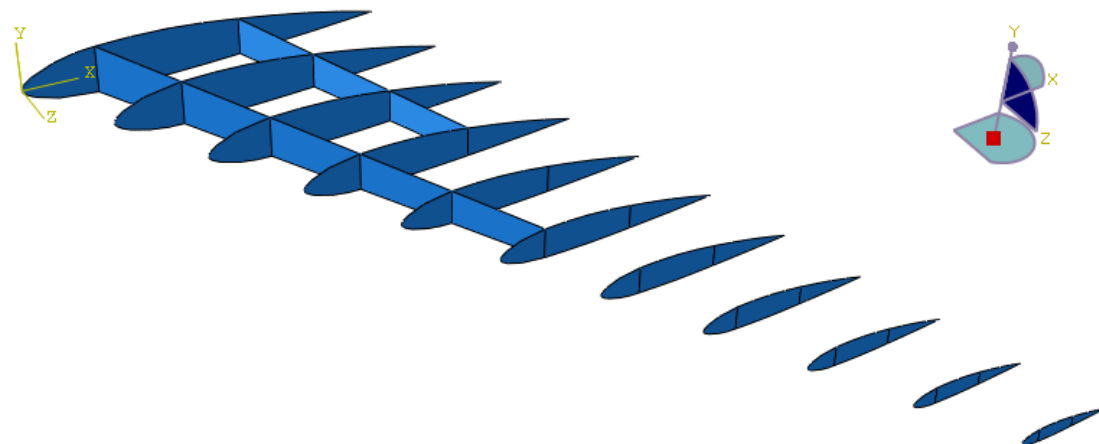


Figure 3.4 – Creation of the spars in the FEM. Model 1

Once the creation of the spars partitions are performed from the rib partitions, the internal structure of the wing is already finished. The combination of the 11 ribs and the 2 spars are shown in Figure 3.5.



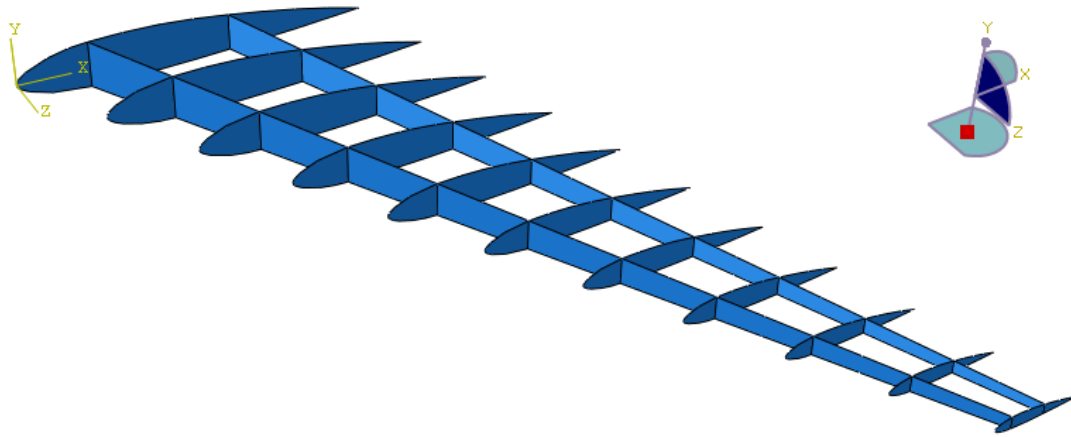


Figure 3.5 – Internal structure of the wing. Model 1

The final step of the wing model creation is to create the skin that covers the internal structure. It is performed in a similar way than the spars. An extrusion from the root to the tip by using the lofting tool in the *Part Module* is performed by joining the boundaries of the ribs, as shown in Figure 3.6.

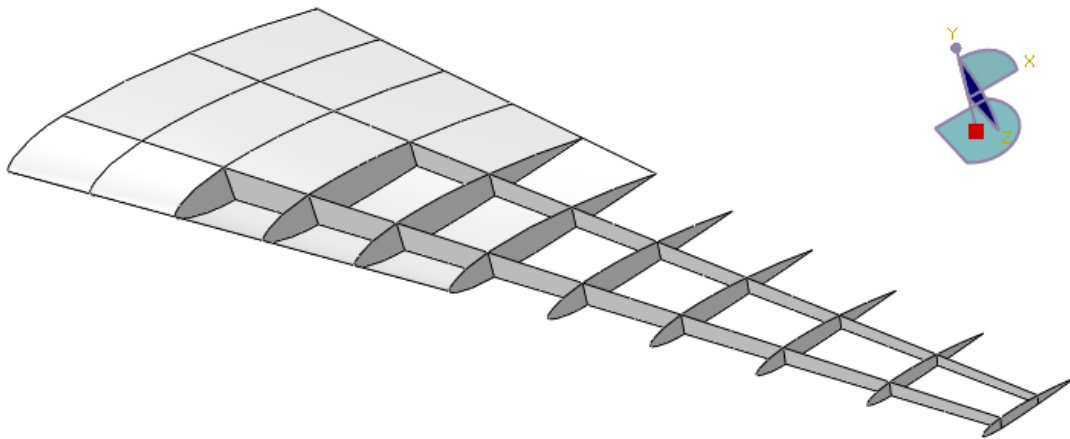


Figure 3.6 – Creation of the wing skin on the wing. Model 1

When the creation of the skin through an extrusion is finished, the final structure is obtained, showing it in figure below:

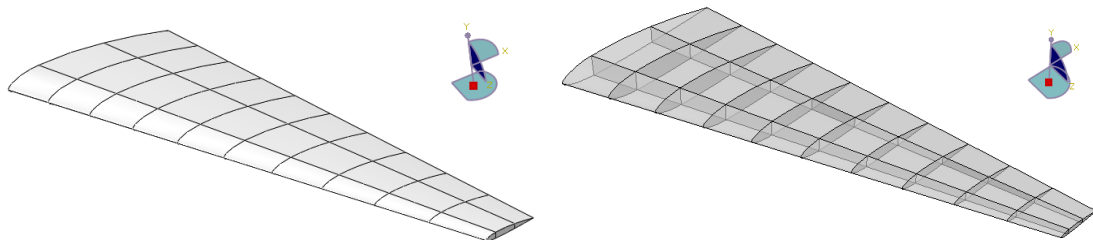


Figure 3.7 – Wing skin (left) and complete structure of the wing (right). Model 1

In addition, to introduce the loads required for the analysis, the skin is divided in several panels in order to apply the corresponding pressure to the wing. Through the partition tool, the panels are created and numbered as can be seen in Figure 3.8.

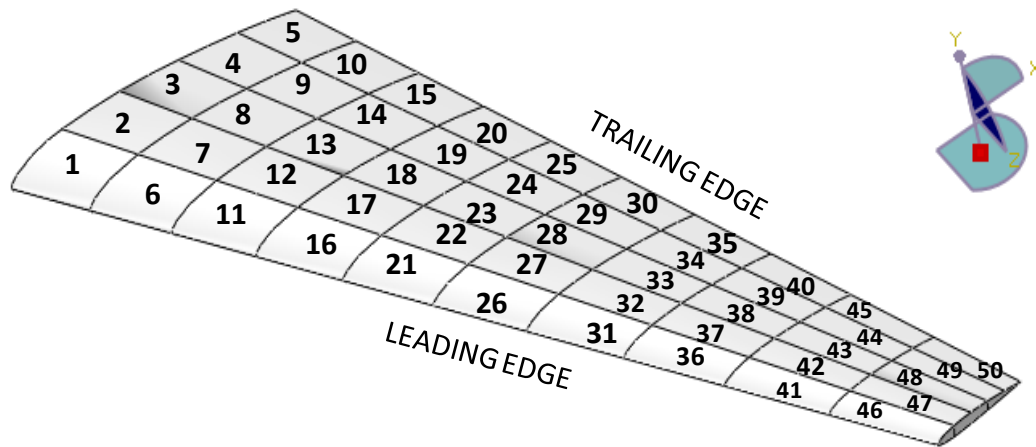


Figure 3.8 – Numbering of the panels in the upper skin of the wing. Model 1

The final step for the wing design is the creation of the meshing in order to be able to apply the finite element method through the ABAQUS/Standard processor. Each of the parts of the wing, the ribs, spars and skin, are divided in finite elements to create the desired mesh in the *Mesh Module*.

In this case, the spars and the skin are modeled through the use of square elements, and the ribs are modeled through the use of triangular elements in the leading edge and trailing edge parts because of the complex shape that they present, and square elements in the central part of the ribs. Therefore, the final meshing of the complete structure is shown in Figure 3.9 and Figure 3.10. The sensitivity analysis performed to validate the current mesh is shown in section 6.1.

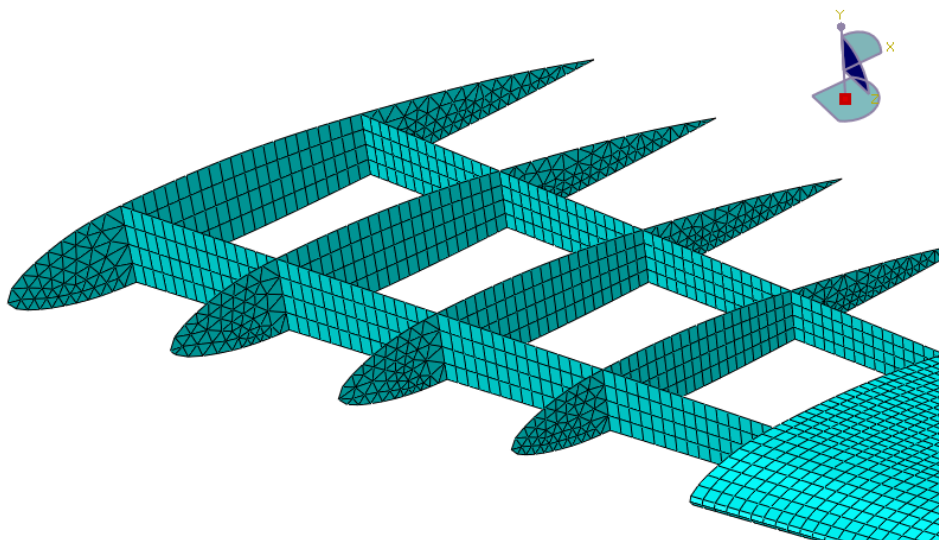


Figure 3.9 – Meshing of the ribs and the spars through the use of triangular and square elements. Model 1

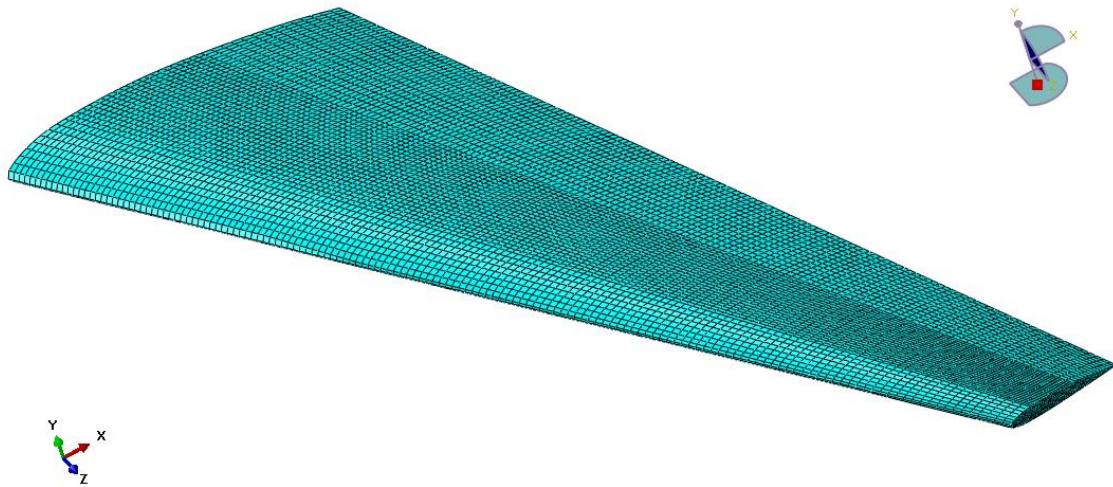


Figure 3.10 – Meshing of the skin through the use of square elements. Model 1

The total number of nodes and elements used in the mesh of this first model is presented in the following table:

Total number of nodes	17622
Total number of elements	19621
Quadrilateral elements (Type S4R)	17230
Triangular elements (Type S3)	2391

Table 3.3 – Mesh characteristics of Model 1

### 3.2. Model 2

The second model varies with respect to the previous model presented in order to approximate the design to the one presented in Figure 2.3. In this case, the wing is formed by two tapered sections instead of one tapered part, but maintaining the same swept angle than the initial model. Maintaining the same airfoil section through the span, characteristics of the 11 ribs used in the model are changed with respect to the previous model. These characteristics are presented in table below:

	Rib 0	Rib 1	Rib 2	Rib 3	Rib 4	Rib 5	Rib 6	Rib 7	Rib 8	Rib 9	Rib 10
<b>Rib Length (m)</b>	11	9.4	7.8	7.2	6.6	6	5.4	4.8	4.2	3.6	3
<b>LE x-coord (m)</b>	0	1.6	3.2	4.8	6.4	8	9.6	11.2	12.8	14.4	16
<b>LE z- coord (m)</b>	0	2.7	5.4	8.1	10.8	13.5	16.2	18.9	21.6	24.3	27

Table 3.4 – Characteristics of the ribs in the FEM. Model 2

Comparing the characteristics of the ribs in the second model with respect to the first model presented in Table 3.2, it is important to realize that the length of the ribs is shortened in such a way that in the trailing edge (sum of the x-coordinate of the leading edge and the rib length), the coordinates of the first three ribs are maintained equal to 11 meters in order to

create the first tapered section. From this point to the rib located at the tip, the second tapered section is created.

Then, once the rib distribution is performed as well as the creation of the spars following the same procedure than the first model, the internal structure of the wing is obtained, as it can be seen in figure below:

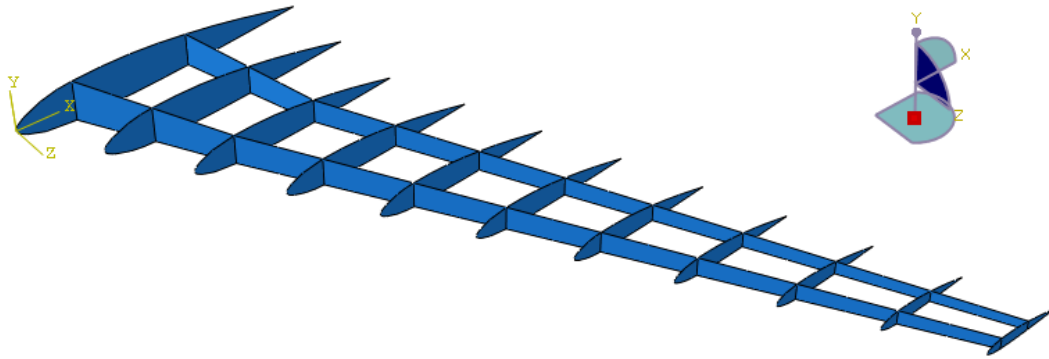


Figure 3.11 – Internal structure of the wing. Model 2

Using the *lofting tool* in the *Part Module*, the skin is created by joining the boundaries of the ribs.

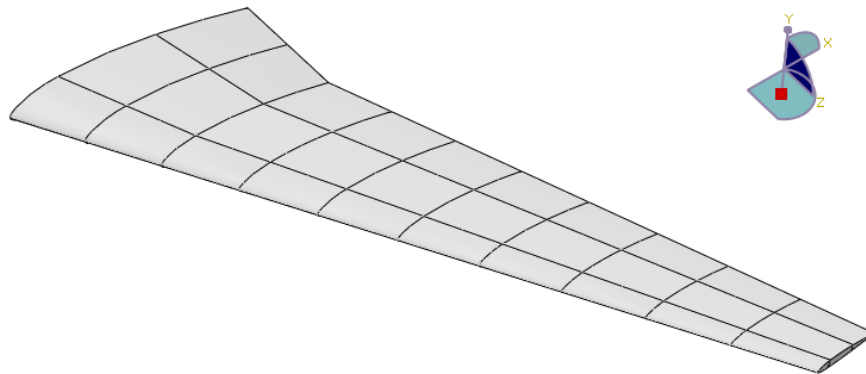


Figure 3.12 – Wing skin. Model 2

When the creation of the skin through an extrusion is finished, the final structure of the second wing model is obtained, as shown in figure below. As mentioned before, two tapered sections have been created, obtaining a wing shape that is very similar to the wing presented in Figure 2.4.

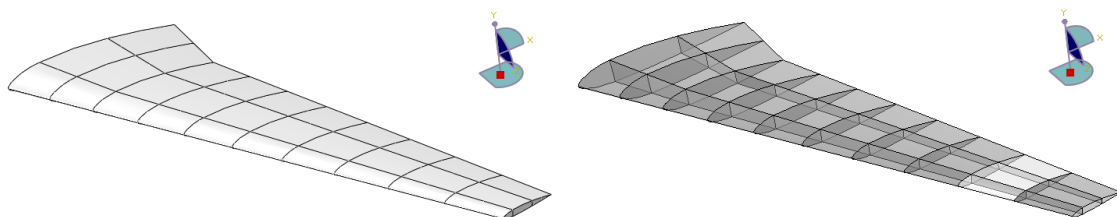


Figure 3.13 – Wing skin (left) and complete structure of the wing (right). Model 2

Also, as in the previous mode, the skin is divided in several panels in order to apply the corresponding pressure load to the wing. In this case, partition has been performed in the upper and lower skin, as the second model withstands different loads comparing with the first model, as it is explained in section 6.3. The numbering of the different panels in the upper and the lower skin is presented in Figure 3.14 and Figure 3.15.

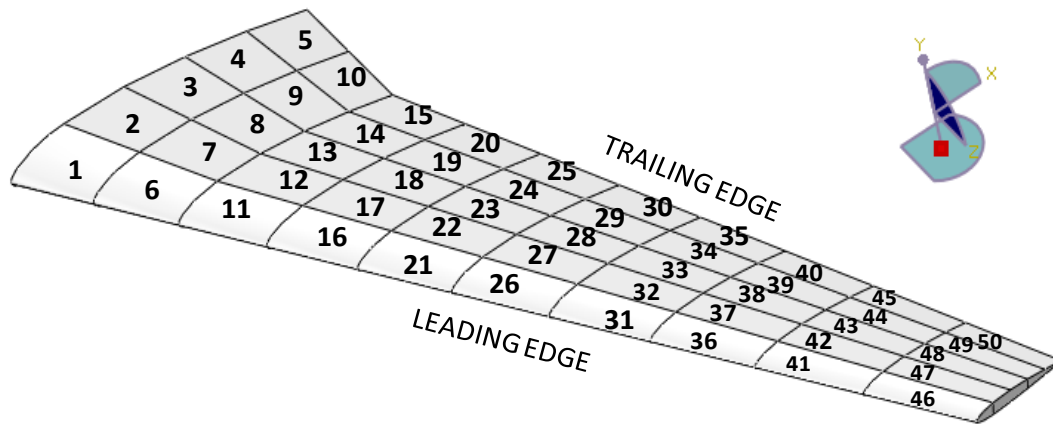


Figure 3.14 – Numbering of the upper skin panels. Model 2

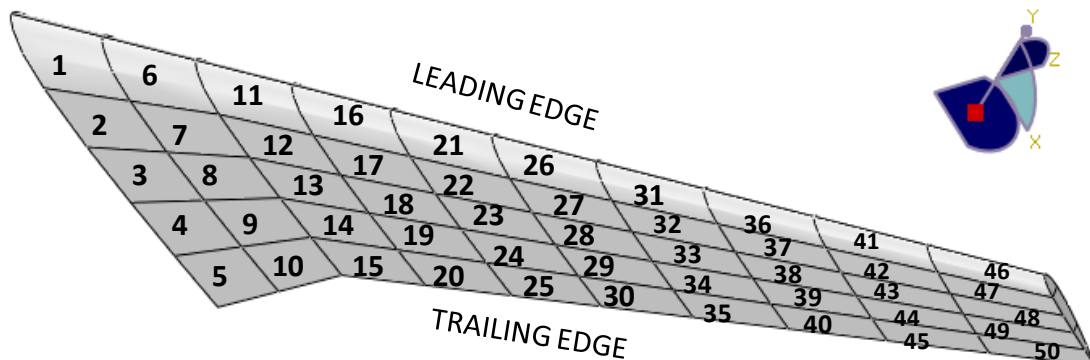


Figure 3.15 – Numbering of the lower skin panel. Model 2

Finally, the mesh creation is performed similarly to the previous model, square elements for the skin and the spars, and a combination of triangular and square elements for the ribs, as shown in the following figures:

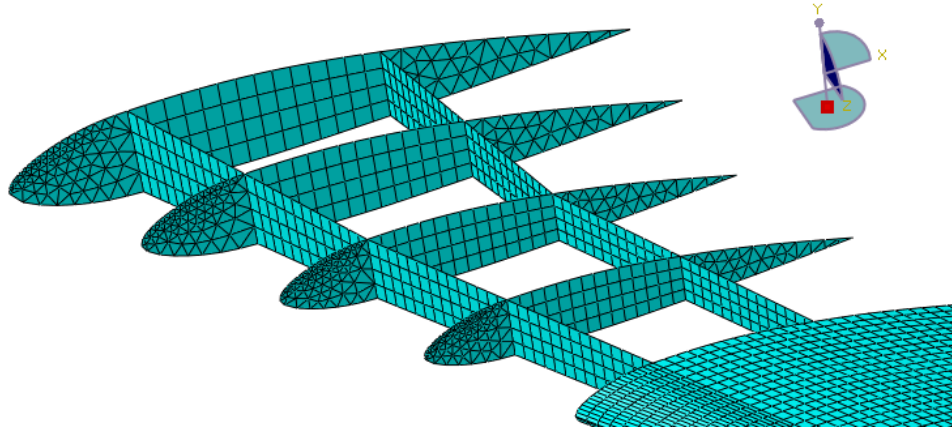


Figure 3.16 – Meshing of the ribs and the spars through the use of triangular and square elements. Model 2

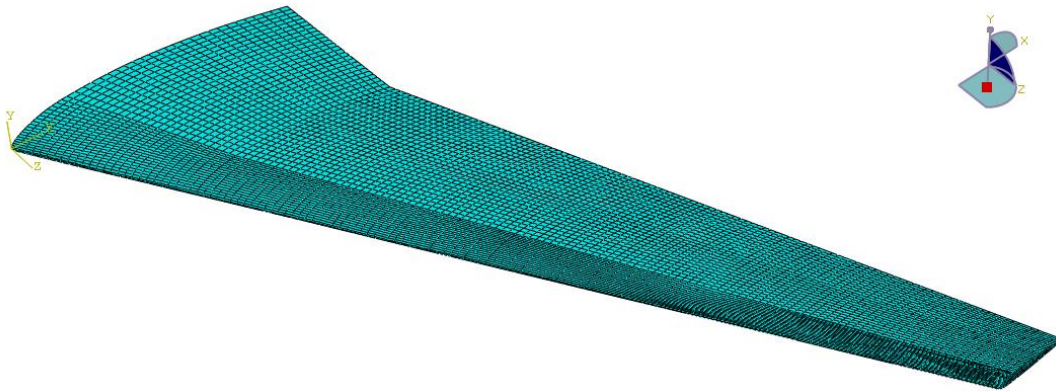


Figure 3.17 – Meshing of the skin through the use of square elements. Model 2

The total number of nodes and elements used in the mesh for this second model is presented in the table below:

Total number of nodes	13182
Total number of elements	14890
Quadrilateral elements (Type S4R)	12848
Triangular elements (Type S3)	2042

Table 3.5 – Mesh characteristics of Model 2

# Chapter 4

## Materials and design restrictions

In this chapter, the materials used for the wing model and the design restrictions are explained. There are two restrictions: the first one is related with the structural failure of the wing and takes into account the failure criteria of the materials used, and the second restriction is related with the maximum vertical displacement of the wing in order to guaranty the functionality of the wing.

### 4.1. Materials

Once the model is created, the material properties have to be assigned to all the sections of the wing. In this project two different materials have been used:

#### **Al 7475-T761**

Al 7475-T761 is a high strength aluminum alloy of very good toughness commonly used in the manufacture of aircrafts in the aeronautic field [14]. Al 7475-T761 material is modeled in ABAQUS as an isotropic material, meaning that their properties are the same in all the directions. The properties of the Al 7475-T761 material are presented in the following table:

Density (Kg/m <sup>3</sup> )	2800
Von Misses stress (MPa)	490
Poisson coefficient	0.33
Young Modulus(GPa)	70.3

Table 4.1 – Aluminum 7475-T761 properties [14]

#### **Carbon Epoxy MTM45-1/IM7**

Carbon Epoxy MTM45-1/IM7 is a composite material that is commonly used in the aeronautical field for the fabrication of structural components, aircraft prototypes, UAVs and missile components [15]. Carbon Epoxy MTM45-1/IM7 is modeled in ABAQUS as a lamina, whose properties are the following:



Density (Kg/m <sup>3</sup> )	1600
Longitudinal modulus, E <sub>1</sub> (GPa)	162
Transverse modulus, E <sub>2</sub> (GPa)	7.93
In-plane shear modulus, G <sub>12</sub> (GPa)	5.3
Out-of-plane shear modulus, G <sub>13</sub> (GPa)	5.3
Out-of-plane shear modulus, G <sub>23</sub> (GPa)	4
Poisson coefficient	0.35
Longitudinal tensile strength, X <sub>T</sub> (MPa)	2899
Longitudinal compressive strength, X <sub>C</sub> (MPa)	1414
Transverse tensile strength, Y <sub>T</sub> (MPa)	37
Transverse compressive strength, Y <sub>C</sub> (MPa)	169
Longitudinal shear strength, S <sub>12</sub> (MPa)	134
Transverse shear strength, S <sub>13</sub> (MPa)	120

Table 4.2 – Carbon Epoxy MTM45-1/IM7 properties [15]

## 4.2. Failure criteria

Failure criteria associated to the models depends on the material that is used in each analyzed case. Two different failure criteria are introduced below.

### - Von Mises Yield Criterion

The Von Mises Stress defined in this failure criterion is the maximum stress that the model can withstand without plastic strains. It is defined from the principal stresses  $\sigma_1$ ,  $\sigma_2$ , and  $\sigma_3$ .

$$\sigma_{VM} = \sqrt{\frac{(\sigma_1 - \sigma_2)^2 + (\sigma_2 - \sigma_3)^2 + (\sigma_3 - \sigma_1)^2}{2}} \quad (15)$$

Von Mises Yield Criterion is applied when Al 7475-T761 is used. The maximum stress obtained in the FEM cannot be higher than the VM stress specified for the material because that means that the material has reached the plastic region.

### - Hashin Failure Criterion

Hashin failure criterion defines the damage initiation criteria for fiber-reinforced composite materials. In ABAQUS, based in Hashin's theory [16], the different modes of failure can be fiber rupture in tension or in compression, and for the case of matrix it may fail also in tension or in compression. The general forms of this criterion are the following:



$$\text{Fiber Tension (HSNFTCRTC)} \quad e_{ft}^2 = \left(\frac{\sigma_1}{X_T}\right)^2 + \alpha \left(\frac{\tau_{12}}{S_{12}}\right)^2 \quad (16)$$

$$\text{Fiber Compression (HSNFCCRTC)} \quad e_{fc}^2 = \frac{\sigma_1}{X_C} \quad (17)$$

$$\text{Matrix Tension (HSNMTCRTC)} \quad e_{mt}^2 = \left(\frac{\sigma_2}{Y_T}\right)^2 + \left(\frac{\tau_{12}}{S_{12}}\right)^2 \quad (18)$$

$$\text{Matrix Compression (HSNMCRTC)} \quad e_{mc}^2 = \left(\frac{\sigma_2}{Y_C}\right)^2 + \left(\frac{\tau_{12}}{S_{12}}\right)^2 \quad (19)$$

Hashin Failure criteria establishes that the variables defined above must not be higher than one, as this indicates that the initiation criterion in a damage mode has been satisfied.

Physically, fiber tension is related with the fiber breakage in the case that the maximum principal stress is higher than the longitudinal tensile strength of the composite, or with fiber de-bonding in the case that the shear stress is higher than the longitudinal shear strength of the composite. In ABAQUS, the fiber tension failure is measured by HSNFTCRTC, which indicates the maximum value of the fiber tensile initiation criterion. In this project,  $\alpha$  defined in fiber tension formula is considered equal to zero, indicating that the shear stress does not contribute to the fiber tensile initiation criterion, in accordance with Hashin and Rotem criterion [17].

Fiber compression is related with the micro-buckling of the fibers, and in ABAQUS, this is defined by HSNFCCRTC parameter, which indicates the maximum value of the fiber compressive initiation criterion.

With respect to the matrix failures, matrix compression predicts matrix crushing and it is measured by HSNMCRTC in ABAQUS, and matrix tension is used to predict matrix cracking, measured by HSNMTCRTC in ABAQUS. [18]

### 4.3. Maximum vertical displacement

Apart from the design restriction related with the different materials presented in the previous section, maximum vertical displacement of the wing must be also taken into account, as high displacements can involve important aerodynamic losses and vibration problems. Therefore, the maximum displacement of the wing is defined as a ten percent of the maximum length of the wing. Thus, the restriction in vertical displacement has a maximum of 2.7 meters in order to introduce the necessary rigidity to avoid the problems described.

$$\text{Vertical displacement } U_2 < 2.7 \text{ m} \quad (20)$$

# Chapter 5

## Applied loads

The analysis of the loads that act on the wing is essential to determine the lift required to introduce in the project. The “Aircraft Recovery Manual” of the airbus A330-300 provides the information of each of the wing parts as well as its corresponding weight [19]. Because of the complexity of the problem as there are a lot of wing components, the selection of the lift load in cruise conditions is performed from the maximum takeoff weight of the aircraft. In this case, as shown in Table 5.1 for the first weight variant the maximum take-off weight is 212000 kg. This value must be multiplied by a safety factor that is selected as 2.5 in order to be more conservative than the specified in FAR 25.303 (safety factor equal to 1.5) because of the simplifications used in the project [20]. Also, it is multiplied by the gravity (assumed to be equal to  $10 \text{ m/s}^2$ ) in order to obtain the desired lift load.

### General Aircraft Characteristics Data

**\*\*ON A/C A330-300**

1. The following table provides characteristics of A330-300 Models, these data are specific to each Weight Variant:

Aircraft Characteristics				
	WV000	WV001	WV002	WV003
Maximum Taxi Weight (MTW)	212 900 kg	184 900 kg	212 900 kg	215 900 kg
Maximum Ramp Weight (MRW)	(469 364 lb)	(407 635 lb)	(469 364 lb)	(475 978 lb)
Maximum Take-Off Weight (MTOW)	212 000 kg	184 000 kg	212 000 kg	215 000 kg
	(467 380 lb)	(405 650 lb)	(467 380 lb)	(473 994 lb)
Maximum Landing Weight (MLW)	174 000 kg	174 000 kg	177 000 kg	177 000 kg
	(383 604 lb)	(383 604 lb)	(390 218 lb)	(390 218 lb)
Maximum Zero Fuel Weight (MZFW)	164 000 kg	164 000 kg	167 000 kg	167 000 kg
	(361 558 lb)	(361 558 lb)	(368 172 lb)	(368 172 lb)

Table 5.1 – Aircraft Weight data of A330-300 [19]

The wing is assumed to carry the entire lift load, neglecting the contribution of the horizontal tail plane, as it is much lower than the one produced by the wing because it is only used for stability effects.

Therefore, the value of the lift load in the wing with the included safety factor and the gravity has a value of 5.3 MN. Because of the symmetry of the aircraft, the lift load for the analyzed wing is half of this value, which is 2.65 MN. From this value, the calculation of the pressures that must be applied in the two models presented in Chapter 3 is performed. Two

different load distributions are taken into account, the first one consists on a simplified triangular distribution across the span and the chord of the wing, and the second one consists on a real distribution of loads, both of them explained in the following sections.

### 5.1. Triangular load distribution

The first case consists on a triangular pressure distribution that is applied through the span-wise and chord-wise direction on the wing, as shown in figure below:

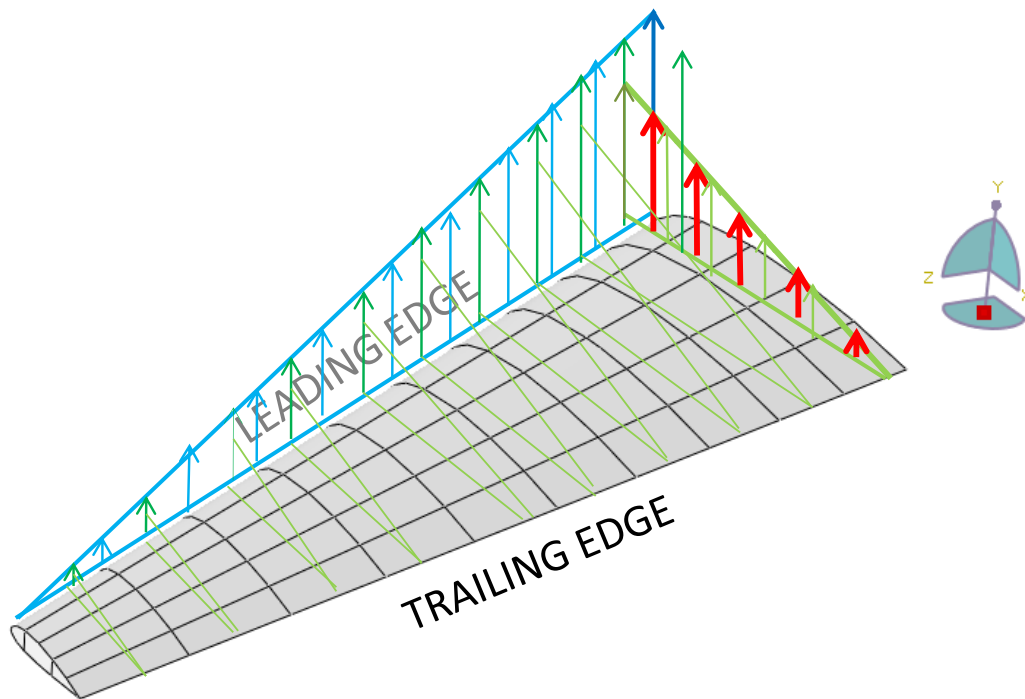


Figure 5.1 – Triangular load distribution in the wing. Example of triangular distribution in Model 1.

The calculation of the pressure distribution starts from the calculation of the load applied in each of the sections defined across the span of the wing. Each of these calculated loads are the resultant force of the section and they are used to obtain the load applied in each panel defined across the chord of the wing. Therefore, the vertical component of the load in each panel and their pressure are obtained by taking into account the area of each panel as well as the angle of inclination of the panel with respect to the vertical.

Starting with the calculations of the loads across the span, the wing is divided in ten sections, each one defined between the eleven ribs used in the model, as shown in figure below:

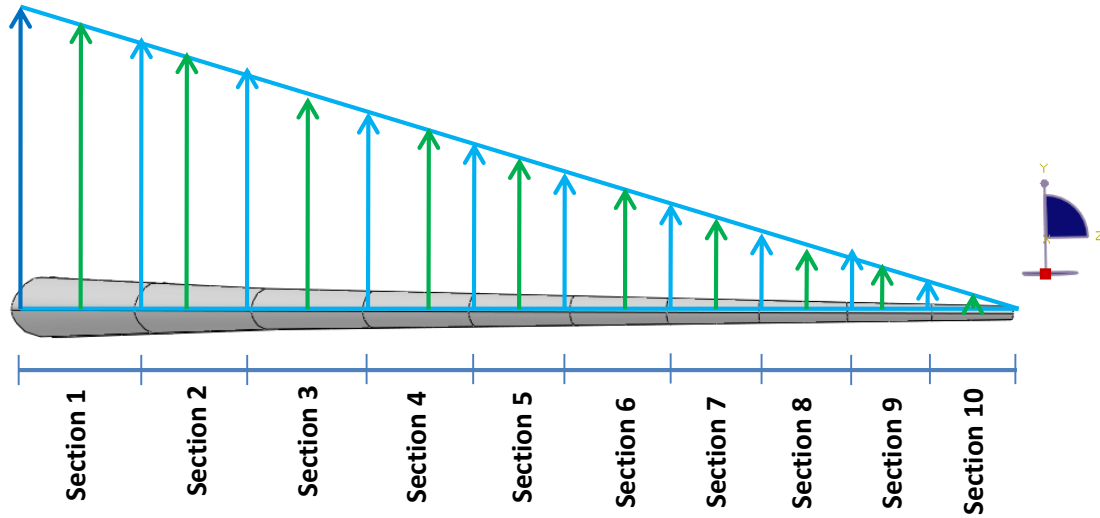


Figure 5.2 – Triangular load distribution across the span of the wing. Model 1 and model 2.

Then, starting from the known maximum lift load, one can calculate the force that is applied the middle of the sections (dark green arrows in Figure 5.2) by knowing that the force decreases linearly from the root to the tip in a triangular distribution, being the force in the root (dark blue arrow in Figure 5.2) the maximum applied force  $F_{max}$  equal to:

$$F_{max} = \frac{Q_{max}}{\sum Factor_i} \quad (21)$$

where  $Q_{max} = 2650000N$  and the  $Factor_i$  is the factor that must be multiplied to  $F_{max_i}$  in order to obtain the maximum force applied in each section  $i$ :

$$F_{section_i} = Factor_i \cdot F_{max} \quad (22)$$

As the applied load across the span is triangular, the corresponding factor decreases from the root to the tip, having the maximum value at the root ( $z=0m$ ) and having zero value at the tip ( $z=27m$ ). By knowing this, the value of  $Factor_i$  in each of the sections is calculated and shown in Table 5.2.

Rib	0	1	2	3	4	5	6	7	8	9	10
z-value	0	2.7	5.4	8.1	10.8	13.5	16.2	18.9	21.6	24.3	27
Factor on Ribs	1	0.9	0.8	0.7	0.6	0.5	0.4	0.3	0.2	0.1	0
Section $i$	-	1	2	3	4	5	6	7	8	9	10
Factor on Section $i$	-	0.95	0.85	0.75	0.65	0.55	0.45	0.35	0.25	0.15	0.05

Table 5.2 – Factors in the sections of the wing span. Model 1 and model 2.

Knowing the value of  $Factor_i$ , the maximum force  $F_{max_i}$  can be calculated:

$$F_{max} = \frac{Q_{max}}{\sum Factor_i} = \frac{2650000}{5} = 530000N \quad (23)$$

Thus,  $F_{section}$  can be calculated for each section  $i$ , obtaining the following results:

Section $i$	-	1	2	3	4	5	6	7	8	9	10
Force in section $i$ (N)	-	503500	450500	397500	344500	291500	238500	185500	132500	79500	26500

Table 5.3 – Total force in the sections of the wing span. Model 1 and model 2.

Then, the values of  $F_{section_i}$  shown in Table 5.3 are the resultant vertical force of the triangular distribution across the chord, having the maximum value at the leading edge and decreasing linearly from the leading edge to the trailing edge as shown in Figure 5.3.

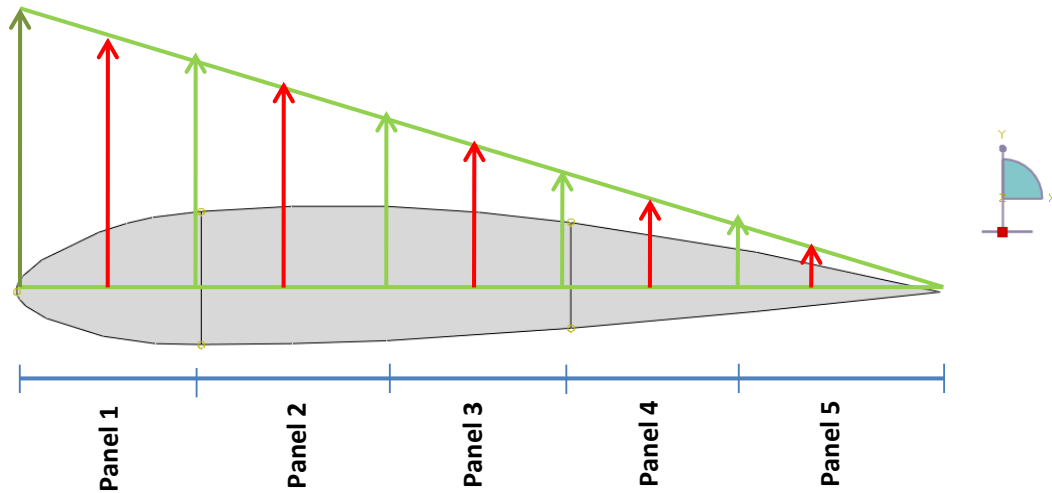


Figure 5.3 – Triangular load distribution across the chord of the wing. Model 1 and model 2.

Therefore, in order to obtain the force acting in each of the panels, same procedure is followed to obtain the factors that must multiply the maximum force  $F_{max_j}$  of each section to know the force acting in each panel of the wing.

$$F_{panel_{ij}} = Factor_j \cdot F_{max_j} \quad (24)$$

Knowing the value of the  $x$ -coordinate of each panel and knowing that the maximum factor is equal to 1 in the leading edge and the factor equal to 0 in the trailing edge, the value of the  $Factor_j$  in each panel can be obtained as the distribution is linear. As the same airfoil has been used across wing span, all the sections has the same value of  $Factor_j$ , that are collected in table below.

Panel $j$	-	1	2	3	4	5
Factor in panel $j$ (N)	-	0.90	0.70	0.50	0.30	0.10

Table 5.4 – Factors in the panels of the wing chord. Model 1 and model 2.

Therefore, the maximum force in each section (dark green arrow in Figure 5.3) is defined as:

$$F_{max_j} = \frac{F_{section_i}}{\sum Factor_j} \quad (25)$$

The values of  $F_{max_j}$  in each section in order to calculate the force  $F_{panel_{ij}}$  that must be applied in each panel are collected in table below:

Section $i$	1	2	3	4	5
Maximum Force (N)	201519.54	180294.51	159083.39	137872.27	116668.49
Section $i$	6	7	8	9	10
Maximum Force (N)	95456.77	74238.91	53031.54	31816.68	10606.18

Table 5.5 – Maximum force in the sections of the wing span. Model 1 and model 2.

Therefore, the force  $F_{panel_{ij}}$  in each panel can be calculated for each panel of the two models defined in Figure 3.8 and Figure 3.14. Note that forces applied in each panel are the same for the two models as the z-value defined in Table 5.2 as well as the airfoil shape are the same in both models. Then, results are shown in table below:

Section 1	Force (N)	Section 2	Force (N)	Section 3	Force (N)	Section 4	Force (N)	Section 5	Force (N)
Panel 1	29214.807	Panel 6	28267.193	Panel 11	27153.856	Panel 16	25823.801	Panel 21	24259.737
Panel 2	24581.751	Panel 7	23821.422	Panel 12	22874.780	Panel 17	21744.780	Panel 22	20371.430
Panel 3	17618.142	Panel 8	17009.855	Panel 13	16361.939	Panel 18	15550.583	Panel 23	14600.600
Panel 4	10466.046	Panel 9	10128.095	Panel 14	9730.915	Panel 19	9256.236	Panel 24	8679.470
Panel 5	3512.588	Panel 10	3398.691	Panel 15	3264.871	Panel 20	3104.999	Panel 25	2910.827

Section 6	Force (N)	Section 7	Force (N)	Section 8	Force (N)	Section 9	Force (N)	Section 10	Force (N)
Panel 26	22253.543	Panel 31	19692.661	Panel 36	16316.164	Panel 41	11651.841	Panel 46	4864.294
Panel 27	18721.683	Panel 32	16556.291	Panel 37	13701.601	Panel 42	9814.994	Panel 47	4036.053
Panel 28	13380.640	Panel 33	11829.076	Panel 38	9820.150	Panel 43	7004.059	Panel 48	2892.726
Panel 29	7962.219	Panel 34	7046.524	Panel 39	5838.961	Panel 44	4170.392	Panel 49	1717.321
Panel 30	2669.489	Panel 35	2361.590	Panel 40	1963.018	Panel 45	1402.057	Panel 50	577.351

Table 5.6 – Vertical force applied in each panel of the wing. Model 1 and model 2.

Finally, in order to calculate the pressure in each panel that must be introduced in ABAQUS program, the angle with respect to the resultant force must be calculated as well as the area of each of the panel, as shown in formula below:

$$P_{panel_{ij}} = \frac{F_{panel_{ij}}}{Area_{ij} \cdot \cos \alpha} \quad (26)$$

Table 5.6 shows only the vertical component of the force that must be applied in order to obtain the maximum force of 2.65 MN calculated at the beginning of the section. For the calculation of the pressure, the resultant force of the panel (purple arrows in Figure 5.4) that is perpendicular to the panel surface must be calculated, so the angle between these two forces must be known.

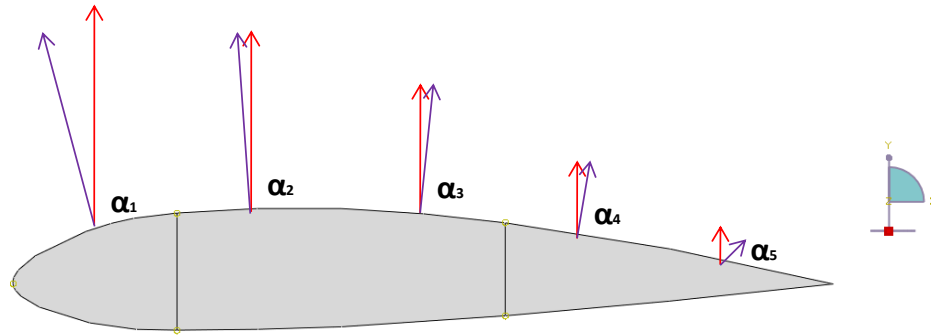


Figure 5.4 – Angle of the panel resultant load with respect to the vertical component load

Simple geometric calculations are performed to obtain the following results:

	$\alpha_1$	$\alpha_2$	$\alpha_3$	$\alpha_4$	$\alpha_5$
Degrees	23.509	1.575	-5.001	-8.645	-12.595

Table 5.7 – Value of the angles formed by the resultant and the vertical component.

These values of  $\alpha$  are taken into account for the future calculation of the pressures to be introduced in ABAQUS. As the airfoil is the same for the two models presented, values of  $\alpha$  are always the same.

## 5.2. Real loads distribution

The pressure distribution in the wing is very different than the one proposed in section 5.1, in which a triangular distribution is presented across the chord and the span of the wing. A real distribution of the loads is shown in figure below as an example.

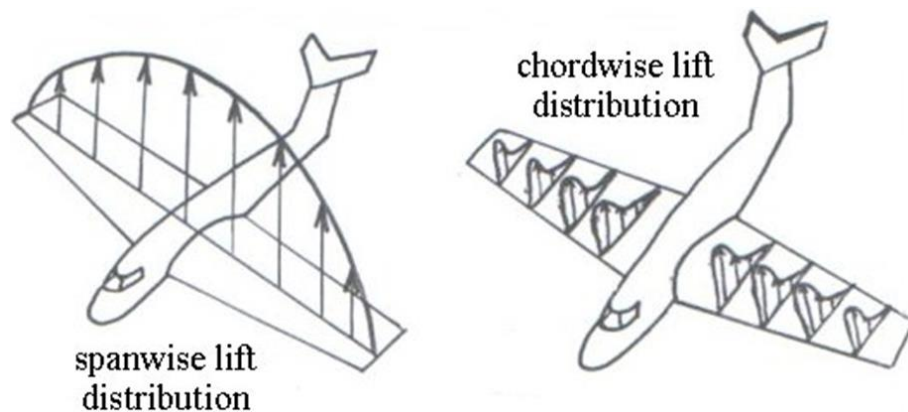


Figure 5.5 – Span-wise and chord-wise lift distribution in a tapered wing [21]

In real aircrafts, the distribution of pressures across the wing span is almost elliptical, depending on the taper ratio and the twist and sweep angle. For simplicity, the distribution of loads along the wing span is chosen to be elliptical. On the other hand, the distribution of pressures along the chord of the wing depends on the angle of attack. In this case, the approximate distribution of pressures is the following:

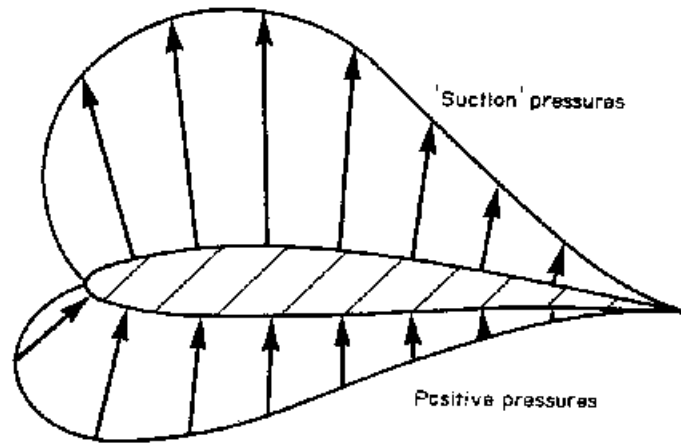
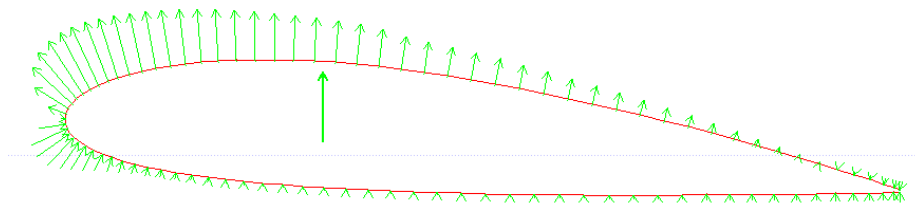


Figure 5.6 – Example of pressure distribution in a general airfoil [22]

To obtain a realistic distribution of pressures in the wing, the pressure coefficient of the NACA 2415 airfoil is obtained by using XFLR5 software [23], for an angle of attack of 5 degrees and Reynolds Number equal to 1000000. The corresponding pressure coefficient are adjusted in order to obtain the desired factors that are used to obtain the pressure in each panel, in a similar way than explained in the case of triangular distribution.

Thus, as the section used for each of the wing models is the same, the analysis is performed through the NACA 2415 airfoil, obtaining the following pressure distribution:

Figure 5.7 – Pressure distribution in NACA 2415 airfoil ( $\alpha = 5$  deg;  $Re = 1000000$ )

In relation with the pressure coefficients, the following tables collect the value of the  $c_p$  along the entire airfoil:

**Upper Part**

x/c	cp	x/c	cp	x/c	cp	x/c	cp	x/c	cp
1.000	0.208	0.798	-0.214	0.508	-0.634	0.242	-1.143	0.059	-1.508
0.993	0.192	0.770	-0.257	0.479	-0.677	0.220	-1.183	0.047	-1.537
0.980	0.160	0.742	-0.299	0.451	-0.720	0.198	-1.223	0.036	-1.559
0.964	0.118	0.713	-0.341	0.422	-0.764	0.177	-1.262	0.027	-1.567
0.945	0.070	0.684	-0.382	0.395	-0.820	0.157	-1.300	0.019	-1.548
0.923	0.020	0.654	-0.423	0.368	-0.916	0.138	-1.337	0.012	-1.478
0.901	-0.029	0.625	-0.464	0.341	-0.992	0.120	-1.373	0.007	-1.312
0.877	-0.078	0.595	-0.506	0.316	-1.025	0.103	-1.408	0.003	-0.998
0.851	-0.125	0.566	-0.548	0.290	-1.062	0.087	-1.443	0.001	-0.489
0.825	-0.170	0.537	-0.591	0.266	-1.102	0.073	-1.476	0.000	0.131

Table 5.8 – Pressure coefficients in the upper part of the NACA 2415 airfoil



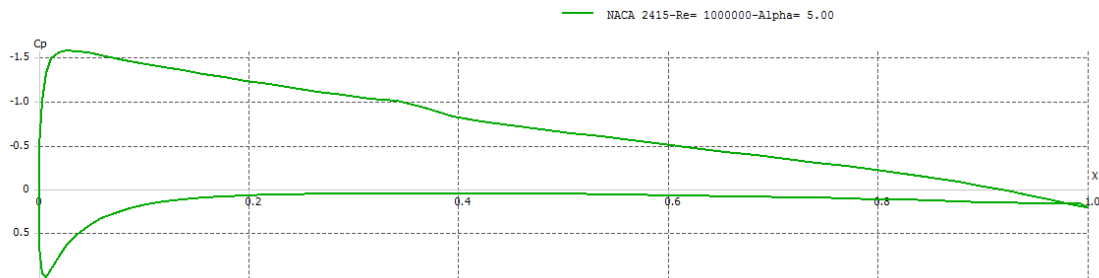
Lower Part

x/c	cp	x/c	cp	x/c	cp	x/c	cp	x/c	cp
0.000	0.131	0.073	0.269	0.266	0.056	0.537	0.058	0.825	0.121
0.001	0.659	0.087	0.218	0.290	0.054	0.566	0.063	0.851	0.130
0.003	0.947	0.103	0.176	0.316	0.053	0.595	0.068	0.877	0.140
0.007	0.994	0.120	0.144	0.341	0.053	0.625	0.073	0.901	0.148
0.012	0.904	0.138	0.118	0.368	0.052	0.654	0.079	0.923	0.155
0.019	0.768	0.157	0.099	0.395	0.051	0.684	0.084	0.945	0.159
0.027	0.632	0.177	0.084	0.422	0.048	0.713	0.090	0.964	0.162
0.036	0.513	0.198	0.072	0.451	0.049	0.742	0.097	0.980	0.164
0.047	0.414	0.220	0.064	0.479	0.051	0.770	0.104	0.993	0.165
0.059	0.334	0.242	0.059	0.508	0.054	0.798	0.112	1.000	0.208

Table 5.9 – Pressure coefficients in the lower part of the NACA 2415 airfoil

Note that positive values of  $c_p$  indicate positive pressure in the airfoil while negative  $c_p$  indicates “suction” pressure in the airfoil.

Graphical view of these tables is shown in figure below:

Figure 5.8 – Pressure distribution along the NACA 2415 airfoil ( $\alpha = 5$  deg;  $Re = 1000000$ )

As mentioned before, the distribution of the pressure distribution is calibrated in order to obtain the desired factors used to perform the distribution of loads across the chord of the airfoil.

The next table shows the factors obtained from the calibration of the values of the pressure coefficients:

Upper Part (Calibrated)

x/c	cp	x/c	cp	x/c	cp	x/c	cp	x/c	cp
1.000	0.133	0.798	-0.137	0.508	-0.404	0.242	-0.729	0.059	-0.962
0.993	0.123	0.770	-0.164	0.479	-0.432	0.220	-0.755	0.047	-0.981
0.980	0.102	0.742	-0.191	0.451	-0.459	0.198	-0.781	0.036	-0.995
0.964	0.075	0.713	-0.217	0.422	-0.487	0.177	-0.805	0.027	-1.000
0.945	0.045	0.684	-0.244	0.395	-0.523	0.157	-0.830	0.019	-0.988
0.923	0.013	0.654	-0.270	0.368	-0.585	0.138	-0.853	0.012	-0.943
0.901	-0.019	0.625	-0.296	0.341	-0.633	0.120	-0.876	0.007	-0.837
0.877	-0.050	0.595	-0.323	0.316	-0.654	0.103	-0.899	0.003	-0.637
0.851	-0.080	0.566	-0.350	0.290	-0.678	0.087	-0.921	0.001	-0.312
0.825	-0.109	0.537	-0.377	0.266	-0.703	0.073	-0.942	0.000	0.083

Table 5.10 – Factors (Calibrated pressure coefficients) used in the upper part of the NACA 2415 airfoil

Lower Part (Calibrated)

x/c	cp	x/c	cp	x/c	cp	x/c	cp	x/c	cp
0.000	0.083	0.073	0.172	0.266	0.035	0.537	0.037	0.825	0.077
0.001	0.420	0.087	0.139	0.290	0.034	0.566	0.040	0.851	0.083
0.003	0.604	0.103	0.113	0.316	0.034	0.595	0.043	0.877	0.089
0.007	0.634	0.120	0.092	0.341	0.034	0.625	0.047	0.901	0.095
0.012	0.577	0.138	0.076	0.368	0.033	0.654	0.050	0.923	0.099
0.019	0.490	0.157	0.063	0.395	0.032	0.684	0.054	0.945	0.102
0.027	0.403	0.177	0.053	0.422	0.031	0.713	0.058	0.964	0.104
0.036	0.328	0.198	0.046	0.451	0.031	0.742	0.062	0.980	0.105
0.047	0.264	0.220	0.041	0.479	0.033	0.770	0.066	0.993	0.106
0.059	0.213	0.242	0.038	0.508	0.035	0.798	0.071	1.000	0.133

Table 5.11 – Factors (Calibrated pressure coefficients) used in the lower part of the NACA 2415 airfoil

As it is shown, the maximum value obtained from the pressure coefficients is  $-1.567$  obtained at  $x/c=0.027$  in the upper part of the airfoil. This value is converted to  $-1$  in order to obtain the corresponding values for the load distribution across the chord.

Then, in order to calculate the loads that are acting in each of the sections of the wing the same procedure than in the previous load case is followed. In this case, the elliptical distribution of loads across the span and the complicated distribution of loads across the chord make the problem more difficult.

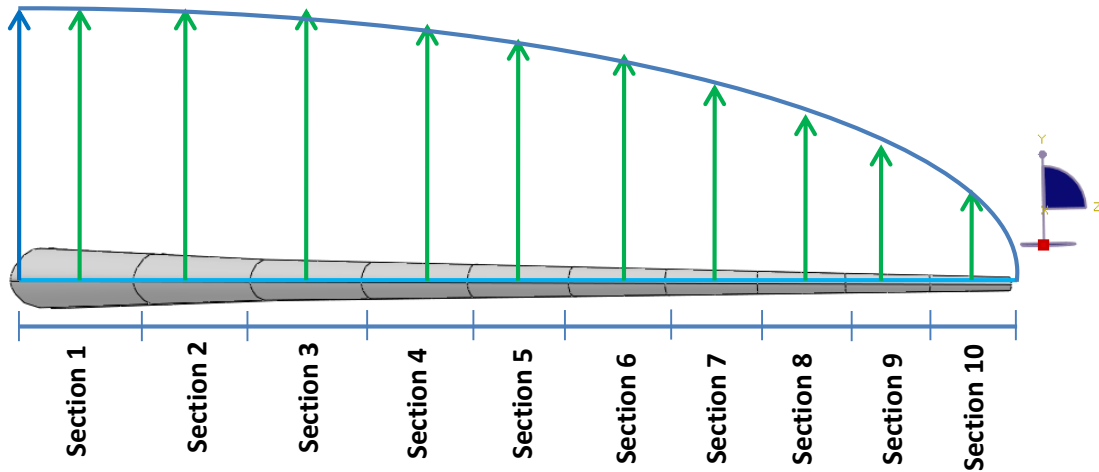


Figure 5.9 – Elliptical load distribution across the span of the wing.

As in the previous section, the maximum applied force  $F_{max}$  is:

$$F_{max_i} = \frac{Q_{max}}{\sum Factor_i} \quad (27)$$

where  $Q_{max} = 265\text{MN}$  and the  $Factor_i$  is the factor that must be multiplied to  $F_{max_i}$  in order to obtain the maximum force applied in each section  $i$ :

$$F_{section_i} = Factor_i \cdot F_{max} \quad (28)$$

In this case, the load distribution is elliptical, so in order to obtain the value of the factor in the middle of the sections defined in Figure 5.2, the formula of the ellipse must be applied:

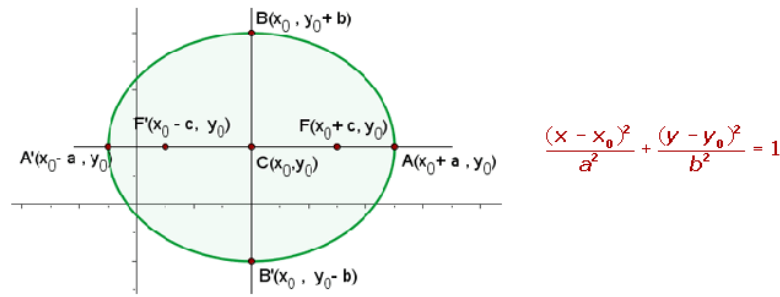


Figure 5.10 – Ellipse characteristics

Then, being  $x$  the  $z$ -coordinate of the wing that define the middle point of each section, and  $y$  the unknown factor, the value of the factor for each of the sections is obtained, showing them in table below:

Section $i$	1	2	3	4	5	6	7	8	9	10
Factor on Section $i$	0.999	0.989	0.968	0.937	0.893	0.835	0.760	0.661	0.527	0.312

Table 5.12 – Factor for distribution of loads across the wing span

Thus, the calculation of  $F_{max_i}$  is performed as follows:

$$F_{max} = \frac{Q_{max}}{\sum Factor_i} = \frac{2650000}{7.88} = 336251N \quad (29)$$

Thus,  $F_{section}$  can be calculated for each section  $i$ , obtaining the following results:

Section $i$	1	2	3	4	5	6	7	8	9	10
Force in section $i$ (N)	335829.9	332446.2	325573.2171	314982.6	300281.3	280824.6	255528.3	222408.8	177131.0	104994.2

Table 5.13 – Total force in the sections of the wing span.

Therefore, the maximum force in each section is defined as:

$$F_{max_j} = \frac{F_{section_i}}{\sum Factor_j} \quad (30)$$

where  $Factor_j$  of each section is calculated by using the mean value of the factors (calibrated  $c_p$ ) corresponding to each panel of the section. As said before, all the sections have the same airfoil shape so the value of the  $Factor_j$  has the same for all the sections.

Results for  $Factor_j$  are shown in table below:

#### Upper Panels

Panel j	1	2	3	4	5
Factor in panel j (N)	0.802	0.639	0.391	0.203	-0.023

#### Lower Panels

Panel j	1	2	3	4	5
Factor in panel j (N)	0.307	0.043	0.035	0.054	0.097

Table 5.14 – Factors for distribution of loads across the chord (upper and lower skin)

Thus, the corresponding  $F_{max_j}$  is equal to:

Section i	1	2	3	4	5
Maximum Force (N)	131799.39	130471.40	127774.03	123617.66	117848.02
Section i	6	7	8	9	10
Maximum Force (N)	110212.04	100284.30	87286.28	69516.59	41205.89

Table 5.15 – Maximum force in the wing span

Therefore, applying the following formula, the force in each panel of the upper and the lower skin can be obtained.

$$F_{panel_{ij}} = Factor_j \cdot F_{max_j} \quad (31)$$

Results are collected in tables below:

#### UPPER SKIN

Section 1	Force (N)	Section 2	Force (N)	Section 3	Force (N)	Section 4	Force (N)	Section 5	Force (N)
Panel 1	105667.121	Panel 6	104602.438	Panel 11	102439.880	Panel 16	99107.606	Panel 21	94481.933
Panel 2	84157.326	Panel 7	83309.371	Panel 12	81587.028	Panel 17	78933.078	Panel 22	75249.015
Panel 3	51549.948	Panel 8	51030.540	Panel 13	49975.532	Panel 18	48349.874	Panel 23	46093.229
Panel 4	26808.228	Panel 9	26538.113	Panel 14	25989.462	Panel 19	25144.049	Panel 24	23970.495
Panel 5	-3079.491	Panel 10	-3048.462	Panel 15	-2985.438	Panel 20	-2888.325	Panel 25	-2753.517

Section 6	Force (N)	Section 7	Force (N)	Section 8	Force (N)	Section 9	Force (N)	Section 10	Force (N)
Panel 26	88359.963	Panel 31	80400.623	Panel 36	69979.760	Panel 41	55733.320	Panel 46	33035.869
Panel 27	70373.245	Panel 32	64034.123	Panel 37	55734.550	Panel 42	44388.142	Panel 47	26311.026
Panel 28	43106.612	Panel 33	39223.629	Panel 38	34139.787	Panel 43	27189.629	Panel 48	16116.625
Panel 29	22417.324	Panel 34	20398.003	Panel 39	17754.183	Panel 44	14139.796	Panel 49	8381.350
Panel 30	-2575.103	Panel 35	-2343.141	Panel 40	-2039.443	Panel 45	-1624.254	Panel 50	-962.775

Table 5.16 – Force on the upper panels of the wing

Note that at the trailing edge panels on the upper skin, there is a negative force that indicates that there is a pressure force in the rear part of the upper skin instead of suction force, in accordance with pressure distribution presented in Figure 5.8.

## LOWER SKIN

Section 1	Force (N)	Section 2	Force (N)	Section 3	Force (N)	Section 4	Force (N)	Section 5	Force (N)
Panel 1	40485.792	Panel 6	40077.864	Panel 11	39249.292	Panel 16	37972.549	Panel 21	36200.247
Panel 2	5704.783	Panel 7	5647.303	Panel 12	5530.550	Panel 17	5350.647	Panel 22	5100.915
Panel 3	4651.905	Panel 8	4605.033	Panel 13	4509.828	Panel 18	4363.128	Panel 23	4159.486
Panel 4	7154.058	Panel 9	7081.975	Panel 14	6935.562	Panel 19	6709.955	Panel 24	6396.779
Panel 5	12730.279	Panel 10	12602.011	Panel 15	12341.476	Panel 20	11940.019	Panel 25	11382.740

Section 6	Force (N)	Section 7	Force (N)	Section 8	Force (N)	Section 9	Force (N)	Section 10	Force (N)
Panel 26	33854.647	Panel 31	30805.069	Panel 36	26812.371	Panel 41	21353.923	Panel 46	12657.516
Panel 27	4770.400	Panel 32	4340.689	Panel 37	3778.085	Panel 42	3008.945	Panel 47	1783.549
Panel 28	3889.972	Panel 33	3539.569	Panel 38	3080.799	Panel 43	2453.612	Panel 48	1454.376
Panel 29	5982.299	Panel 34	5443.422	Panel 39	4737.891	Panel 44	3773.354	Panel 49	2236.652
Panel 30	10645.194	Panel 35	9686.290	Panel 40	8430.833	Panel 45	6714.489	Panel 50	3980.006

Table 5.17 – Force in the lower panel of the wing

Finally, in order to calculate the pressure in each panel that must be introduced in ABAQUS program, the angle with respect to the resultant force must be calculated as well as the area of each of the panel, as shown in formula below:

$$P_{panel_{ij}} = \frac{F_{panel_{ij}}}{Area_{ij} \cdot \cos \alpha} \quad (32)$$

For the calculation of the pressure, the resultant force of the panels in the upper and lower skin (purple arrows in Figure 5.11) that is perpendicular to the panel surface must be calculated, so the angle between these two forces must be known.

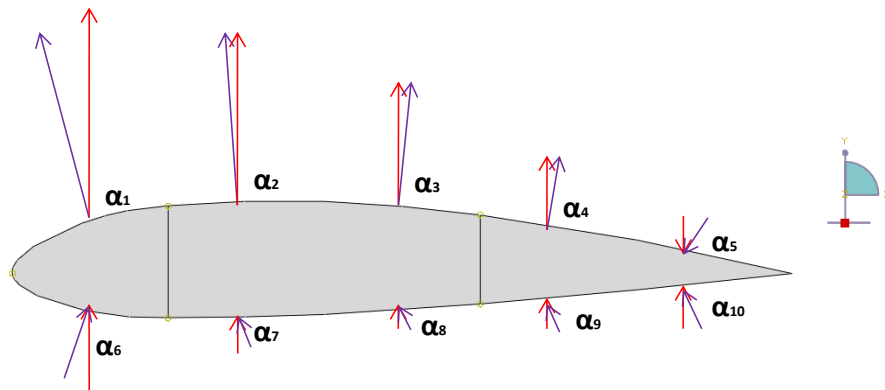


Figure 5.11 – Angle of the vertical component versus the resultant of the forces in the second model

Results for the upper part are shown in table below, for the upper and the lower panels of each of the sections:

UPPER SKIN	$\alpha_1$	$\alpha_2$	$\alpha_3$	$\alpha_4$	$\alpha_5$
Degrees	23.509	1.575	-5.001	-8.645	-12.595
LOWER SKIN	$\alpha_1$	$\alpha_2$	$\alpha_3$	$\alpha_4$	$\alpha_5$
Degrees	-15.802	1.176	3.863	5.315	6.003

Table 5.18 – Value of the angles formed by the resultant and the vertical component

# Chapter 6

## Studied cases

The aim of the project is to perform a structural analysis of the A330-300 wing. In order to do this, the simplified wing models shown in Chapter 3 are analyzed by using ABAQUS software. These two models are analyzed as follows:

- The first model consists on a simple tapered wing shown in section 3.1. This wing is made of aluminum (See Chapter 4) and it supports a triangular load distributed along the span and across the chord of the wing, as explained in section 5.1. Analysis is presented in section 6.1.
- The second model is formed by two tapered sections shown in section 3.2. This wing model is analyzed in three different ways:
  - o Second wing model made of aluminum under triangular load distribution (see section 5.1). Analysis is presented in section 6.2
  - o Second wing model made of aluminum under real load distribution (see section 5.2). Analysis is presented in section 6.3
  - o Second wing model made of carbon fiber under real load distribution (see section 5.2). Further improvement of the model has been performed by introducing holes in the ribs and stringers in the upper and lower skins. Analysis is presented in section 6.4

Therefore, as shown in Chapter 3, the creation of each of the designs proposed are performed by using the finite element program ABAQUS, which also is used to perform the complete analysis in order to obtain the final results of each of the different cases presented. Results obtained are studied in order to perform an optimization process to obtain the minimum weight possible by taking into account the maximum deformations and the maximum stresses that the structure can withstand.

### 6.1. Case 1

The first case analyzed has the tapered wing model shown in section 3.1 made of aluminum and with the triangular load distribution shown in section 5.1.

In order to introduce the triangular loads in the model, an equivalent pressure is introduced in each of the panels, whose area is presented in the following table in accordance with the numbering introduced in Figure 3.8.

	Area (m <sup>2</sup> )		Area (m <sup>2</sup> )		Area (m <sup>2</sup> )		Area (m <sup>2</sup> )		Area (m <sup>2</sup> )
Panel 1	6.77	Panel 2	5.74	Panel 3	5.74	Panel 4	5.83	Panel 5	5.84
Panel 6	6.26	Panel 7	5.3	Panel 8	5.32	Panel 9	5.39	Panel 10	5.4
Panel 11	5.75	Panel 12	4.87	Panel 13	4.88	Panel 14	4.95	Panel 15	4.96
Panel 16	5.24	Panel 17	4.44	Panel 18	4.45	Panel 19	4.51	Panel 20	4.52
Panel 21	4.72	Panel 22	4.01	Panel 23	4.01	Panel 24	4.07	Panel 25	4.08
Panel 26	4.21	Panel 27	3.57	Panel 28	3.58	Panel 29	3.63	Panel 30	3.64
Panel 31	3.70	Panel 32	3.14	Panel 33	3.15	Panel 34	3.19	Panel 35	3.20
Panel 36	3.19	Panel 37	2.71	Panel 38	2.71	Panel 39	2.75	Panel 40	2.75
Panel 41	2.68	Panel 42	2.27	Panel 43	2.28	Panel 44	2.31	Panel 45	2.31
Panel 46	2.14	Panel 47	1.84	Panel 48	1.84	Panel 49	1.87	Panel 50	1.87

Table 6.1 – Area of the upper panels of the simple tapered wing model

By taking into account the corresponding areas and the angles presented in Table 5.7, the values of Table 5.6 are introduced in the following formula:

$$P_{panel_{ij}} = \frac{F_{panel_{ij}}}{Area_{ij} \cdot \cos \alpha} \quad (33)$$

Thus, the pressures to be introduced in the model are the following:

Section 1	Pressure (Pa)	Section 2	Pressure (Pa)	Section 3	Pressure (Pa)	Section 4	Pressure (Pa)	Section 5	Pressure (Pa)
Panel 1	29214.807	Panel 6	28267.193	Panel 11	27153.856	Panel 16	25823.801	Panel 21	24259.737
Panel 2	24581.751	Panel 7	23821.422	Panel 12	22874.780	Panel 17	21744.780	Panel 22	20371.430
Panel 3	17618.142	Panel 8	17009.855	Panel 13	16361.939	Panel 18	15550.583	Panel 23	14600.600
Panel 4	10466.046	Panel 9	10128.095	Panel 14	9730.915	Panel 19	9256.236	Panel 24	8679.470
Panel 5	3512.588	Panel 10	3398.691	Panel 15	3264.871	Panel 20	3104.999	Panel 25	2910.827

Section 6	Pressure (Pa)	Section 7	Pressure (Pa)	Section 8	Pressure (Pa)	Section 9	Pressure (Pa)	Section 10	Pressure (Pa)
Panel 26	22253.543	Panel 31	19692.661	Panel 36	16316.164	Panel 41	11651.841	Panel 46	4864.294
Panel 27	18721.683	Panel 32	16556.291	Panel 37	13701.601	Panel 42	9814.994	Panel 47	4036.053
Panel 28	13380.640	Panel 33	11829.076	Panel 38	9820.150	Panel 43	7004.059	Panel 48	2892.726
Panel 29	7962.219	Panel 34	7046.524	Panel 39	5838.961	Panel 44	4170.392	Panel 49	1717.321
Panel 30	2669.489	Panel 35	2361.590	Panel 40	1963.018	Panel 45	1402.057	Panel 50	577.351

Table 6.2 – Pressure applied in the upper panels of the simple tapered wing model

The graphical view of the model used as an input for the processing in ABAQUS is shown in figure below. Note that the root of the wing is constrained in order to simulate the attachment to the aircraft fuselage.

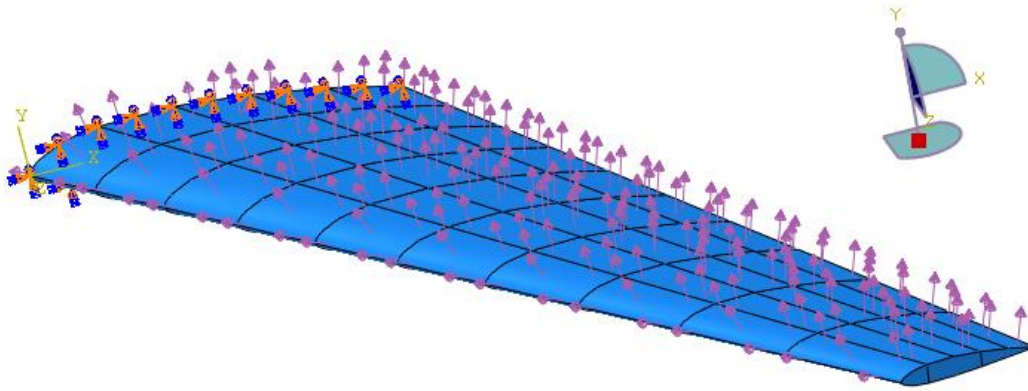


Figure 6.1 – Tapered wing with triangular distribution of loads.

Therefore, once all the pre-processing has been performed in ABAQUS, processing of all the data is performed and the results are obtained. Results obtained in ABAQUS must fulfill the requirements imposed by the model, as shown in Chapter 4 (maximum deformation and maximum VM for aluminum)

First analysis is performed with a minimum established thickness of 2 mm in order to avoid buckling problems due to low thickness. Then, the results obtained by using 2mm of thickness in all the sections of the wing are the following:

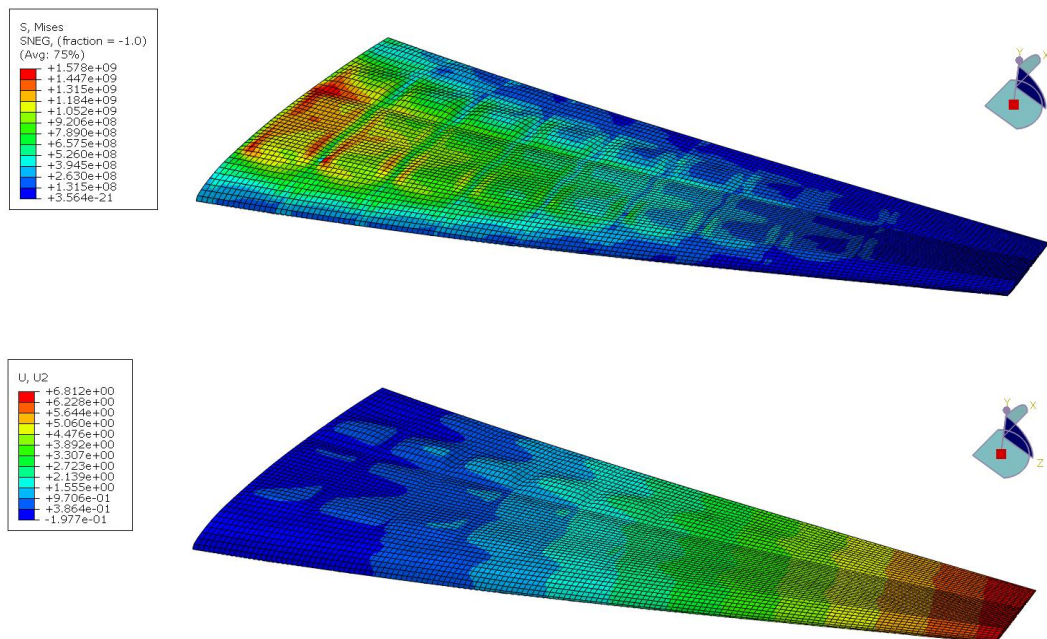


Figure 6.2 – VM in Pascal (upper) and vertical displacements in meters (lower) with thickness of 2 mm. Model 1

Regarding to the maximum allowable stress (490 MPa), one can see that due to the low thickness, most of the wing skin is subjected to stresses ( $1578\text{MPa} > 490\text{MPa}$ ) much higher than the mentioned design restriction value explained in Chapter 4. Regarding to the maximum vertical displacement ( $6.812 > 2.7\text{m}$ ), one can see that the maximum value allowed is reached in the middle of the wing span, so failure of the model is considered. Although the



mass of the wing is only 2841.38 Kg, the high stresses and vertical displacements on the wing make this wing model invalid.

In order to solve the problem due to the low thickness (2mm) in the model, a thickness of 15 mm is assigned to the entire models, obtaining the following results:

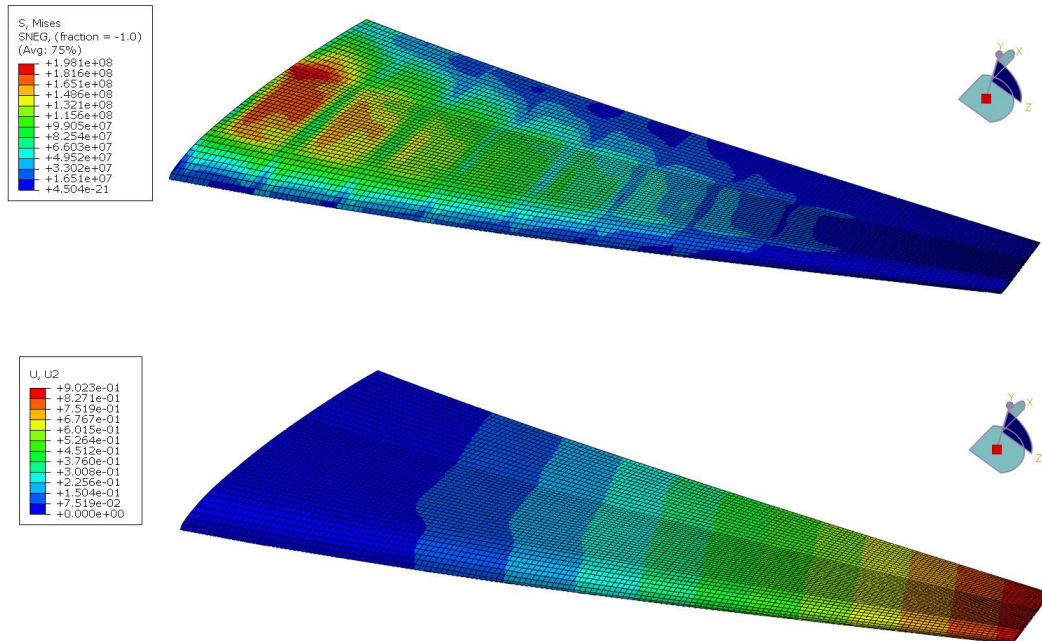


Figure 6.3 – VM in Pascal (upper) and vertical displacements in meters (lower) with thickness of 15 mm. Model 1

As it is shown in figure above, the results obtained for the Von Mises ( $198.1\text{MPa} < 490\text{MPa}$ ) and the maximum displacements ( $0.9023\text{m} < 2.7\text{m}$ ) are much lower than the design restrictions imposed in Chapter 4. This model is considered valid as the design restrictions are fulfilled, but the mass of the wing is 20310.92 Kg, a very high value so an optimization process must be performed in order to decrease the weight and improve the results with the design with the design restrictions fulfilled.

In order to improve the design characteristics, a sensitivity analysis must be performed in the wing, studying the influence of the thickness modifications in the spars, ribs and skin of the wing. By modifying the thickness of each of the wing components while the remaining parts have a thickness of 2 mm, the following results have been obtained:

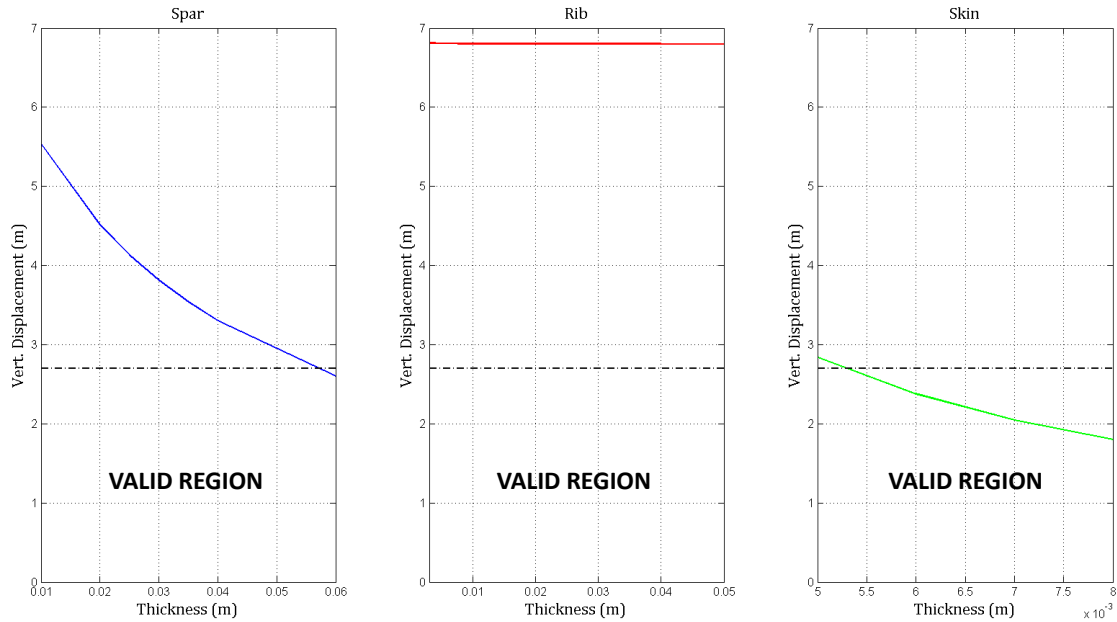


Figure 6.4 – Influence of thickness in the vertical displacement in each part with the remaining at 2mm of thickness.

According to graph above, the vertical displacement is highly affected by the thickness of the spars and the skin, while the thickness of the ribs does not affect the vertical displacement. It is important to know that although the restriction of the vertical displacement is fulfilled rapidly when increasing the thickness of the skin, the slope of the spar is higher, meaning that they fulfill an important role to maintain the vertical displacement as low as possible.

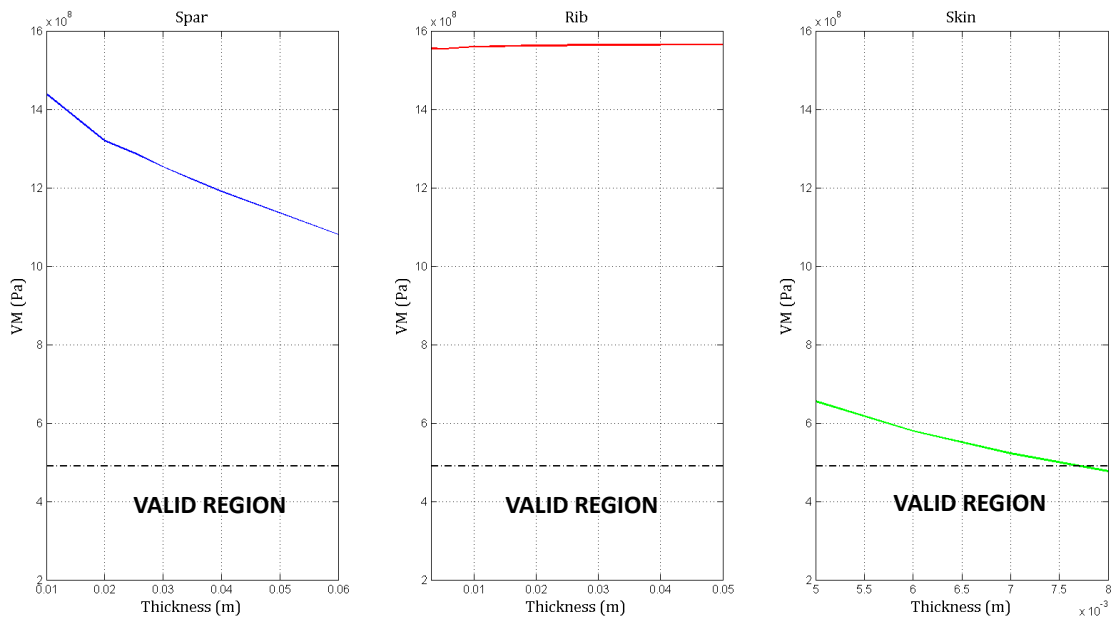


Figure 6.5 – Influence of thickness in the Von Mises Stress in each part with the remaining at 2mm of thickness.

According to the Von Mises stress, one can easily see that the main important part is the skin, which is directly affected by the loads applied in the model. Also, the influence of the spar is important while the ribs are not important in carrying the loads applied.

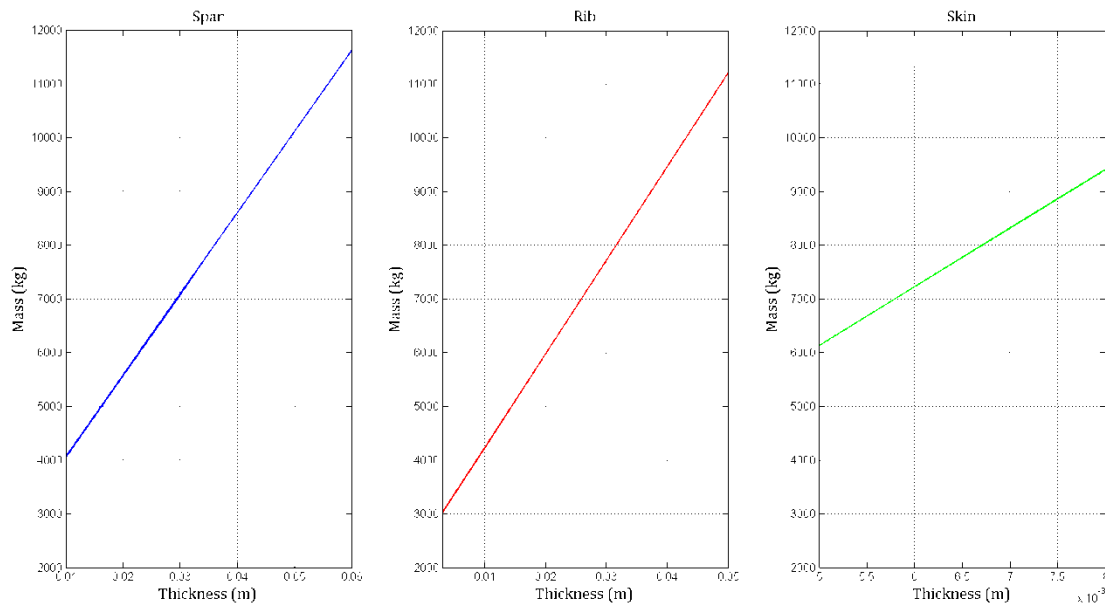


Figure 6.6 – Influence of thickness in the mass in each part with the remaining at 2mm of thickness.

The last graph refers to the variation of mass with respect to the thickness. In general, improvement of the skin is better in terms of mass with respect to the rib and spar thickness modifications.

Also, apart from the sensitivity analysis, it is important to interpret the visual results obtained from ABAQUS, so the optimization process can be performed more efficiently as one can see the zones in where the stresses are higher. As shown in Figure 6.2 and Figure 6.3, higher stresses occur near the root, where the clamped root of the wing is situated as well as the higher loads. These loads decrease from the root to the tip, so the thickness of the skin can vary as well in order to perform the optimization process, taking also into account the importance of the spars to perform the best optimization, as the more thickness the spars have, the less stresses the skin withstands.

Thus, the optimized wing is presented in figure below, as well as the thickness used in each of the part.

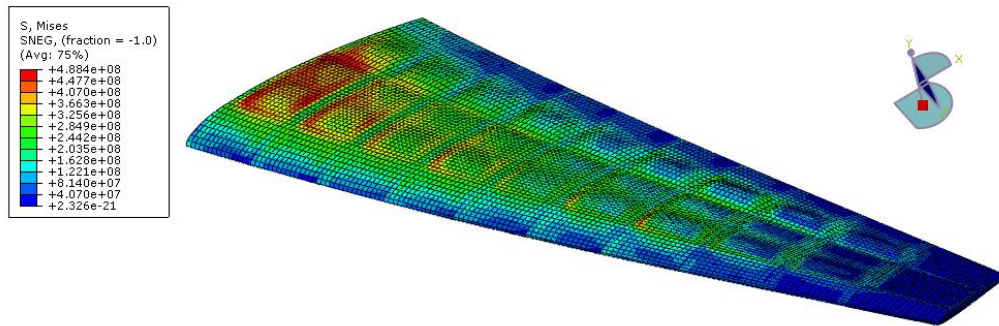


Figure 6.7 – Von Mises in Pascal of the optimized aircraft wing. Case 1

As shown, higher loads appear near the root, where the region is subjected to higher compressive loads. Also, stress concentration appears in points between the front spar and the ribs.

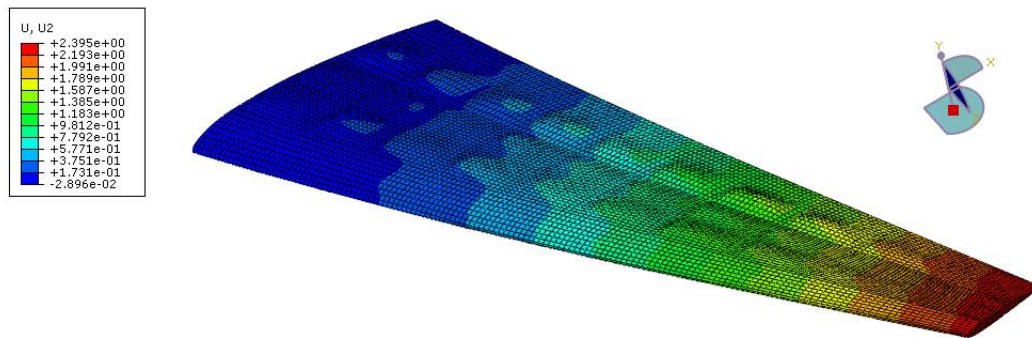


Figure 6.8 – Vertical displacement in meters of the optimized aircraft wing. Case 1

As it is expected, maximum displacement of the wing occurs in the point that is further than the root. The existence of small elevations principally in the rear panels of the wing are not a problem as the restriction of maximum vertical displacement is fulfilled.

The corresponding thickness assigned to each part of the wing to obtain these results is shown in tables below:

**Ribs**

Rib 0	Rib 1	Rib 2	Rib 3	Rib 4	Rib 5	Rib 6	Rib 7	Rib 8	Rib 9	Rib 10
0.002	0.002	0.002	0.002	0.002	0.002	0.002	0.002	0.002	0.002	0.002

**Spars**

Front Spar	Rear Spar
0.028	0.028

**Skin**

Section1	Section2	Section3	Section4	Section5	Section6	Section7	Section8	Section9	Section10
0.005	0.005	0.005	0.004	0.004	0.003	0.002	0.002	0.002	0.002

Table 6.3 – Thickness in mm of the ribs, spars and skin. Case 1

As the ribs do not influence the vertical displacement and the Von Mises stress, minimum thickness has been assigned to them. In the other hand, the thickness of the spars

has been increased to improve the characteristics related to vertical displacement and the thickness of the skin has been decreased from the root to the tip as lower loads are applied near the tip. Therefore, the following results have been obtained:

Von Mises (MPa)	488.4
Vertical Displacement (m)	2.395
Mass (Kg)	8749.52

Table 6.4 – Results of optimization process. Case 1

Results obtained in this first model can be used in order to validate the selected mesh. A mesh sensitivity analysis is performed to analyze the influence of the elements size in the results. The size of the elements near the root has been chosen to be modified as it is the critical region in terms of maximum stresses. The error is calculated with respect to the previous case analyzed in order to assure that the mesh used for the analysis (*Case (c)*) is correct.

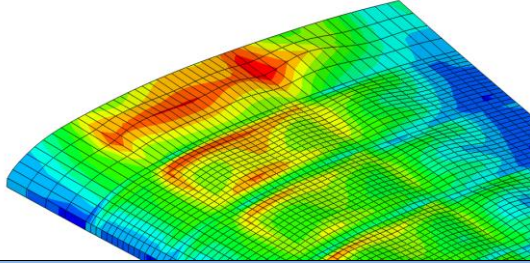
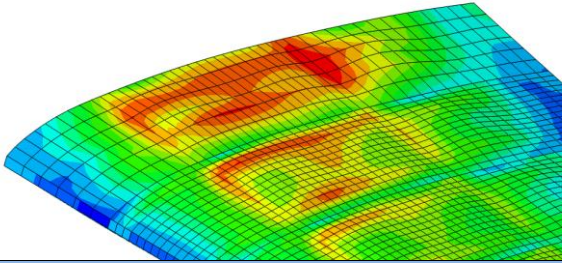
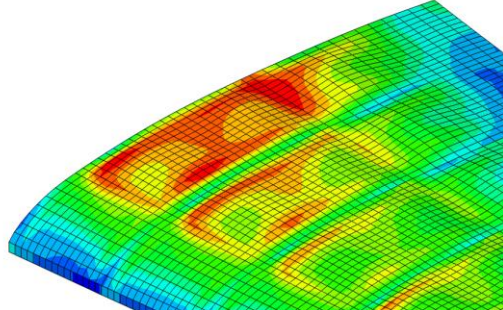
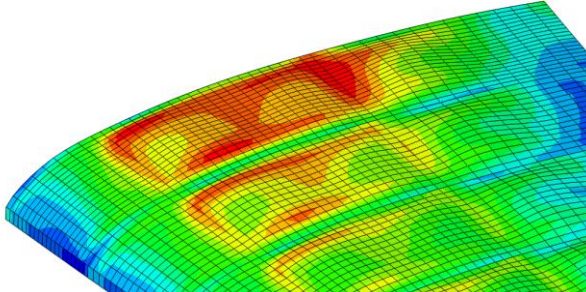
<b>Case (a)</b>		<b>Case (b)</b>	
Max VM (MPa) = 4.921	-	Max VM (MPa) = 4.870	$\Delta=1.03\%$
Max Displ. (m) = 2.394	-	Max Displ. (m) = 2.394	$\Delta=0\%$
Element size = 0.716364		Element size = 0.477576	
			
<b>Case (c)</b>		<b>Case (d)</b>	
Max VM (MPa) = 4.885	$\Delta=0.3\%$	Max VM (MPa) = 4.890	$\Delta=0.1\%$
Max Displ. (m) = 2.395	$\Delta= 0.04\%$	Max Displ. (m) = 2.395	$\Delta=0\%$
Element size = 0.19916		Element size = 0.143273	
			

Figure 6.9 – Mesh sensitivity analysis. Case 1

As shown, results obtained are similar in terms of stresses and displacements, with a low error comparing with the previous analyzed meshing. That means that the results obtained are almost independent of the size of the mesh elements presented above. Also, the computational cost is very low, as the difference in time of computing the results is very small. Therefore, the mesh (*Case (c)*) used for the analysis of the wing model is considered valid.



## 6.2. Case 2

The second case analyzed has the two tapered sections wing model shown in section 3.2 made of aluminum and with the triangular load distribution shown in section 5.1. In order to introduce the triangular loads in the model, an equivalent pressure is introduced in each of the panels, whose area is presented in the following table in accordance with the numbering introduced in Figure 3.14.

	Area (m <sup>2</sup> )		Area (m <sup>2</sup> )		Area (m <sup>2</sup> )		Area (m <sup>2</sup> )		Area (m <sup>2</sup> )
Panel 1	6.52	Panel 2	5.53	Panel 3	5.74	Panel 4	5.61	Panel 5	5.61
Panel 6	5.50	Panel 7	4.67	Panel 8	5.32	Panel 9	4.73	Panel 10	4.73
Panel 11	4.79	Panel 12	4.06	Panel 13	4.88	Panel 14	4.13	Panel 15	4.14
Panel 16	4.40	Panel 17	3.74	Panel 18	4.45	Panel 19	3.8	Panel 20	3.8
Panel 21	4.02	Panel 22	3.41	Panel 23	4.01	Panel 24	3.47	Panel 25	3.47
Panel 26	3.64	Panel 27	3.09	Panel 28	3.58	Panel 29	3.14	Panel 30	3.14
Panel 31	3.26	Panel 32	2.76	Panel 33	3.15	Panel 34	2.81	Panel 35	2.81
Panel 36	2.87	Panel 37	2.43	Panel 38	2.71	Panel 39	2.48	Panel 40	2.48
Panel 41	2.49	Panel 42	2.11	Panel 43	2.28	Panel 44	2.15	Panel 45	2.15
Panel 46	2.11	Panel 47	1.79	Panel 48	1.84	Panel 49	1.82	Panel 50	1.82

Table 6.5 – Area of the upper panels of the two tapered sections wing model

Note that the areas of the second model are smaller than the first model areas presented in Table 6.1, because the entire surface of the wing has been reduced with the introduction of the two tapered sections.

By taking into account the corresponding areas and the angles presented in Table 5.18, the values of Table 5.16 and Table 5.17 are introduced in the following formula:

$$P_{panel_{ij}} = \frac{F_{panel_{ij}}}{Area_{ij} \cdot \cos \alpha} \quad (34)$$

Thus, the pressures to be introduced in the model are the following:

Section 1	Pressure (Pa)	Section 2	Pressure (Pa)	Section 3	Pressure (Pa)	Section 4	Pressure (Pa)	Section 5	Pressure (Pa)
Panel 1	30333.289	Panel 6	32173.604	Panel 11	32594.309	Panel 16	30752.068	Panel 21	28482.632
Panel 2	25510.931	Panel 7	27028.994	Panel 12	27433.715	Panel 17	25810.299	Panel 22	23951.690
Panel 3	17614.378	Panel 8	17004.461	Panel 13	16358.301	Panel 18	15547.254	Panel 23	14597.346
Panel 4	10893.112	Panel 9	11559.766	Panel 14	11680.866	Panel 19	11002.495	Panel 24	10195.874
Panel 5	3656.257	Panel 10	3880.019	Panel 15	3911.196	Panel 20	3692.971	Panel 25	3422.230

Section 6	Pressure (Pa)	Section 7	Pressure (Pa)	Section 8	Pressure (Pa)	Section 9	Pressure (Pa)	Section 10	Pressure (Pa)
Panel 26	25736.803	Panel 31	22349.459	Panel 36	18134.333	Panel 41	12540.204	Panel 46	4933.226
Panel 27	21626.282	Panel 32	18832.499	Panel 37	15277.826	Panel 42	10557.493	Panel 47	4148.058
Panel 28	13377.812	Panel 33	11826.424	Panel 38	9818.074	Panel 43	7002.581	Panel 48	2892.063
Panel 29	9218.794	Panel 34	8011.725	Panel 39	6484.546	Panel 44	4487.591	Panel 49	1767.217
Panel 30	3094.275	Panel 35	2689.124	Panel 40	2176.529	Panel 45	1506.254	Panel 50	593.164

Table 6.6 – Pressure applied in the upper panels of the two tapered sections wing model

The graphical view of the model used as an input for the processing in ABAQUS is shown in figure below.

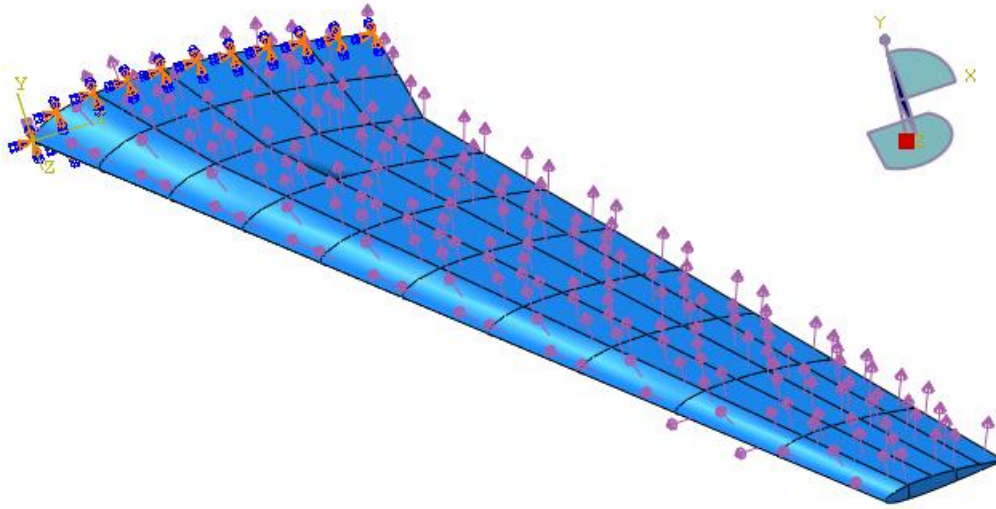


Figure 6.10 – Two tapered sections wing with triangular distribution of loads.

Therefore, once all the pre-processing has been performed in ABAQUS, processing of all the data is performed and the results are obtained. Results obtained in ABAQUS must fulfill the requirements imposed by the model, as shown in Chapter 4 (maximum deformation and maximum Von Mises stress for the aluminum material).

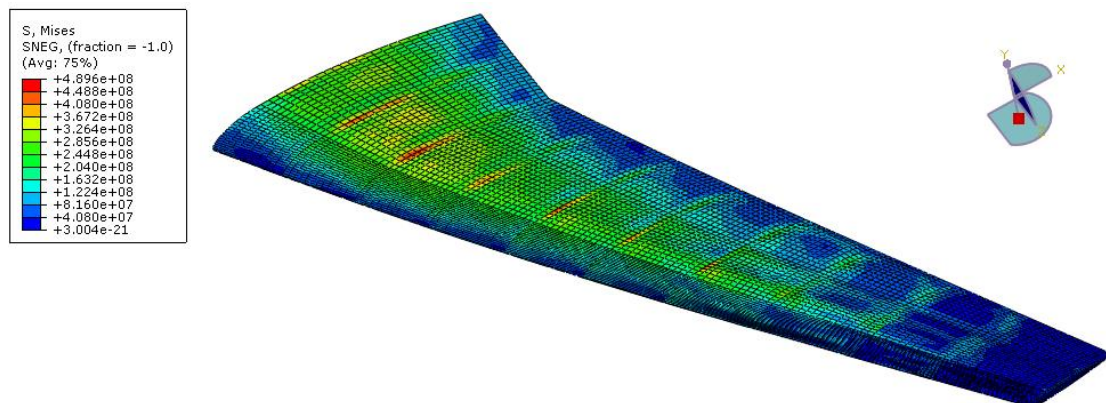


Figure 6.11 – Von Mises stress in Pascal of the optimized aircraft wing. Case 2

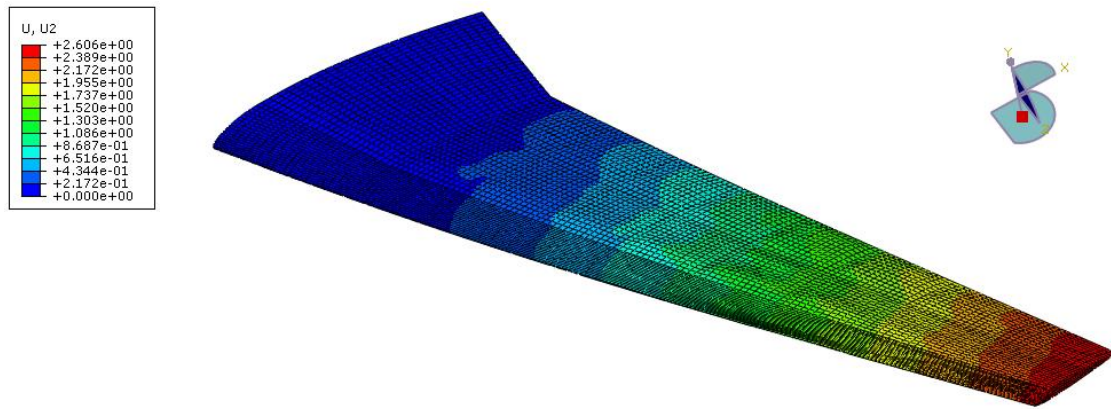


Figure 6.12 – Vertical displacement in meters of the optimized aircraft wing. Case 2

The corresponding thickness assigned to each part of the wing is shown in tables below:

**Ribs**

Rib 0	Rib 1	Rib 2	Rib 3	Rib 4	Rib 5	Rib 6	Rib 7	Rib 8	Rib 9	Rib 10
0.002	0.007	0.006	0.004	0.003	0.003	0.003	0.002	0.002	0.002	0.002

**Spars**

Front Spar	Rear Spar
0.045	0.045

**Skin**

Section1	Section2	Section3	Section4	Section5	Section6	Section7	Section8	Section9	Section10
0.006	0.006	0.006	0.004	0.003	0.002	0.002	0.002	0.002	0.002

Table 6.7 – Thickness in mm of the ribs, spars and skin. Case 2

In this case, the thickness of the ribs has been increased from the minimum allowed thickness in order to solve the stress concentration that is shown in Figure 6.11. The increase of thickness in the ribs has solved the problem without adding a lot of mass to the model, being a better option than directly increase the thickness of the panels in which the stress concentration is located.

Therefore, results for this second model are the following:

Von Mises (MPa)	489.6
Vertical Displacement (m)	2.606
Mass (Kg)	11015.10

Table 6.8 – Results of optimization process. Case 2

Note that results in this second model are more critical comparing with the previous model. That is because the applied pressures have been increased due to the decrease of panel areas, so the thickness used in each of the parts have been increased and due to this, the corresponding mass of the wing.



### 6.3. Case 3

The third case analyzed has the same model than the previous case, but in this case with the real load distribution shown in section 5.2. In order to introduce the real loads in the model, an equivalent pressure is introduced in each of the panels, taking into account the areas of the upper panel presented in Table 6.5, but also the areas of the lower panel introduced in the table below and whose panel numbering is shown in Figure 3.15.

	Area (m <sup>2</sup> )		Area (m <sup>2</sup> )		Area (m <sup>2</sup> )		Area (m <sup>2</sup> )		Area (m <sup>2</sup> )
Panel 1	6.08	Panel 2	5.51	Panel 3	5.52	Panel 4	5.53	Panel 5	5.53
Panel 6	5.13	Panel 7	4.65	Panel 8	4.65	Panel 9	4.67	Panel 10	4.67
Panel 11	4.07	Panel 12	4.05	Panel 13	4.06	Panel 14	4.07	Panel 15	4.07
Panel 16	4.11	Panel 17	3.73	Panel 18	3.74	Panel 19	3.75	Panel 20	3.75
Panel 21	3.75	Panel 22	3.4	Panel 23	3.41	Panel 24	3.42	Panel 25	3.42
Panel 26	3.40	Panel 27	3.08	Panel 28	3.08	Panel 29	3.09	Panel 30	3.1
Panel 31	3.04	Panel 32	2.75	Panel 33	2.76	Panel 34	2.77	Panel 35	2.77
Panel 36	2.68	Panel 37	2.43	Panel 38	2.44	Panel 39	2.44	Panel 40	2.44
Panel 41	2.32	Panel 42	2.11	Panel 43	2.11	Panel 44	2.12	Panel 45	2.12
Panel 46	1.97	Panel 47	1.78	Panel 48	1.79	Panel 49	1.79	Panel 50	1.79

Table 6.9 – Area of the lower panels of the two tapered sections wing model

In this case, the corresponding areas and the angles presented in Table 5.18, the values of Table 5.6 are introduced in the following formula:

$$P_{panel_{ij}} = \frac{F_{panel_{ij}}}{Area_{ij} \cdot \cos \alpha} \quad (35)$$

Thus, the pressures to be introduced in the model are the following:

#### UPPER SKIN

Section 1	Pressure (Pa)	Section 2	Pressure (Pa)	Section 3	Pressure (Pa)	Section 4	Pressure (Pa)	Section 5	Pressure (Pa)
Panel 1	17673.570	Panel 6	28267.193	Panel 11	27153.856	Panel 16	25823.801	Panel 21	24259.737
Panel 2	15224.035	Panel 7	23821.422	Panel 12	22874.780	Panel 17	21744.780	Panel 22	20371.430
Panel 3	9015.213	Panel 8	17009.855	Panel 13	16361.939	Panel 18	15550.583	Panel 23	14600.600
Panel 4	4838.821	Panel 9	10128.095	Panel 14	9730.915	Panel 19	9256.236	Panel 24	8679.470
Panel 5	-561.600	Panel 10	3398.691	Panel 15	3264.871	Panel 20	3104.999	Panel 25	2910.827

Section 6	Pressure (Pa)	Section 7	Pressure (Pa)	Section 8	Pressure (Pa)	Section 9	Pressure (Pa)	Section 10	Pressure (Pa)
Panel 26	26471.964	Panel 31	26895.141	Panel 36	26590.259	Panel 41	24408.865	Panel 46	17074.000
Panel 27	22783.062	Panel 32	23209.478	Panel 37	22944.638	Panel 42	21044.931	Panel 47	14704.414
Panel 28	12087.055	Panel 33	12499.621	Panel 38	12645.941	Panel 43	11970.935	Panel 48	8792.571
Panel 29	7229.170	Panel 34	7350.479	Panel 39	7249.087	Panel 44	6659.460	Panel 49	4663.123
Panel 30	-839.026	Panel 35	-853.106	Panel 40	-841.338	Panel 45	-772.905	Panel 50	-541.208

Table 6.10 – Pressure applied in the upper panels of the two tapered sections wing model

## LOWER SKIN

Section 1	Pressure (Pa)	Section 2	Pressure (Pa)	Section 3	Pressure (Pa)	Section 4	Pressure (Pa)	Section 5	Pressure (Pa)
Panel 1	6920.362	Panel 6	8119.270	Panel 11	10022.295	Panel 16	9601.911	Panel 21	10032.520
Panel 2	1035.569	Panel 7	1214.730	Panel 12	1365.856	Panel 17	1434.792	Panel 22	1500.585
Panel 3	844.655	Panel 8	992.585	Panel 13	1113.325	Panel 18	1169.268	Panel 23	1222.568
Panel 4	1298.894	Panel 9	1522.594	Panel 14	1710.936	Panel 19	1796.531	Panel 24	1877.940
Panel 5	2314.731	Panel 10	2713.380	Panel 15	3049.021	Panel 20	3201.558	Panel 25	3346.635

Section 6	Pressure (Pa)	Section 7	Pressure (Pa)	Section 8	Pressure (Pa)	Section 9	Pressure (Pa)	Section 10	Pressure (Pa)
Panel 26	10348.303	Panel 31	10531.212	Panel 36	10397.530	Panel 41	9565.760	Panel 46	6677.471
Panel 27	1549.157	Panel 32	1578.765	Panel 37	1555.095	Panel 42	1426.340	Panel 47	1002.205
Panel 28	1265.854	Panel 33	1285.373	Panel 38	1265.498	Panel 43	1165.497	Panel 48	814.351
Panel 29	1943.820	Panel 34	1973.053	Panel 39	1949.583	Panel 44	1787.056	Panel 49	1254.561
Panel 30	3452.864	Panel 35	3516.133	Panel 40	3474.308	Panel 45	3184.672	Panel 50	2235.725

Table 6.11 – Pressure applied in the lower panels of the two tapered sections wing model

The graphical view of the model used as an input for the processing in ABAQUS is shown in figure below. Note that the root of the wing is constrained in order to simulate the attachment to the aircraft fuselage and that the trailing edge panels of the upper skin are affected by a positive pressure, not by a “suction” pressure.

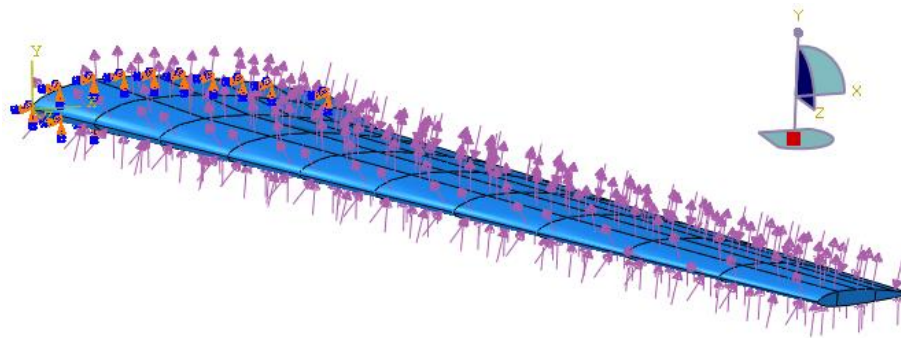


Figure 6.13 – Two tapered sections wing with real distribution of loads.

Therefore, once all the pre-processing has been performed in ABAQUS, processing of all the data is performed and the results are obtained. Results obtained in ABAQUS must fulfill the requirements imposed by the model, as shown in Chapter 4 (maximum deformation and maximum VM for the aluminum). Visual results obtained for the upper and lower skin of the wing model are presented in figures below.

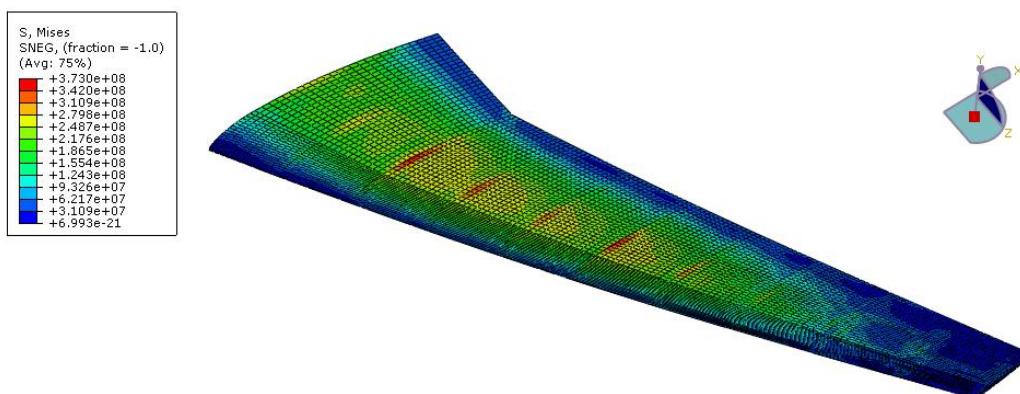


Figure 6.14 – Von Mises in Pascal in the upper panel of the optimized aircraft wing. Case 3

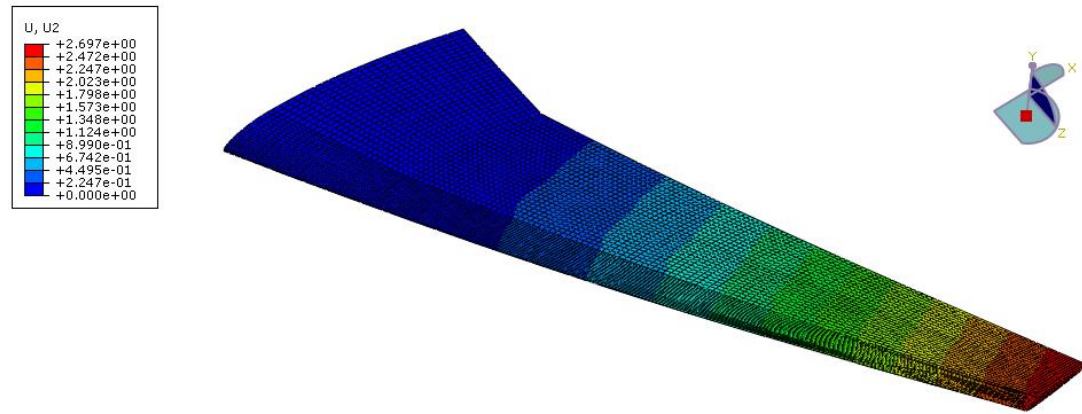


Figure 6.15 – Vertical displacement in meters in the upper panel of the optimized aircraft wing. Case 3

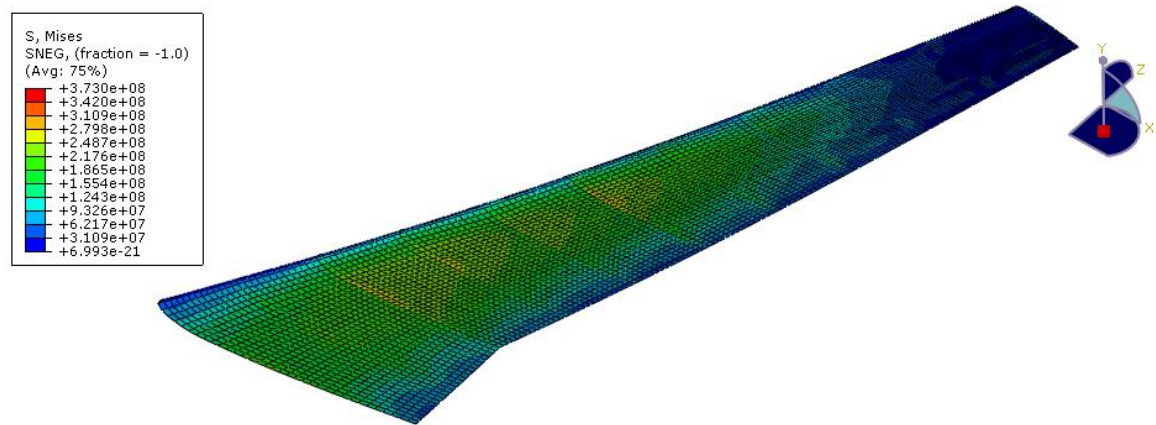


Figure 6.16 – Von Mises stress in Pascal in the lower panel of the optimized aircraft wing. Case 3

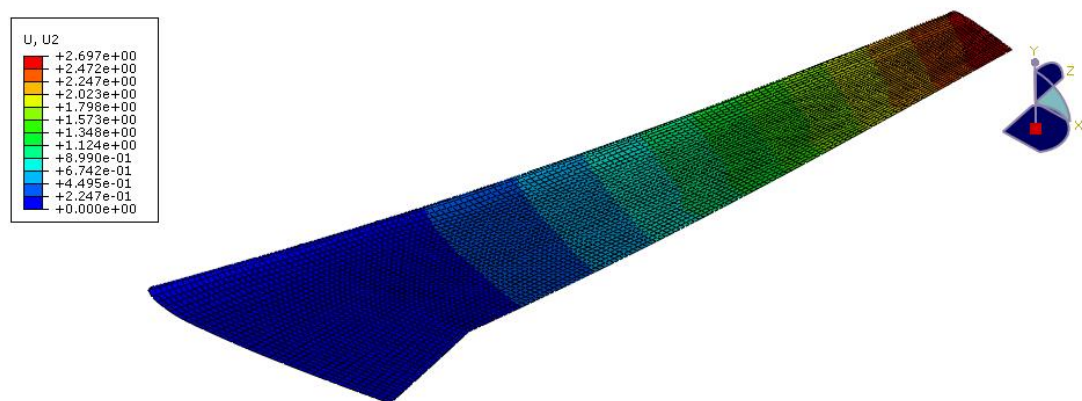


Figure 6.17 – Vertical displacement in meters in the lower of the optimized aircraft wing. Case 3

The corresponding thickness assigned to each part of the wing is shown in tables below:

#### Ribs

Rib 0	Rib 1	Rib 2	Rib 3	Rib 4	Rib 5	Rib 6	Rib 7	Rib 8	Rib 9	Rib 10
0.002	0.002	0.002	0.002	0.002	0.002	0.002	0.002	0.002	0.002	0.002

#### Spars

Front Spar	Rear Spar
0.021	0.021

#### Skin

Section1	Section2	Section3	Section4	Section5	Section6	Section7	Section8	Section9	Section10
0.015	0.014	0.013	0.012	0.010	0.007	0.006	0.005	0.005	0.004

Table 6.12 – Thickness in mm of the ribs, spars and skin. Case 2

In this case, due to the elliptical distribution of loads across the span of the wing, the loads applied to the parts that are further than the root are higher, so the thickness of the skin has been increased more comparing with the previous models.

Therefore, results for this third model are the following:

Von Mises (MPa)	373.0
Vertical Displacement (m)	2.697
Mass (Kg)	13271.38

Table 6.13 – Results of optimization process. Case 2

In this model, the vertical displacement is more restrictive than the Von Mises stress as the higher loads applied near the root creates higher vertical displacement than in the previous models with triangular distribution. Due to this, the stress concentration that appears near the ribs are not so important comparing with the ones presented in section 6.2, so there is no need to increase the thickness of the ribs.

## 6.4. Case 4

The third case analyzed is repeated, but with different material. Aluminum is therefore substituted by Carbon Epoxy MTM45-1/IM7 material, whose principal characteristics are the high stiffness and the low weight. These characteristics make the carbon fiber a very attractive material within the aeronautic field.

An initial analysis is performed by using carbon fiber with the following ply sequence:  $[45/-45/0/90]_{ns}$ , where each ply has a thickness of 0.1mm and being 0 degrees the z-direction across the longitudinal span of the wing defined by a local reference system located at the front spar, as shown in Figure 6.18. The distribution of plies goes from the outer part (aerodynamic surface) to the inner part as the normal is defined inwards. The number  $n$  is the number of repetitions of the ply sequence and is defined in order to fulfill the Hashin Failure

Criteria, which has to be lower than one. The sub-index  $S$  indicates that the ply sequence is symmetric ( $[45/-45/0/90]_{nS} \rightarrow [45/-45/0/90/90/0/-45/45]_n$ ).

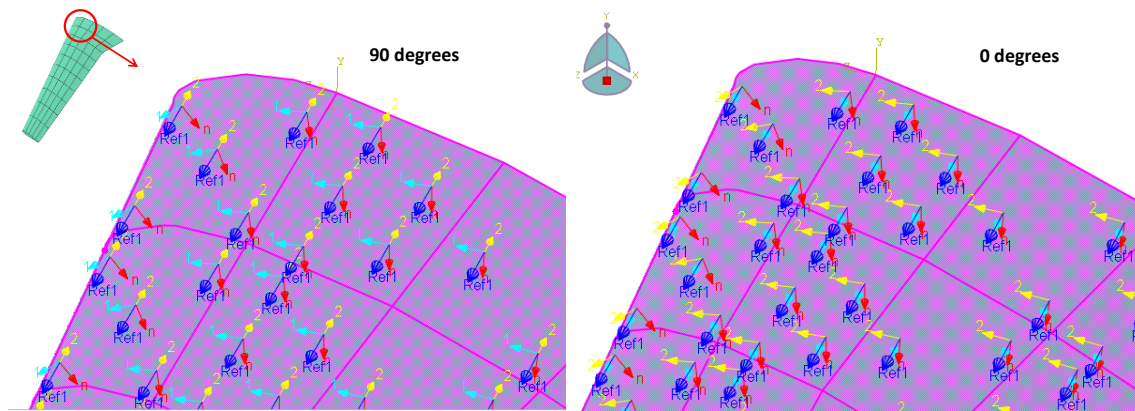


Figure 6.18 – Ply orientation (defined by light blue arrows) and normal direction (red arrows) in the wing model

As a first approximation in order to fulfill all the design restrictions, all the aircraft components use the same ply sequence with the same  $n$ , which in this case is 20. Thus, under  $[45/-45/0/90]_{20S}$ , the following results have been obtained for Hashin Failure Criteria presented in section 4.2 :

HSNFCCRT	HSNFTCRT	HSNMC CRT	HSNMTCRT	Mass (Kg)
0.1971	0.01111	0.17	0.3846	9643.59

Table 6.14 – HASHIN Failure Criteria for  $[45/-45/0/90]_{20S}$  in all the wing components.

As shown, the values obtained for Hashin Failure Criteria are much lower than one. This occurs because in this case, the critical constraint is the vertical displacement, which must have a value lower than 2.7m. The value obtained in this initial approach is 2.694 m, as shown in figure below.

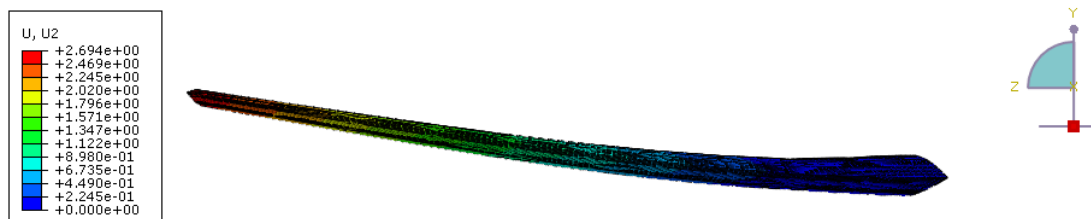


Figure 6.19 – Vertical displacement in meters for  $[45/-45/0/90]_{20S}$  in all the wing components.

Analyzing the results, the mass is lower than the model presented in section 6.3, meaning that the carbon fiber can be used instead of aluminum because of the significant weight reduction. The weight can also be reduced if an optimization process is performed. In order to perform the optimization process, the following characteristics has been taken into account.



- Minimum ply sequence of  $[45/-45/0/90]_{25}$  (1.6mm of thickness) is assigned to the ribs as it is demonstrated in section 6.1 that they do not affect significantly the results of the analysis.
- As shown in Table 6.14 critical case for Hashin Failure Criteria is the matrix tension case (HSNMTCRT), which occurs in the lower skin of the wing as can be seen in figure below.

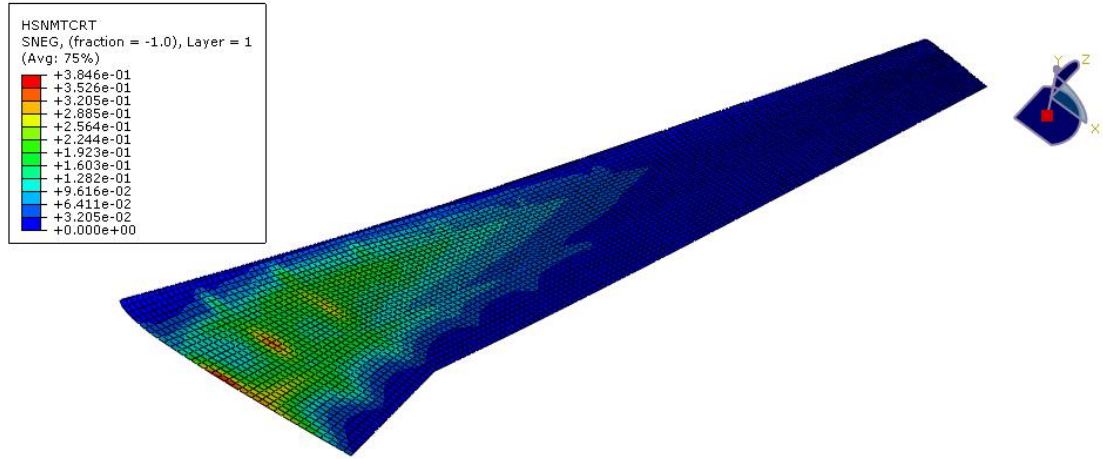


Figure 6.20 – HSNMTCRT in the lower skin of the wing under  $[45/-45/0/90]_{205}$  in all the wing components

Then, a sensitivity analysis is performed by adding repeated fiber in each of the directions to see the better ply orientation that improves the behavior of the skin in terms of matrix tension HSNMTCRT criteria, as well as the vertical displacement, which has been the critical aspect in the initial analysis.

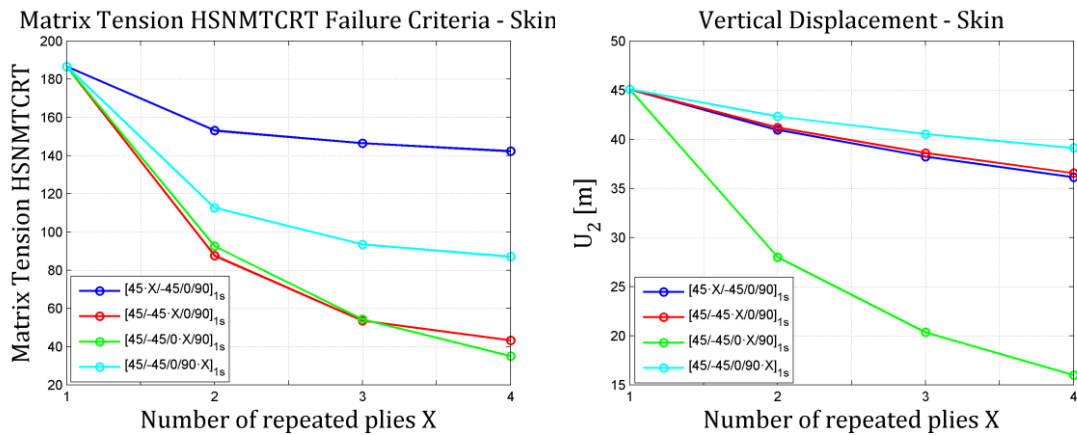


Figure 6.21 – Skin Sensitivity Analysis for HSNMTCRT failure criteria and vertical displacement.

As it is shown in the figure above, the best ply orientation for the critical Hashin Criteria in the skin is the one that adds four plies at 0 degrees in the ply sequence. This new ply sequence with four plies orientated in the longitudinal direction of the wing reduces a lot the vertical displacement of the wing, as it can be seen in the graph at the right hand side of the figure.

- In the case of the spars, same sensitivity analysis is performed in order to see what is the better ply orientation that improves the behavior of the spars in terms of matrix

tension criteria and vertical displacement. As before, for  $[45/-45/0/90]_{1s}$  in all the wing components, ply sequence of the spar is modified by including X plies of each ply:

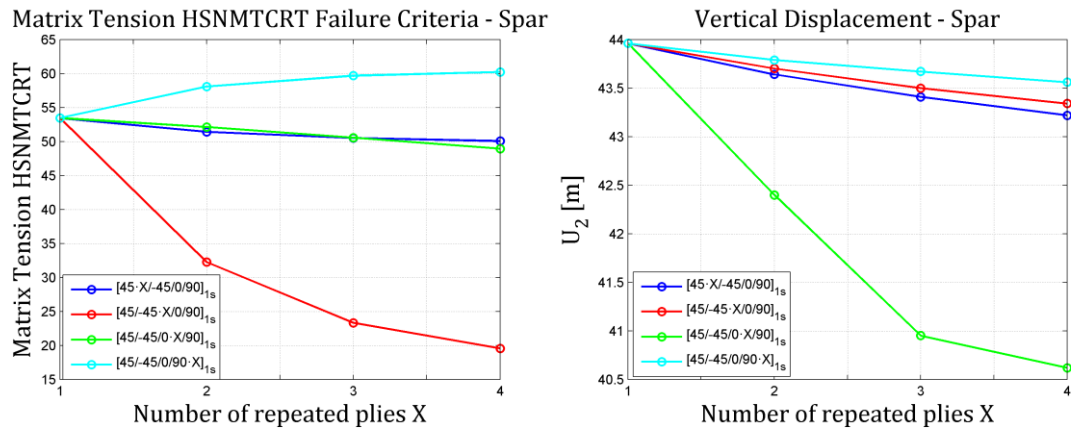


Figure 6.22 – Spar Sensitivity Analysis for HSNMTCRT failure criteria and vertical displacement

Therefore, one can see that the in the spars, fibers at -45 degrees can be included in order to improve the Hashin failure criteria of these structural components. The vertical displacement is improved if several plies at 0 degrees are introduced but in this case the skin reduces more significantly the vertical displacement.

Thus, the optimization process has been performed with the following ply orientations in each of the components:

RIBS		SPARS	
[45/-45/0/90]2s		[45/-45/-45/-45/0/90]3s	

SKIN							
Skin Section 1		Skin Section 2		Skin Section 3		Skin Section 4	
Upper	[45/-45/0/90/90/90/90]6s	[45/-45/0/90/90/90/90]6s	[45/-45/0/90/90/90/90]6s	[45/-45/0/90/90/90/90]6s	[45/-45/0/90/90/90/90]6s	[45/-45/0/90/90/90/90]6s	[45/-45/0/90/90/90/90]6s
Lower	[45/-45/0/90/90/90/90]9s	[45/-45/0/90/90/90/90]9s	[45/-45/0/90/90/90/90]9s	[45/-45/0/90/90/90/90]9s	[45/-45/0/90/90/90/90]9s	[45/-45/0/90/90/90/90]9s	[45/-45/0/90/90/90/90]9s
Skin Section 5		Skin Section 6		Skin Section 7			
Upper	[45/-45/0/90/90/90/90]5s	[45/-45/0/90/90/90/90]5s	[45/-45/0/90/90/90/90]5s	[45/-45/0/90/90/90/90]5s	[45/-45/0/90/90/90/90]5s	[45/-45/0/90/90/90/90]5s	[45/-45/0/90/90/90/90]5s
Lower	[45/-45/0/90/90/90/90]7s	[45/-45/0/90/90/90/90]7s	[45/-45/0/90/90/90/90]7s	[45/-45/0/90/90/90/90]7s	[45/-45/0/90/90/90/90]7s	[45/-45/0/90/90/90/90]7s	[45/-45/0/90/90/90/90]7s
Skin Section 8		Skin Section 9		Skin Section 10			
Upper	[45/-45/0/90/90/90/90]4s	[45/-45/0/90/90/90/90]4s	[45/-45/0/90/90/90/90]4s	[45/-45/0/90/90/90/90]4s	[45/-45/0/90/90/90/90]4s	[45/-45/0/90/90/90/90]4s	[45/-45/0/90/90/90/90]4s
Lower	[45/-45/0/90/90/90/90]4s	[45/-45/0/90/90/90/90]4s	[45/-45/0/90/90/90/90]4s	[45/-45/0/90/90/90/90]4s	[45/-45/0/90/90/90/90]4s	[45/-45/0/90/90/90/90]4s	[45/-45/0/90/90/90/90]4s

Table 6.15 –Optimized ply sequence in the wing components

Ply sequence of the ribs has been chosen in order to maintain the minimum thickness (1.6mm) to avoid possible bucking. Spars have 4 plies at -45 degrees in order to improve the matrix tension failure criteria, as explained before. For the skin, it is important to note that the number of ply repetitions has decreased from the root to the tip has in the root there are higher loads that are more critical for the analysis results. Besides, the lower part of the sections near the root has more number of ply repetitions as the matrix tension failure criteria occurs in the lower part, as shown in Figure 6.20.

Therefore, result for vertical displacement, which is the critical restriction in this case, is shown in figure below:

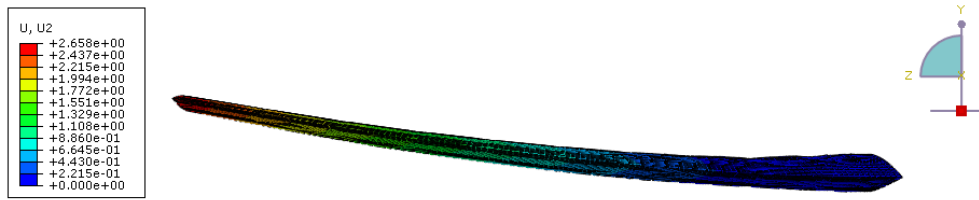


Figure 6.23 – Vertical displacement in meters for last model

On the other hand, results for the most critical cases in Hashin Failure Criteria (fiber compression HSNFCCRT and matrix tension HSNMTCRT) are shown in figures below.

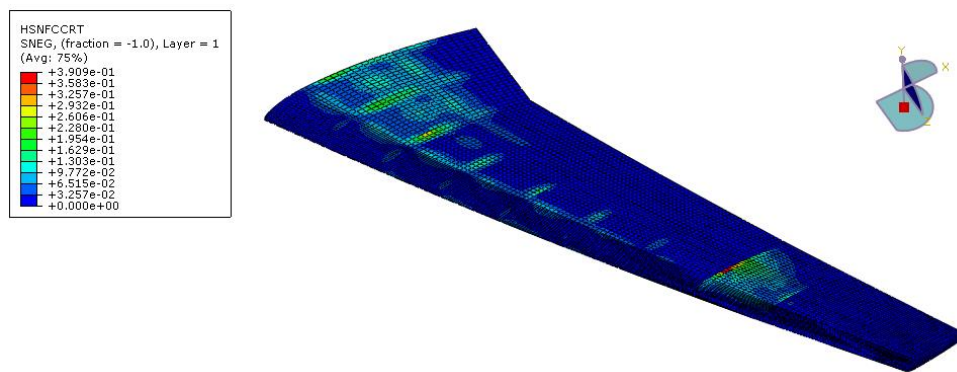


Figure 6.24 – HSNFCCRT in the upper skin of the wing under optimized ply sequence in all the wing components

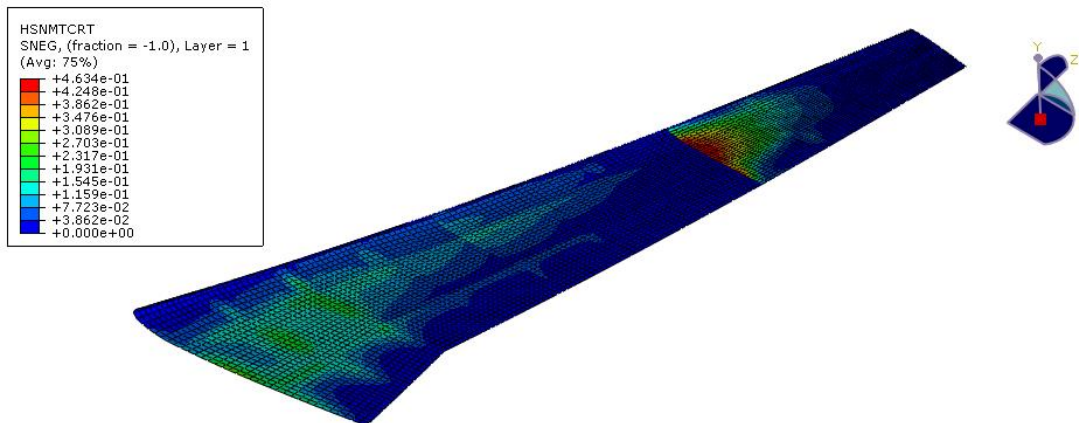


Figure 6.25 – HSNMTCRT in the lower skin of the wing under optimized ply sequence in all the wing components

As shown, critical results in Hashin Failure criteria are obtained in the sections that are near the tip, occurring this due to the change in the numbering of the ply sequence shown in Table 6.15. But in this case, it is not a problem as the most restrictive parameter is the vertical displacement.



Therefore, results for HASHIN failure criteria are shown in table below:

HSNFCCRT	HSFTCRT	HSNMCCRT	HSNMTCRT	Mass (Kg)
0.3909	0.02907	0.1607	0.4634	5425.70

Table 6.16 – HASHIN Failure Criteria for optimized ply orientation in all the wing components.

As also can be seen, mass of the wing has been decreased more than 4 tons with respect to the model that is not optimized. Also, comparing with respect to the aluminum model shown in section 6.3, the mass has been decreased about 8 tons, so optimization process using carbon fiber material is very important in terms of weight reduction maintaining the capability of the wing in withstanding the aerodynamic loads proposed.

The reduction of weight can also be improved by introducing holes in the ribs, whose supported stresses are very low compared with the rest of the aircraft components. Besides, the introduction of stringers in the upper and lower skin can be used to decrease the thickness of the skin by removing some plies.

Thus, the holes have been introduced in the model by performing a circular cut in the ribs shown in the figure below through the *extrusion tool* in ABAQUS. Circular holes have not been included in the most inner ribs because they support higher loads than the most outer ribs. Figure below shows the internal structure of the wing, which includes the previously mentioned circular holes in the outer ribs.

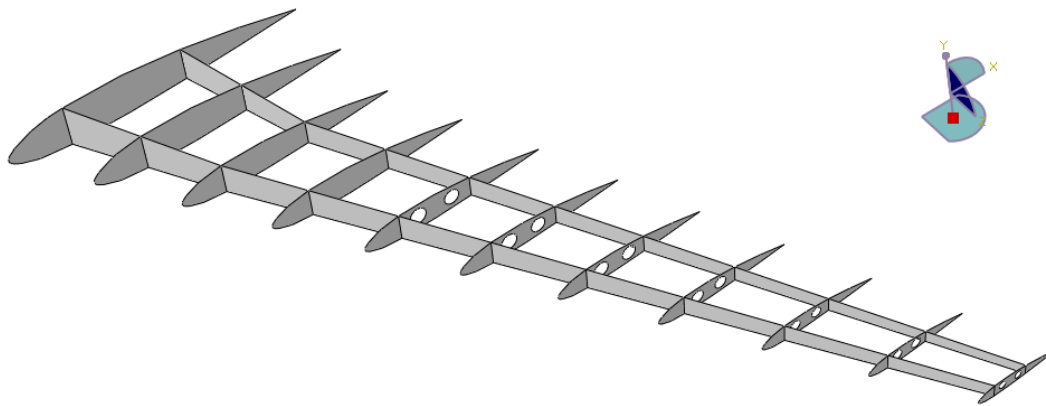


Figure 6.26- Internal structure of the wing with circular holes in the outer ribs. Model 4

The next step is the introduction of stringers that allows the reduction of thickness in the skin. As shown in Figure 6.24 and Figure 6.25, higher stresses appear in the panels that are between the two spars of the wing, so stringers are introduced between these two spars as well as in the outer middle of the panels located at the trailing edge, as shown in figure below:

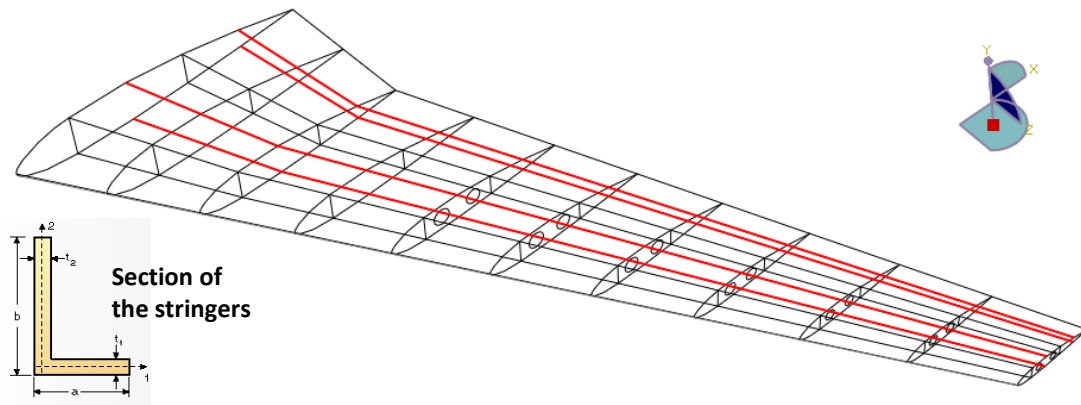


Figure 6.27 – Location and section of the stringers in the upper and lower skin of the wing. Model 4

These stringers have been modeled by using beam elements with an L-section with the following characteristics:

	Profile	a (mm)	b (mm)	t <sub>1</sub> (mm)	t <sub>2</sub> (mm)
Upper Stringers	L	130	130	10	10
Lower Stringers	L	110	110	10	10

Table 6.17 – Characteristics of the stringers in the upper and lower panels.

Besides, the material used is also the carbon fiber, but with unidirectional plies in order to create an isotropic material whose properties are shown in Table 6.18. The analysis of the stringers has been performed by comparing the longitudinal stresses (denoted by  $S_{11}$ ) obtained in ABAQUS with respect to the longitudinal tensile and compressive strength of the material. In this case, the maximum and minimum values of  $|S_{11}|$  must be lower than the longitudinal tensile and compressive strength, respectively.

Density (Kg/m <sup>3</sup> )	1600
Longitudinal tensile strength, X <sub>T</sub> (MPa)	2899
Longitudinal compressive strength, X <sub>C</sub> (MPa)	1414
Poisson coefficient	0.35
Young Modulus(GPa)	162

Table 6.18 – Isotropic Carbon Epoxy MTM45-1/IM7 properties

Then, in order to perform the analysis, the mesh of the model has been changed, introducing more triangular elements in the ribs that have holes in order to have a better representation of the holes in the mesh, as shown in figure below.

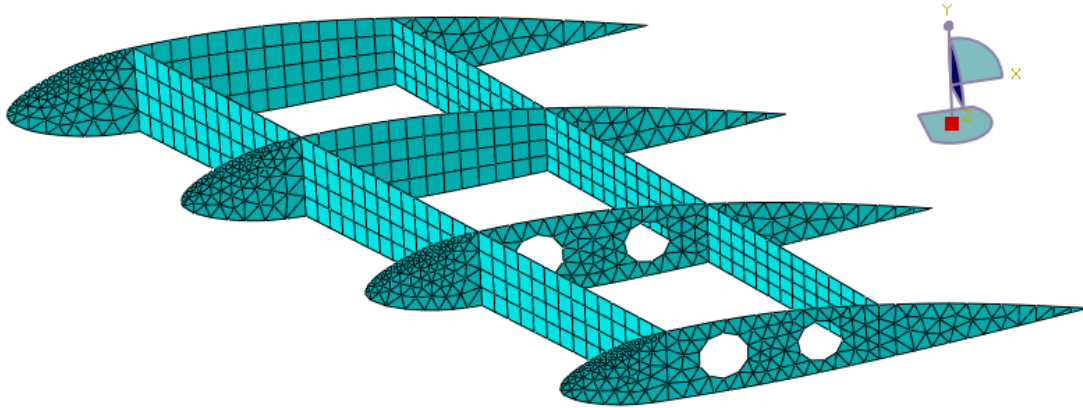


Figure 6.28 – Mesh of the internal structure of the wing. Example from Rib 2 to Rib 5. Model 4

The general characteristics of the mesh used for this final optimization process are collected in the following table:

Total number of nodes	13282
Total number of elements	15878
Beam elements (Type B31)	556
Quadrilateral elements (Type S4R)	12456
Triangular elements (Type S3)	2866

Table 6.19 – Mesh characteristics of Model 4 (with holes and stringers)

Therefore, the process has been performed with the following ply orientations in all the components except the stringers:

RIBS		SPARS	
[45/-45/0/90]2s		[45/-45/-45/-45/0/90]3s	

SKIN				
Skin Section 1		Skin Section 2		Skin Section 3
Upper [45/-45/0/90/90/90/90]5s		Upper [45/-45/0/90/90/90/90]5s		Upper [45/-45/0/90/90/90/90]5s
Lower [45/-45/0/90/90/90/90]7s		Lower [45/-45/0/90/90/90/90]7s		Lower [45/-45/0/90/90/90/90]7s
Skin Section 5		Skin Section 6		Skin Section 7
Upper [45/-45/0/90/90/90/90]4s		Upper [45/-45/0/90/90/90/90]4s		Upper [45/-45/0/90/90/90/90]4s
Lower [45/-45/0/90/90/90/90]5s		Lower [45/-45/0/90/90/90/90]5s		Lower [45/-45/0/90/90/90/90]5s
Skin Section 8		Skin Section 9		Skin Section 10
Upper [45/-45/0/90/90/90/90]3s		Upper [45/-45/0/90/90/90/90]3s		Upper [45/-45/0/90/90/90/90]3s
Lower [45/-45/0/90/90/90/90]3s		Lower [45/-45/0/90/90/90/90]3s		Lower [45/-45/0/90/90/90/90]3s

Table 6.20 –Optimized ply sequence in the wing components (with holes and stringers)

Comparing the ply sequence of this optimized wing with respect to the one presented in Table 6.15, one can easily see the decrease of thickness in both the upper and lower skin because of the addition of the stringers.

Finally, the results obtained for this optimized wing with holes and stringers are the following:

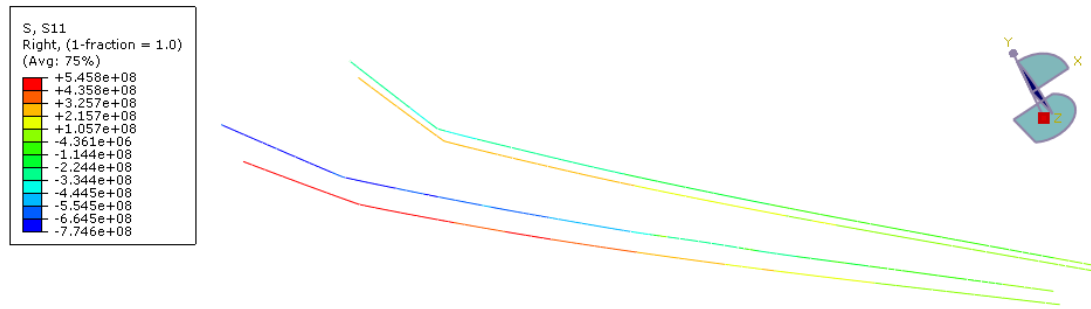


Figure 6.29 – Longitudinal stresses in Pascal for the stringers

Analyzing the results obtained in the stringers, the maximum compressive value is obtained in the upper part of the wing and the maximum tensile value is obtained in the lower part, as expected. Both values are lower than the longitudinal tensile and compressive strength imposed by the isotropic material used for the stringers, so stringers are validated.

The critical modes of failure of Hashin criteria (fiber compression and matrix tension) are shown in figures below:

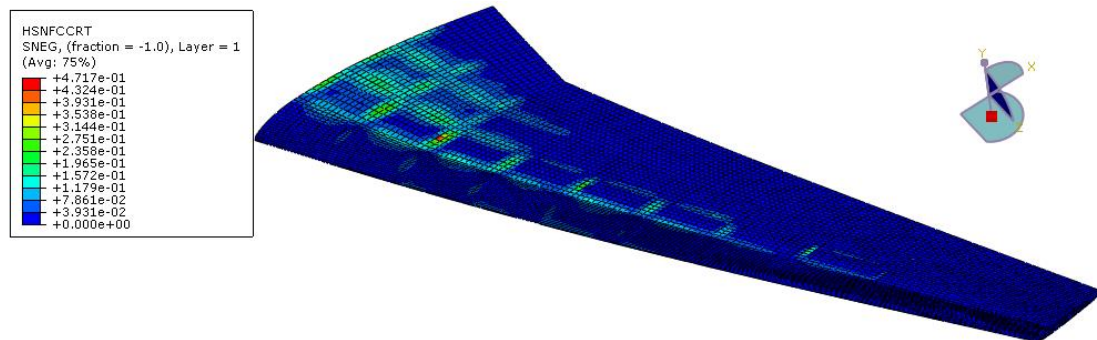


Figure 6.30 – HSNFCCRT in the upper skin of the wing with holes and stringers

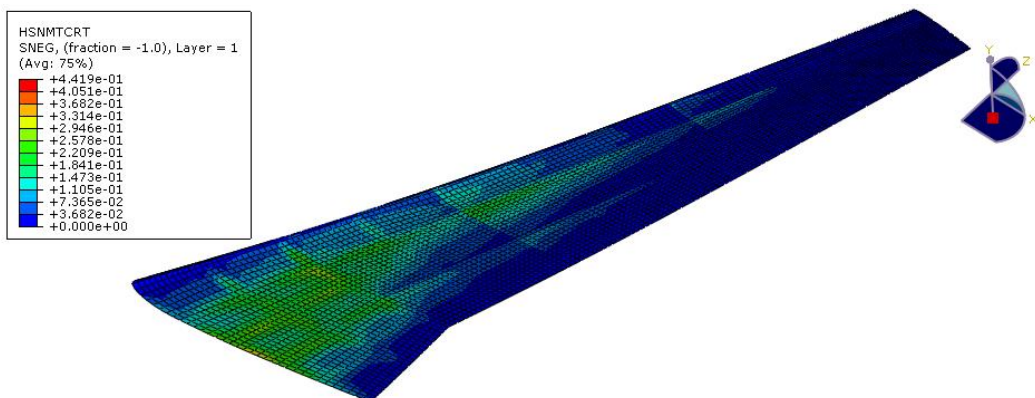


Figure 6.31 – HSNMTCRT in the lower skin of the wing with holes and stringers

With respect to the results of fiber compression (HSNFCCRT) and matrix tension (HSNMTCRT) shown in figures above, one can see that the high stresses that appear due to the

high change in thickness from one section to another are not present anymore due to the introduction of the stringers that allows less abrupt decrease in thickness in the skin.

Therefore, results for HASHIN failure criteria are shown in the following table:

HSNFCCRT	HSFTCRT	HSNMCCRT	HSNMTCRT	Mass (Kg)
0.4717	0.03448	0.1878	0.4419	4765.44

Table 6.21 – HASHIN Failure Criteria for optimized ply orientation in all the wing components.

Results for the vertical displacement of the model are shown in figure below. As shown, vertical displacement is the critical parameter in terms of design restriction when the model is subjected to a real distribution of aerodynamic loads using carbon fiber materials.

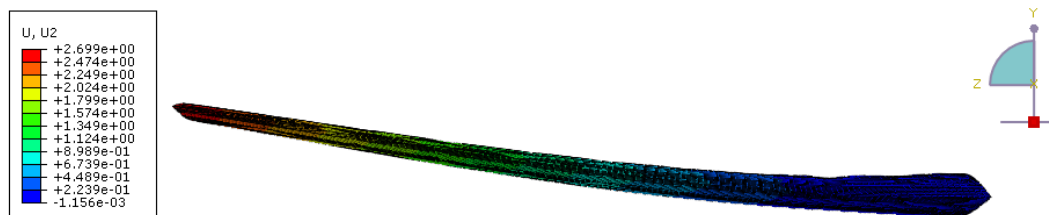


Figure 6.32 – Vertical displacement in meters for last model

## 6.5. Summary of the results

Results of the different models presented in the project are collected in table below:

Wing models made of Al 7475-T761				
Model	Applied Loads	Mass (Kg)	Von Mises (MPa)	Vertical Displ. (m)
Model 1	Triangular	8749.52	488.4	2.395
Model 2	Triangular	11015.1	489.6	2.606
Model 2	Real Distributed	13271.38	373.0	2.697

Table 6.22 – Results for wing models made of Al 7475-T761

Wings made of Al 7475-T761 have the Von Mises stress as the critical parameter when it is subjected to triangular loads. The introduction of the second wing model under triangular loads has as a consequence the increase in weight due to the decrease of the area of the upper panels of the skin, so higher pressure are applied to the model. When the real distributed loads are applied to the second model, the critical parameter changes to the vertical displacement, as in this case, pressure in the upper panels of the wing are also introduced. Also, the introduction of an elliptical load distribution across the span increases a lot the load applied in the panels compared with respect to the triangular load.

Wing models made of Carbon Epoxy MTM45-1/IM7					
Model	Applied Loads	Mass (Kg)	HSNFCCRT	HSNMTCRT	Vertical Displ. (m)
Model 2	Real Distributed	5425.70	0.3909	0.4634	2.658
Model 2 (Holes+Stringers)	Real Distributed	4765.44	0.4717	0.4419	2.699

Table 6.23 – Results for wing models made of Carbon Epoxy MTM45-1/IM7

When composite material is introduced to the model in substitution to Al 7475-T761, the failure criteria changes from the Von Mises to the Hashin Failure Criteria. Wing models made of carbon fiber material have as a critical parameter the vertical displacement, but the optimization of the ply sequence is also needed in order to obtain the lowest possible values of Hashin Failure Criteria. Comparing carbon fiber models created, the introduction of holes in the ribs is very effective in the weight reduction of the wing if the ribs are not subjected to high stresses. In relation with the stringers, they are very useful in order to decrease the thickness of the skin as well as to prevent bucking problems if the thickness of the panels is relatively low.

# Chapter 7

## Conclusions

The realization of the current project through the use of ABAQUS software has demonstrated the validity of the application of finite element method in the analysis of a structural wing model under simulated aerodynamic loads. The prediction of the stresses in the wing as well as the displacements are accurately obtained by introducing the simulated loads and the corresponding boundary conditions that creates a model that represents a real aircraft wing. As explained in section 1.1, it has been demonstrated that the finite element modelling has allowed a significant money and time saving as the construction and the testing of the structural members of the wing and the wing itself has been avoided by simply creating a model using finite element software. Results obtained in this numerical procedure can be extrapolated to a real model and, comparing the results obtained in the finite element software with respect to the results obtained from one test, once both results are considered perfectly correlated, the time and money saving is done by the reduction of the need of construction of real models and tests.

Apart from the advantages presented before, finite element analysis is also important in terms of predicting results in the real model. In the current model, the behavior of the different structural members of the wing under different loads has been understood. Also, in relation with the ply orientation when dealing with composite materials, the fiber orientation is different depending on the structural member studied. Therefore, the conclusions obtained from the results obtained in the different analyzed models can be summarized as follows:

- Wing models made of aluminum material and subjected to a simplified triangular load has the Von Mises stress as the more restrictive parameter. Changing the wing geometry in such a way that the area of the panels in which the load is applied decreases, provokes an increase of the pressure in each of the panels, so the mass of the wing increases as the thickness associated to the structural members of the wing has increased to fulfill the imposed design criteria.
- Minimum thickness must be defined for all the structural members of the wing, as in a linear static analysis, buckling problems are not taken into account.
- In relation with the thickness that must be associated to each structural member in order to withstand the applied loads, minimum thickness can be associated to the ribs, as it is demonstrated that the increase of thickness in the ribs poorly improves the values in the Von Mises stress and the vertical displacement. With respect to the increase of the thickness in the spars and the skin, the spars are able to improve the maximum displacement with higher thickness, and the skin is able to improve the

stresses on the skin with higher thickness. One can that an optimization process can be performed in the spars and in the skin as the higher thickness in the spars, the lower stresses in the skin.

- With the introduction of a real distribution of aerodynamic loads obtained from an analysis tool for airfoils, the loads affects both the upper and the lower skin of the wing, so in this case, the vertical displacement is the limiting design criteria.
- The principal consequence of the introduction of carbon fiber material in the wing model under real aerodynamic loads is the reduction in weight. In this case, the critical design criterion is the maximum vertical displacement in the wing, but also the fiber tension and the matrix compression must be taken into account in order to avoid failure in the composite material.
- The ply orientation in each of the structural members is important to the optimization of the wing model. For the ribs, minimum thickness must be imposed to avoid buckling problems. In the case of the spars, it has been demonstrated that the introduction of fibers at -45 degrees are better in order to avoid failure in the material and in the case of the skin, it is better to introduce more fibers in the longitudinal direction of the wing, that is at 0 degrees as the matrix failure criteria as well as the vertical displacement are considerably improved.
- The introduction of holes and stringers are essential for a further optimization of the wing. Holes are introduced in order to decrease the weight of the wing as the ribs are not highly affected by the distribution of aerodynamic loads comparing with the other structural members. In relation with the stringers, they are very useful in order to decrease the thickness of the skin they are attached. Also, the location of the stringers are usually between two spars in order to reduce the area of the panels, which can be subjected to compressive loads in the upper skin that provokes failures in buckling.



# Chapter 8

## Future projects

The current project can be used as a starting point for future projects that are related with the structural analysis of an aircraft wing.

The structural analysis of the wing can be therefore performed under different flight conditions, taking into account the different phases during the flight (ground maneuvers, climb, descend, landing...), so that the aerodynamic loads applied on the model change. Apart from these loads, internal forces due to the fuel tanks or the weight of the engine can also be introduced in the model to obtain a better approximation to the real model. Also, dynamic loads and vibrations can be introduced in the model for further improvement of the structural analysis of the wing.

In the current project, linear static analysis has been performed. For future project, non-linear analysis can be introduced in the model in order to compare the results obtained from the linear analysis.

In relation with the wing design, further improvement of the model can be carried out by introducing the control surfaces that has been presented in Figure 2.4 as well as the modelling of the engine that is located in the middle of the two tapered sections with its respective pylon.

Finally, buckling of the upper panels of the skin can be used to perform a buckling analysis as they are subjected to compressive loads, and in a linear static analysis in ABAQUS the effects of buckling are not shown.

# Chapter 9

## Project planning and budget

The project has been divided in several work packages in order to have a better view of the objectives of the project. These work packages have been divided as explained down below.

The starting point of the project has been the collection of information and general characteristics of the aircraft used as a reference for the modelling of the wing in finite element software. Also, the basis of the finite element method used in the ABAQUS software has been reviewed. Then, the project starts by taking into account the following work packages:

- Modelling of the wings.
- Calculation of the different pressures applied in each of the panels of the skin of the wing models
- Analysis of the entire wing model and optimization of it by analyzing the results obtained.

To perform a complete analysis of the wing model, these steps have been repeated with different wing geometries, materials and load distributions in order to obtain all the different studied cases presented in the project.

Finally, the current project has been written to collect the procedure and the results obtained from the Finite Element Model.

A planning has been performed to create a virtual budget in the case that this project is carried out in real life. The estimated work hours in each of the work packages are shown in table below:

Work Package	Hours
Bibliographic research	15
Modelling of the wings	100
Calculation of the distribution of the applied loads	60
Optimization process	40
Report Writing	80
Meeting	20

Table 9.1 – Hours per work package

Therefore, an estimation of the cost is performed by taking into account the cost of one engineering work hour and the cost of the ABAQUS license.

$$315 \text{ h of engineering work} * 30 \frac{\text{€}}{\text{h}} = 9450\text{€} \quad (36)$$

$$\text{ABAQUS License Cost} = \frac{25000\text{€}}{\text{year}} * \frac{1}{4} \text{ year} = 6250 \text{ €} \quad (37)$$

$$\text{Total Cost of the Project} = 9450 + 6250 = 15700\text{€} \quad (38)$$

# Bibliography

- [1] "The worlds of David Darling website" [www.daviddarling.info](http://www.daviddarling.info). Consultation year: 2015
- [2] "The structural model and the normal modes" Lecture 04 Aeroelasticity course 2014/2015. Bachelor in Aerospace Engineering
- [3] "Engineering nomenclature website - Airbus Airplane Wing Structure and Terminology" [www.nomenclaturo.com](http://www.nomenclaturo.com). Consultation year: 2015
- [4] "Introduction to Finite Element Analysis (General Steps)" Lab session course 2014/2015. Bachelor in Aerospace Engineering
- [5] "Finite element analysis website – Finite element analysis in a nut shell" [www.stressebook.com](http://www.stressebook.com). Consultation year: 2015
- [6] ABAQUS 6.14.1 Software
- [7] "Airbus website" [www.airbus.com](http://www.airbus.com). Consultation year: 2015
- [8] "Análisis estructural del ala de un aeronave comercial". Trabajo Fin de Grado. Author: Manuel Robles del Toro
- [9] "Aircraft Characteristics Airport and Maintenance Planning". Airbus Manual. Issued date January 1993, revised January 2012
- [10] Dassault Systemes website. [www.3ds.com](http://www.3ds.com). Consultation year: 2015
- [11] "Abaqus/CAE User's Manual" Dassault Systemes, 2012
- [12] "Abaqus Analysis User's Manual" Dassault Systemes, 2012
- [13] "Airfoil tools website" [www.airfoiltools.com](http://www.airfoiltools.com). Consulting year: 2015
- [14] "Material Data Sheet Aluminum 7475-T761". Aerospace Specification Metals, 2015
- [15] "Analysis of a wing structure by Finite Element Software (ABAQUS)" Laboratory sessions Course 2013/2014. Bachelor in Aerospace Engineering
- [16] Hashin, Z., "Failure Criteria for Unidirectional Fiber Composites," Journal of Applied Mechanics, vol. 47, pp. 329–334, 1980.

- [17] Hashin, Z., and A. Rotem, "A Fatigue Criterion for Fiber-Reinforced Materials," Journal of Composite Materials, vol. 7, pp. 448–464, 1973.
- [18] "Compressive Failure of Fiber Composites" paper. N. A. FLECK. Cambridge University Engineering Department. 2005
- [19] "A330 Aircraft Recovery Manual ARM". Airbus Manual. Issued date July 1993, revised November 2009
- [20] "Federal Aviation Regulations, FAR Part 25.303: Factor of Safety"
- [21] "Remote Control Plane Website" School of aerospace engineering – Universiti Sains Malaysia. [aerospace.eng.usm.my](http://aerospace.eng.usm.my). Consultation year: 2015
- [22] "Thermofluids, surfaces and interfaces website" University of Leeds [www.efm.leeds.ac.uk](http://www.efm.leeds.ac.uk). Consultation year: 2015
- [23] XFLR5 6.10.04 Software